Zeitschrift: IABSE congress report = Rapport du congrès AIPC = IVBH Kongressbericht

Band: 9 (1972)

Rubrik: Theme VI: Experimental study of the behaviour of structures under loads

VI

Etudes expérimentales du comportement des ouvrages sous les sollicitations

Experimentelle Studien über das Verhalten der Bauwerke unter Belastung

Experimental Study of the Behaviour of Structures under Loads

VI a

Contrôle des ouvrages existants

Kontrolle bestehender Bauten

Checking of Actual Structures

Leere Seite
Blank page
Page vide

Kontrollmessungen an Brückenkonstruktionen

Control Measurements of Bridges

Mesures de contrôles de ponts

A. SZITTNER
TU Budapest, Lehrstuhl für Stahlkonstruktionen
Budapest, Ungarn

Die Mitarbeiter des Lehrstuhles für Stahlkonstruktionen der TU Budapest haben in den letzteren Zeiten an den in Ungarn gebauten verschiedenen Brückenkonstruktionen Kontrollmessungen durchgeführt, um die wirkliche und theoretische Kräftespiele gegenüberzustellen. Die Messungen wurden in fünf Gruppen klassiert:

1. Traditionelle Probebelastung,
2. Lastenzug-Einflusslinie,
3. Dynamisches Verhalten der Brücken,
4. Feststellung des Brückenzustandes,
5. Kontrollmessungen während des Baues.

Die Mess- und Auswertungsmethode bzw. die Folgerungen werden auf Grund der Messungen an den untenstehenden Strassenbrückenkonstruktionen vorgestellt:

a/ Hängebrücke mit Spannweite 44 + 290 + 44
b/ Verbundkonstruktion mit Kastenträger (Spannweite: 30 m)
c/ Durchlaufende Fachwerkbrücke mit Eisenbeton-Fahrplatte als Verbundkonstruktion mit Querträger (Spannweite: 3x70 m)
d/ Durchlaufende Verbundkonstruktion mit Kastenträger (Spannweite: 3x25 + 40 + 2x25 m)
e/ Durchlaufende Vollwand-Verbundkonstruktion mit Freikabel-Vorspannung (Spannweite: 57 + 67 + 57 m).

1. Traditionelle Probebelastung

Der Inbetriebnahme der Brücken geht immer ein amtlicher Prozess, die Probebelastung voran, wo den Vorschriften nach, nur die Durchbiegungen gemessen werden sollen. So wird das Kräftespiel und das Verhalten der Konstruktion im Ganzen kontrolliert. Im wissenschaftlichen und praktischen Sinne ist es aber auch wichtig, die wirklichen Spannungen und Beanspruchungen der Brückenelemente mit den theoretischen Werten, gewonnen an den mathematischen Modellen, zu vergleichen.

Durch die Messungen werden

die örtlichen Spannungen und Spannungsspitzen,
die Knotenpunkt-Nebenspannungen,
die Querverteilung und Torsionssteifigkeit, und
die Fahrbahn-Mitwirkung

kontrolliert.

Als Mess-System wurden bei den obenerwähnten Aufgaben Dehnungsmess-Streifen (DMS) mit Messverstärker und mit Registriereinrichtung, oder Dehnungsmesser mechanischen Systems angewendet.

Über die Messungen der örtlichen Spannungen kann nichts Neues gesagt werden. Um die Knotenpunkt-Nebenspannungen festzustellen, wurden die Spannungen (Dehnungen) neben den ausgewählten Knotenpunkten auf jedem Stab bei der Stabmitte und neben dem Knotenblech in den 4 Eckpunkten der Querschnitten gemessen. Auf Grund des Bernoulli-Navier-Satzes werden aus den Messergebnissen die Werte σ_N, σ_{Mx}, σ_{My} und σ_W gerechnet. Auf der Brückenkonstruktion nach Abb.4. in den Knotenpunkten 25 und 28 wurden die Nebenspannungen festgestellt. Bei den Gurtstäben sind die gemessenen Werte ein wenig höher als die gerechneten Werte nach Hartmann-Melan [1], aber bei den Diagonalen, wo die Stabkräfte bzw. die σ_N-Spannungen im absoluten Sinne kleiner sind, sind die Nebenspannungen prozentuell viel höher. Auf Abb.1. wurde die Tendenz vorgestellt, dass die Knotenpunkt-Nebenspannungen mit der Zunahme der Ausnützung des Stabes sich vermindern. Die Nebenspannungen waren immer beachtlich [2].

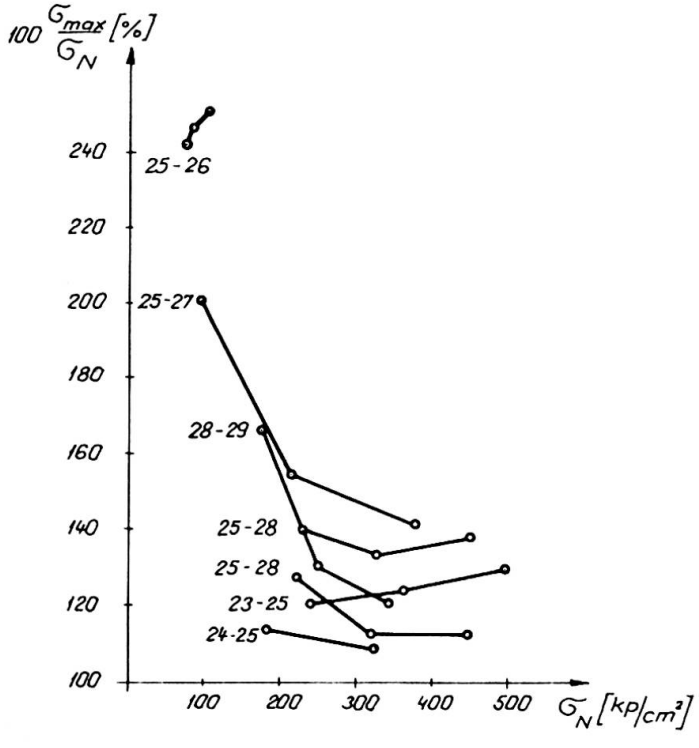

Abb.1.

Auf dieser Brücke wurde auch die Querverteilung kontrolliert. Die Messergebnisse und die Werte - gerechnet nach Cornelius [3] - zeigten weder bei symmetrischer, noch bei asymmetrischer Belastung gute Übereinstimmung. Die Messergebnisse unterstützten viel mehr eine Rechenmethode wobei die Konstruktion als einfacher Träger auf zwei Stützen gerechnet wurde (Abb.2.).

An der selben Konstruktion wurde auch die Mitwirkung der Fahrbahnkonstruktion überprüft. Die Spannungen in dem Untergurt sind wegen der Mitwirkung der Fahrbahnplatte etwa 20-30 % kleiner, als die ohne Mitwirkung gerechneten Werte. Dementsprechend sind aber die Obergurt-Kräfte durch die Verkürzung des Hebelarmes der Zug-Druckkraft etwa 10-15 % höher, als die Werte einfach berechnet.

Diese Differenz vermindert sich bedeutend neben den Stützen, wo die Fahrbahnplatte untergebrochen ist.

2. Lastenzug-Einflusslinien

Im Laufe der traditionellen Probebelastung werden die bei einer genau bestimmten Achsenanordnung gemessenen und berechneten Deformationen und Spannungen verglichen. Man bekommt aber ein besseres Bild über das Verhalten der Konstruktion, oder Konstruktionselemente, wenn die Belastung mit der Hilfe eines in der Fahrbahnachse sich langsam bewegenden Schwerlastwagens wirkt, und die Spannungen und Deformationen mit einer Registriereinrichtung aufgenommen werden. Die auf Grund der Einflusslinien gerechneten Werte werden den wirklichen Registratumwerten gegenübergestellt.

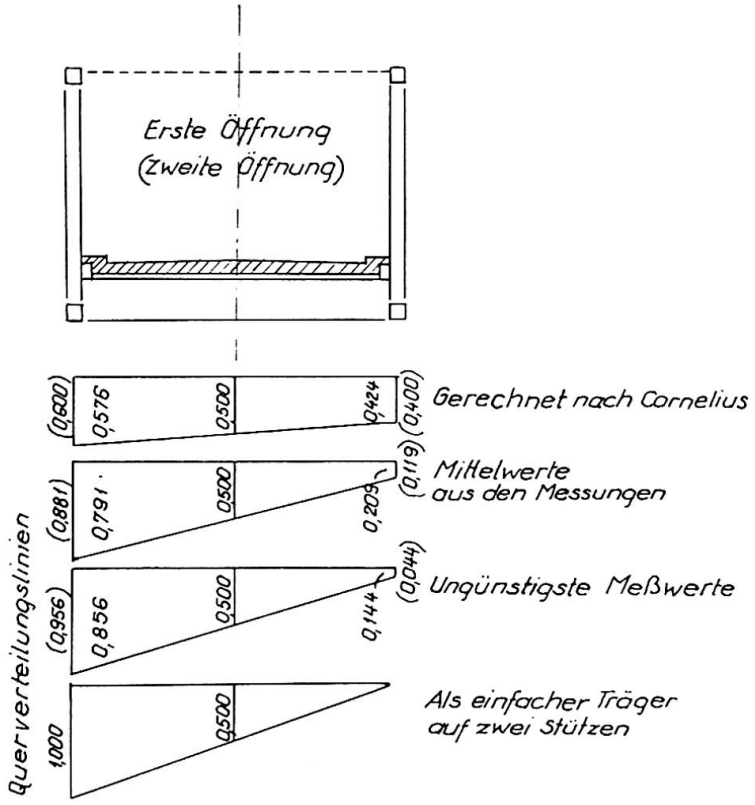

Abb.2.

Abb.3. zeigt die Gegenüberstellung der Lastenzug-Einflusslinie bei einer Verbund-Konstruktion mit Kastenträger (l = 30 m). Die auf den verschiedenen Punkten des Kastenträgergurtes gemessenen Spannungen zeigen gut die Spannungsverteilung der Brücke. Der Durchschnittswert der Messergebnisse stimmt sehr gut mit dem gerechneten Wert [4].

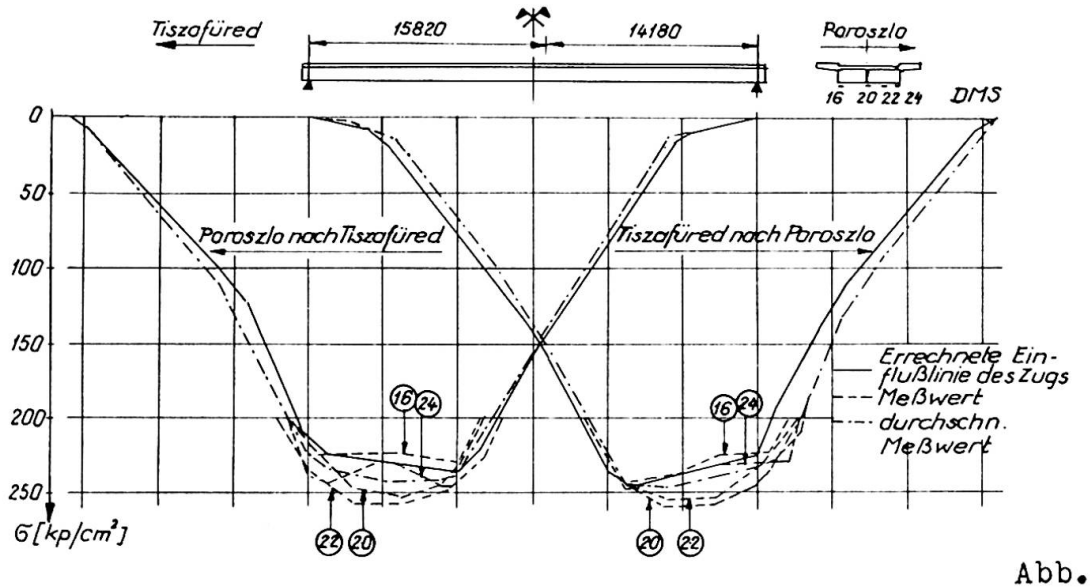

Abb.3.

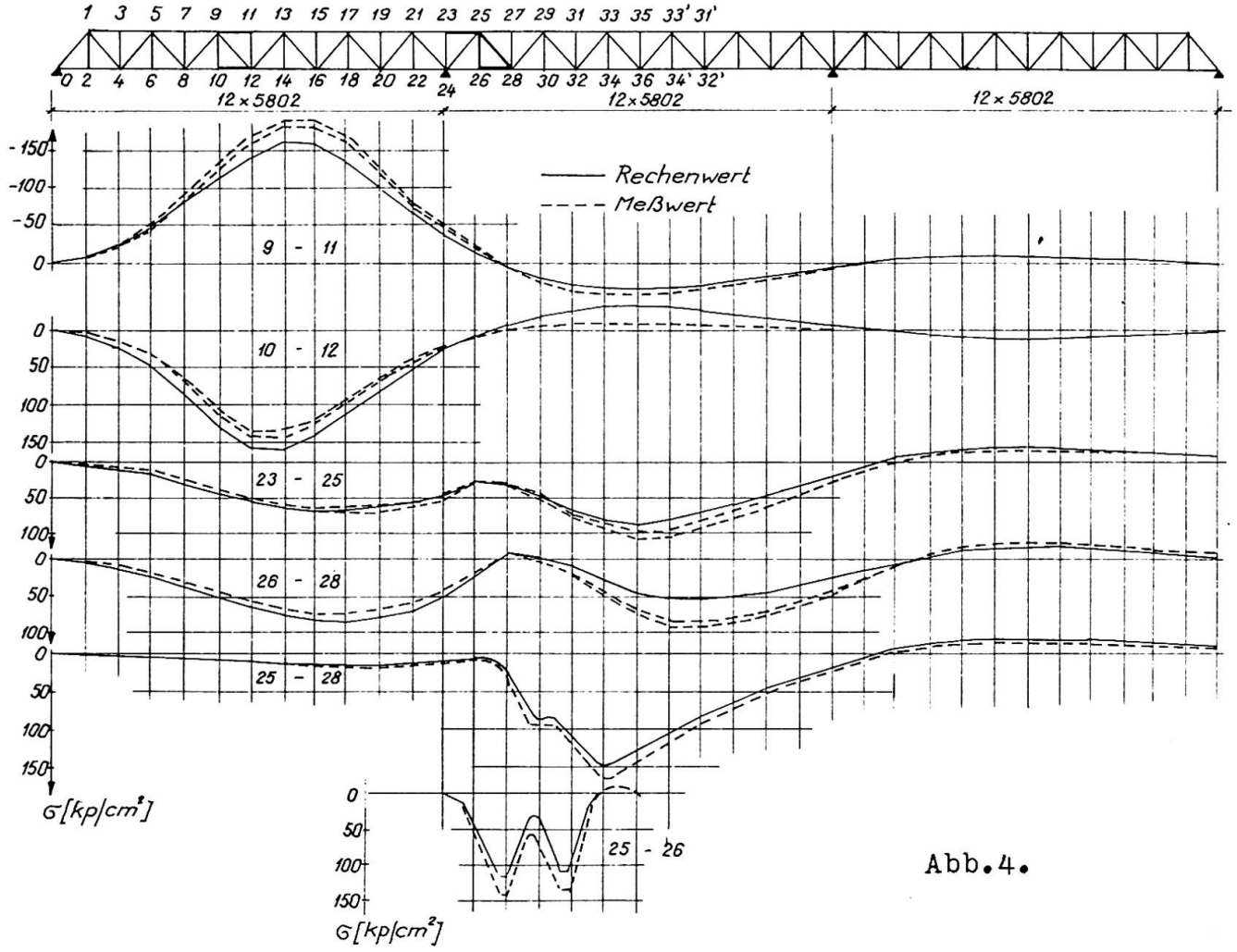
1 3 5 7 9 11 13 15 17 19 21 23 25 27 29 31 33 35 33' 31'
0 2 4 6 8 10 12 14 16 18 20 22 24 26 28 30 32 34 36 34' 32'
12×5802
12×5802
12×5802
Rechenwert
Meßwert
9 - 11
10 - 12
23 - 25
26 - 28
25 - 28
25 - 26
σ[kp/cm²]

Abb.4.

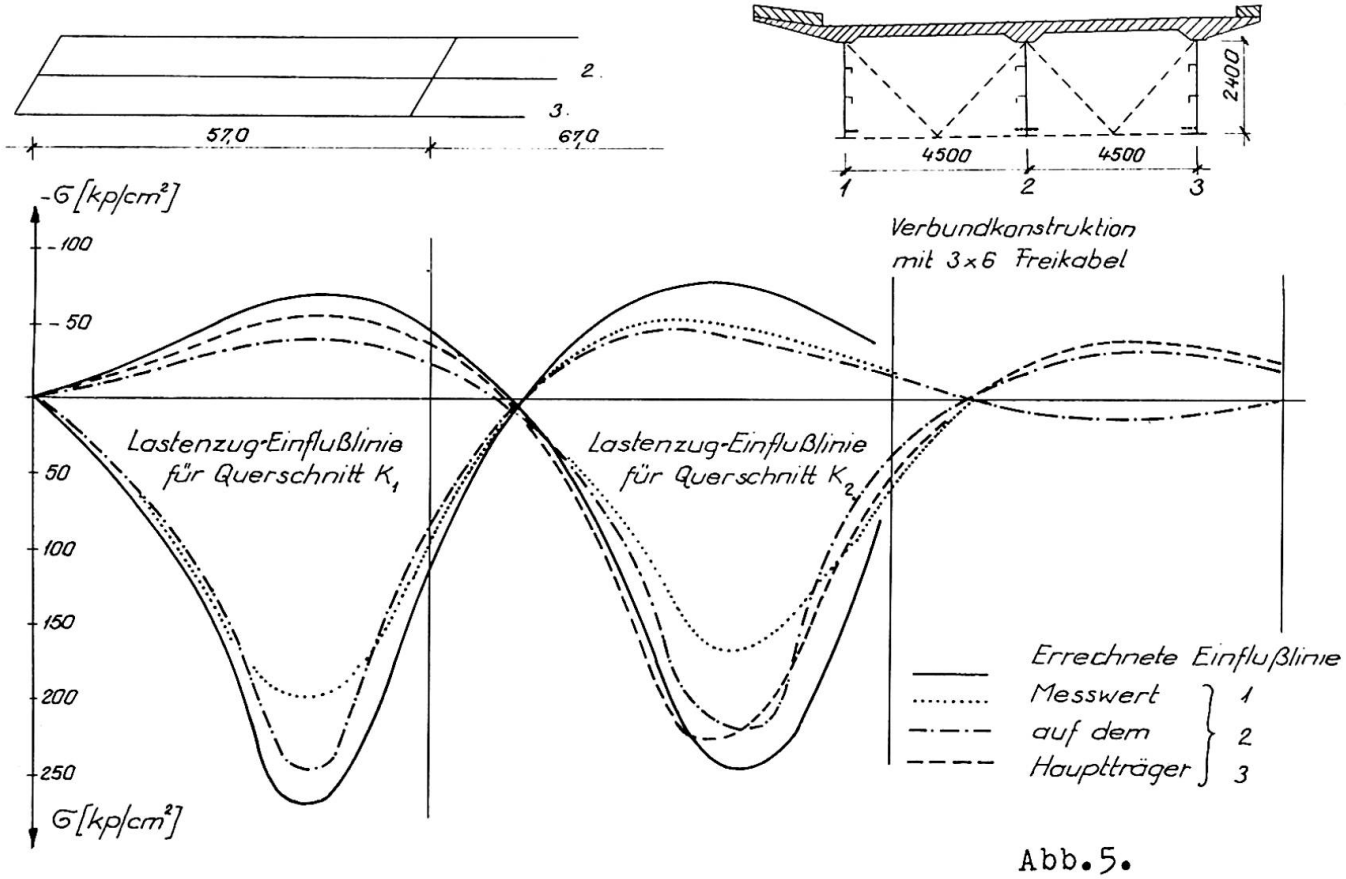
2.
3.
57.0
67.0
2400
4500
4500
1
2
3
Verbundkonstruktion
mit 3×6 Freikabel
-σ[kp/cm²]
Lastenzug-Einflußlinie
für Querschnitt K1
Lastenzug-Einflußlinie
für Querschnitt K2
Errechnete Einflußlinie
Messwert
auf dem
Hauptträger
1
2
3
σ[kp/cm²]

Abb.5.

Auf Abb.4. sind die Lastenzug-Einflusslinien für die Stabspannungen eines durchlaufenden Fachwerkträgers zu sehen. Der Ursprung der Abweichung zwischen den gerechneten und gemessenen Spannungen ist auch jetzt die Mitwirkung der Fahrbahnplatte. Deswegen ist die Obergurtkraft etwa 20 % höher, die Untergurtkraft etwa 10 % niedriger, als die ohne Mitwirkung der Fahrbahnplatte gerechneten Werte. Bei dem Obergurt 23-25 gab es in der Seitenöffnung infolge der Fahrbahnplatten-Unterbrechung keine bedeutende Differenz, aber in der Mittelöffnung war die Differenz schon beachtlich.

In dem Gurtstab 26-28, wo die Stabkräfte etwas kleiner sind, ist die Abweichung ein bischen grösser. Die Differenz meldet sich besonders in dem Charakter der Einflusslinie. Bei den Diagonalen 25-28 und 25-26 ist die Abweichung nicht bedeutend.

Die Lastenzug-Einflusslinien geben ein sehr gutes Bild über die Querverteilung der kastenartig ausgebildeten Brückenquerschnitten. Als Beispiel werden die Messergebnisse einer mit äusseren Kabeln gespannten, schrägen, durchlaufenden Verbundkonstruktion erwähnt (Abb.5.). Wegen des schrägen Grundrisses und der asymmetrischen Fahrbahn-Anordnung sind die Spannungen in den drei Hauptträgern verschieden, andererseits wegen der besseren Betonqualität etwas kleiner, als die nach dem Entwurf gerechneten Werte.

3. Dynamisches Verhalten der Brücken

Die meisten Bemessungsvorschriften berücksichtigen die aus der Bewegung stammende dynamische Zusatzlast mit einem sogenannten dynamischen Faktor, der von der Art der Brücken abhängt und mit der Spannweite sich vermindert. Bei einer konkreten Konstruktion ist die Zusatzlast proportional mit der Nutzlast. Diese Voraussetzung wurde durch die experimentellen Werte nicht unterstützt. Deshalb bestrebte man theoretisch oder experimentell einen Zusammenhang, der das dynamische Verhalten der Brücken treu spiegelt. Die Grunderscheinungen und die Grundgleichungen der Lösung sind theoretisch klar (Effekt von Timoshenko, Zimmermann, usw.), aber eine allgültige Superpositionsregel oder ein Zusammenhang der dynamischen Wirkung ist wegen der zeitlichen und räumlichen Zufälligkeit der Lasten unmöglich zu finden.

Aus diesem Grunde hat der UIC-ORE (Internationaler Eisenbahnverband, Forschungs- und Versuchsamt) für Eisenbahnbrücken eine umfangreiche Experiment-Serie angefangen und die Messergebnisse ausgewertet. In der zusammenfassenden Veröffentlichung [5] hat der ORE die eindeutige Folgerung festgestellt, dass es unmöglich ist, die wirkliche dynamische Wirkung in geschlossener Form sogar bei zwangsbahnartiger Eisenbahn-Belastung festzustellen. Die Anwendung des dynamischen Faktors als Bemessungsmethode spiegelt das wirkliche Kräftespiel nicht.

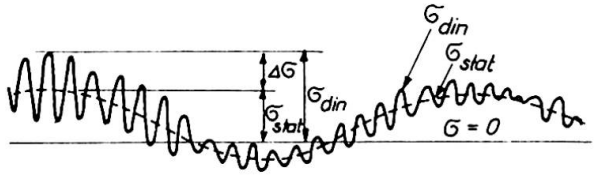

Abb.6.

Gleichzeitig mit den anderen Probebelastungen wurde in dem Geist der Arbeit von UIC-ORE auch dynamische Probebelastung durchgeführt, wo die Lastkraftwagen auf der Brücke in verschiedenen Gruppen und mit verschiedener Geschwindigkeit gefahren wurden.

Die Auswertung der Registraten wurde nach der Abb.6 gemacht. So wurden die charakteristischen Werte von σ_{stat}, σ_{din}, $\mu = \sigma_{din}/\sigma_{stat}$ und $\Delta\sigma = \sigma_{din} - \sigma_{stat}$ für jede Fahrt festgestellt. Mit verschiedenen Lastgruppen wurde erreicht, dass die Ausnützung der Träger verschieden sei. Als Ausnützung wurde ein prozentuelles Verhältnis zwischen dem Messwert σ_{stat} und dem Rechenwert $\sigma_{stat,max}$ genommen.

So wurden die Ergebnisse als Funktion der Ausnützung erstens auf Grund des dynamischen Faktors μ, zweitens auf Grund des dynamischen Mehrwertes $\Delta\sigma$ aufgezeichnet. Wenn die Hüllkurve dazu eingezeichnet wird, ist der Charakter des dynamischen Faktors, bzw. des dynamischen Mehrwertes sehr schön zu sehen.

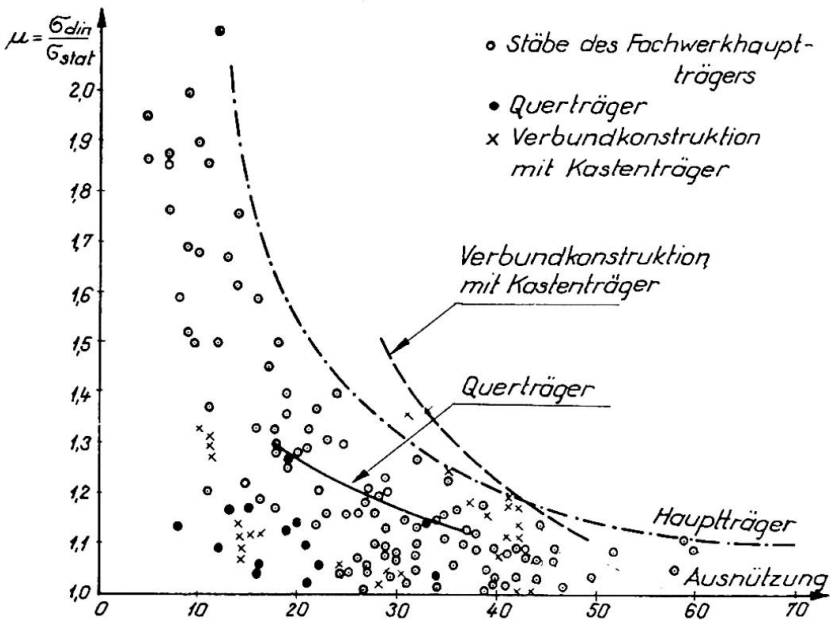

Abb.7.

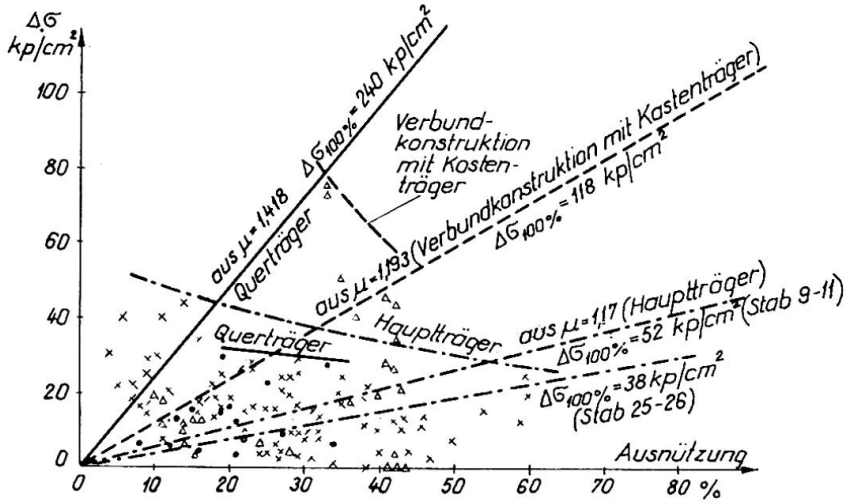

Abb.8.

Als Beispiel wird auf den Abbildungen 7. und 8. die Auswertung der Messergebnisse der Brücke von Tiszafüred (Fachwerkträger und Vollwandträger siehe auf Abb.3,4); auf der Abb.9. die Auswertung der Messergebnisse der Elisabeth-Brücke, und auf Abb.10. die Auswertung der Messergebnisse einer durchlaufenden Verbundkonstruktion vorgestellt.

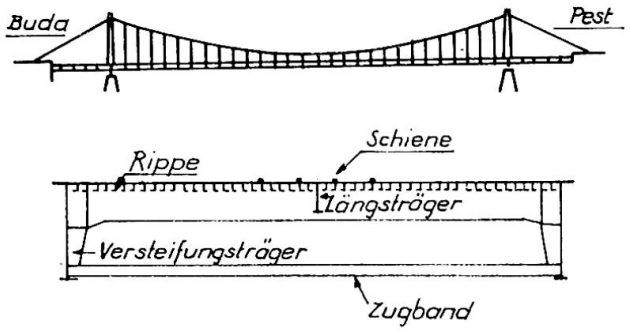

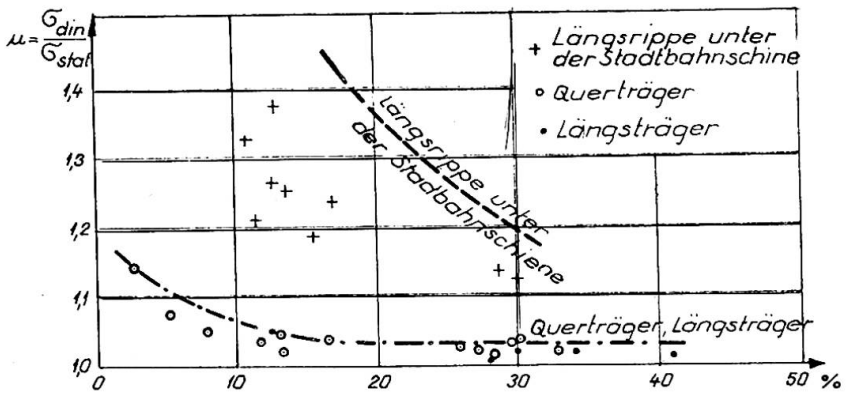

Abb.9.

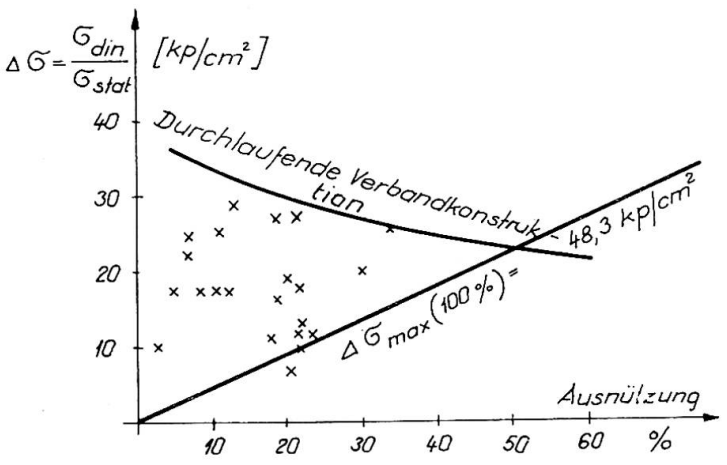

Abb.10.

Auf Grund der Messergebnisse wurden die nachstehenden Folgerungen festgestellt:

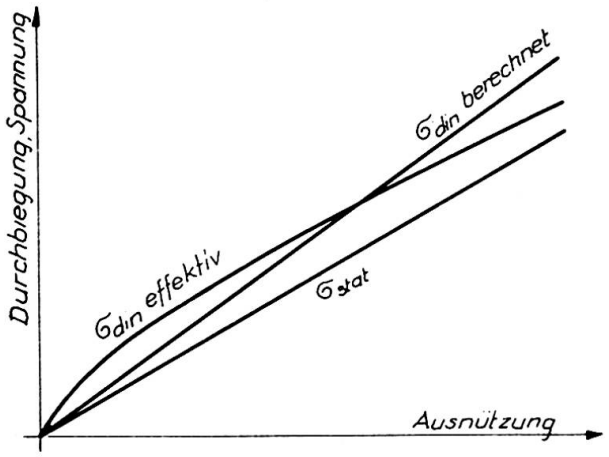

Abb.11.

a/ Der Wert von $\sigma_{din}/\sigma_{stat}$ ist kein Konstant, es vermindert sich mit dem Wachsen der Ausnützung.

b/ Der dynamische Mehrwert $(\sigma_{din} - \sigma_{stat})$ vermindert sich in Tendenz, oder stagniert.

c/ Die dynamische Vollbelastung der Strassenbrücken ist unmöglich. Unseren Erfahrungen nach ist die maximale Ausnützung etwa 60-70 %.

d/ Bei der Dimensionierung der Strassenbrücken wäre auch richtiger, so wie es von UIC-ORE vorgeschlagen wurde, statt des dynamischen Faktors den dynamischen Mehrwert anzuwenden (Abb.11.).

4. Feststellung des Brückenzustandes

Bei den neueren Brückenkonstruktionen, besonders bei den Stahlbeton- und Verbundkonstruktionen, wurden auf Grund des Vorschlages von I. Illésy die Eigenfrequenzen der Konstruktion auch gemessen. Es ist nämlich selbstverständlich, dass die nicht gut sichtbaren mechanischen Aenderungen (Risse, Stützenbewegungen usw.) auch die gut messbare Eigenfrequenz verändern können. Die Eigenfrequenzmessungen sind auf den neueren Brücken durchgeführt und ständig kontrolliert worden. Über die Erfahrungen kann noch nicht berichtet werden.

5. Kontrollmessungen während des Baues

Im Laufe der Bauzeit ist es sehr wichtig, besonders bei den durchlaufenden Verbundkonstruktionen und bei den vorgespannten Konstruktionen das wirkliche Montage-Kräftespiel und die Wirkung der verschiedenen Montagephasen (Stützensenkung, Belastung, Vorspannung usw.) zu beobachten. Diese Aufgabe benötigt eine Messmethode, wo die Messprozesse während der verhältnismässig langweiligen Bauzeit weitergeführt und die Messelemente aufbewahrt werden können. Ausserdem soll die Wirkung der Temperaturänderung beseitigt werden. Bei solchen Aufgaben wurde als Messinstrument der Setzdehnungsmesser Bauart Pfender sehr gut angewendet, der mit einer Messlänge von 100 mm, mit entsprechender Temperaturkompensation, eine Genauigkeit vont 20 kp/cm^2 sichert. Mit dieser Methode wurde in Ungarn der Bau von zwei durchlaufenden Verbundkonstruktionen in der Bauzeit durch mehrere Monate ständig kontrolliert.

Literatur

[1] Hartmann-Melan: Der Brückenbau. Franz Deuticke Verlag, Wien, 1951.

[2] Tóth-Visontai: Statische Messungen an der Strassenbrücke über die Theiss bei Tiszafüred. Periodica Polytechnica Vol. 13. No 3-4. Budapest 1969.

[3] Cornelius: Über den Einfluss der Torsionssteifigkeit auf die verdrehung von Tragwerken. MAN-Forschungsheft, Augsburg, 1951.

[4] Kristóf-Szittner: Dynamische Untersuchungen an der Tisza-Strassenbrücke bei Tiszafüred. Periodica Polytechnica Vol. 13. No 3-4. Budapest 1969.

[5] Frage D 23. Ermittlung der dynamischen Beanspruchungen von Brücken. Bericht üver den Vorversuch an der Rhonebrücke Riddes der SBB. UIC-ORE, Utrecht, 1957.

Zusammenfassung

Der Lehrstuhl für Stahlkonstruktionen der TU Budapest hat an verschiedenen neugebauten Stahlbrücken Kontrollmessungen durchgeführt. Mittels dieser Messungen wurden die auf theoretischem Grunde gerechneten Werte des Kräftespieles, der Querverteilung, der Torsionssteifigkeit, der Knotenpunkt-Nebenspannungen, das dynamische Verhalten der Strassenbrücken und das Kräftespiel in verschiedenen Bauphasen kontrolliert. Der Diskussionsbeitrag gibt einen Überblick über die Messmethoden und die Ergebnisse.

Leere Seite
Blank page
Page vide

Actual Traffic Loadings on Highway Bridges and Stress Levels in Bridge Members

Charges de trafic actuel sur ponts-routes et niveaux de sollicitations dans les membrures des ponts

Gegenwärtige Verkehrslasten auf Strassenbrücken und Beanspruchungs-Niveau in Brückenelementen

EIICHI MURAKAMI
Director
Honshu-Shikoku Bridge Authority

TETSUO KUNIHIRO
Chief, Bridge Section
Public Works Research Institute
Ministry of Construction

MINORU OHTA
Deputy Chief, Second Design Room
Honshu-Shikoku Bridge Authority

HAJIME ASAKURA
Research Engineer, Bridge Section
Public Works Research Institute
Ministry of Construction

Japan

1. Introduction

The design live load specified in the design specifications for highway bridges in Japan, as shown in Fig. 1 and Fig. 2, is fundamentally based on a 20 ton truck and traffic rows composed of a 20 ton truck and 15 ton trucks. The T-load in Fig. 1 is used for design of slab and floor system, while the L-load shown in Fig. 2 is used for design of main girder and main truss. These loads have been used since 1956, but the increase in both weight and number of trucks in these years is so remarkable that the loads shown in the current specifications have reached the state which may not be necessarily appropriate in contrast with the actual traffic situation. Besides, there exist a great number of old bridges which were designed for smaller load, than that of current specifications, and the safety of those bridges under the present heavy load is posing a problem.

In Japan, various surveys of actual traffic loadings and stress levels in highway bridge members are being carried out for the purpose of obtaining the data in re-examination of design live load, and also for control of safety of existing bridges.

2. Stress levels in bridge members[1)]

Stress levels caused in the main girder of 18 plate girder bridges (with span length of 20 to 60 m) and for each member of a truss bridge (with span length of 80 m) under the ordinary traffic loading were measured.

In measuring, the device enabling to automatically count up the frequency by each stress level separately was used. This device is composed of the strain detector in which differential transformer is used and recording device which classifies the detected strain separately by four class levels, and count up the respective frequency.

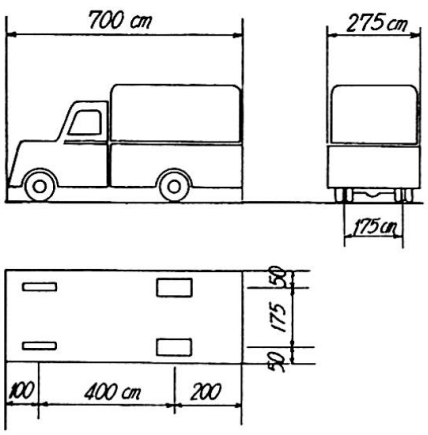

Fig. 1 T - load

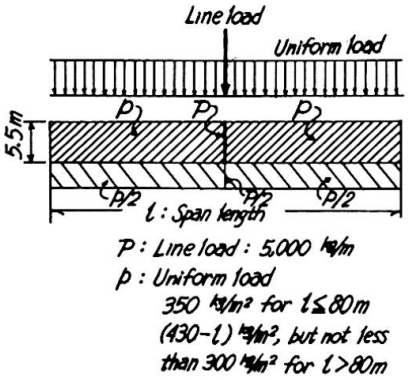

Fig. 2 L - load

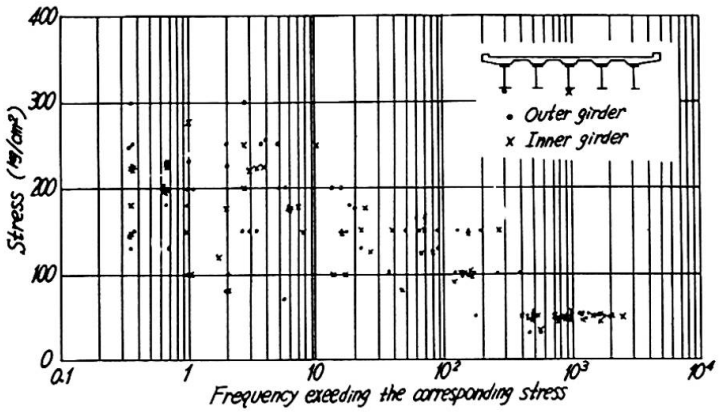

Fig. 3 Stress frequency (Plate girder bridge)

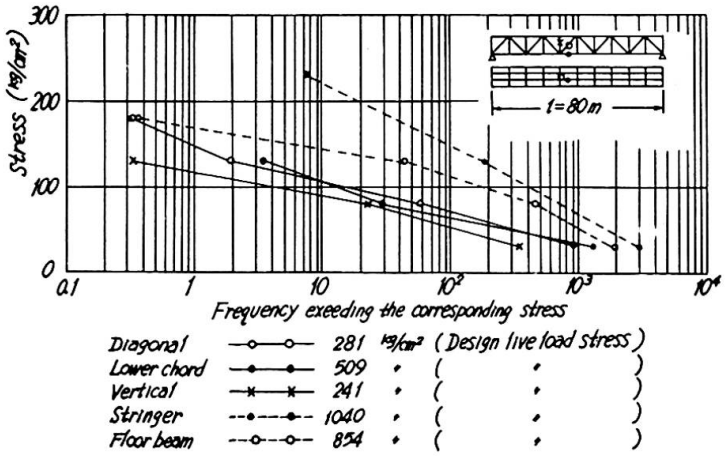

Fig. 4 Stress frequency (Truss bridge)

Type of Vehicles	Passenger Car	Bus	Small Size Truck (Gross Weight of 7.5 ton or less)	Large Size Truck (Gross Weight of 7.6 ton or more)	Total
Ratio (%)	67.9	18.1	1.5	12.5	100

Table 1. Percentage of various vehicles

The bridges for which the survey was made were selected from those which are located on the main national highways served for heavy traffic. The traffic amount per 24 hours at the survey point counts 10,000 to 40,000 vehicles, and the average traffic volume for the entire survey points was about 20,000 vechicles, the percentage of various types of vehicles being as shown in Table 1.

The measurement was curried out for 3 to 5 consecutive days. The result of measurements for plate girder bridges and a truss bridge are indicated in Fig. 3 and Fig. 4, respectively. In those

figures, the frequency at each stress level is shown per one day (24 hours). The relation between the range of the ratio of stress level measured in girder bridges to the calculated stress due to the current design live load (L-load) and the frequency caused per the traffic volume of 10,000 vehicles is shown in Fig. 5.

In the case of truss bridge shown in Fig. 4, the values of measured stress of floor system is greater than those of truss members. However, the ratio of measured stress level to design live load stress for floor system is smaller than that of truss members. This is supposed to be due to the fact the reinforced concrete slab supported by the stringers and floor beams may take charge a portion of the function of stringers or floor beams. Such a function of reinforced concrete slab was not considered in the design calculation.

According to the fact mentioned above, it is known that the live load stress caused in each member of bridge under ordinary traffic load is some 300 kg/cm^2 at most, which is fairly at lower level as compared with the calculated stress level due to design live load.

3. Actual status of wheel load[2)3)]

For the purpose of confirming the actual weight of wheel load of vehicle having great influence on the slab and floor system, measurement of weight of wheel load was carried out at 34 points on national highways in Japan.

The device used for the measurement is composed of weighing part and recording part. The weighing apparatus is the weighing meter consisting of a sheet of steel plate and four loadcells

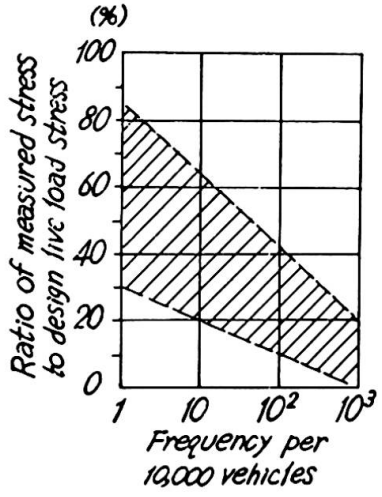

Fig. 5 Ratio of measured stress to design live load stress

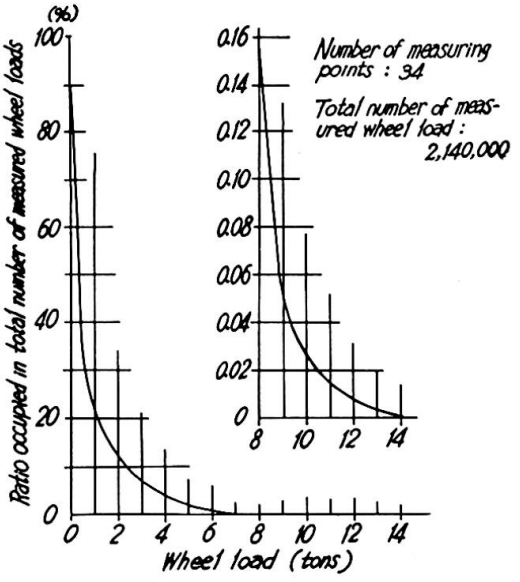

Fig. 6 Cumulative frequency distribution of wheel load

supporting the plate on its four corners. The weighing meter is installed in the reinforced concrete pit in such a way that the loading plate makes a part of the road surface covering the pit, so that the weight of wheel passing over the plate is detected without stopping the vehicles. The recording part has the function of classifying counting automatically each frequency of the detected weight by every 12 classes of level.

The survey points were selected from among the points located on main national highway, and besides, where the traffic is especially crowded. The traffic volume per 24 hours for the lane where the wheel load was measured indicated about 5,000 vehicles at point where the traffic volume was the least, and about 28,000 vehicles where the traffic volume was the most.

The measurement was carried out for 1 to 7 days for each point. It was made clear, as the result of the survey, that the frequency by different level of wheel load showed considerable difference according to the survey point, but on the same point, approximately the same frequency distribution was observed.

Fig. 6 represents the frequency measured by various weight of wheel load. As known from Fig. 6, although about 80% of the whole number of wheel load measured is one ton or less, and the number of heavier wheel load decreases rapidly, the fact that the number of wheel load exceeding design wheel load of 8 ton (which is approximately the same as the wheel load of HS20 of AASHO, see Fig. 1) amounts to 0.16% of whole number of wheel load, namely, that there exist about 32 vehicles of which wheel load exceeds design wheel load of 8 ton, per 10,000 vehicles, may not be ignored from the point of view of design of new bridges or maintenance and safety of the existing bridges. The reason of the existence of wheel loads heavier than design wheel load is due, needless to say, to the operation of large size trucks which are loaded more than the statutory loading limit.

In Japan, the expansion of truck size has been advanced in these years to reduce the cost of transportation. At the same time, the instances of damages of reinforced concrete slab have become remarkable. As one of the causes thereof, the operation of vehicles with weight heavier than design wheel load may be mentioned.

Besides, on account of the fact that the weight and number of wheel loads of trucks increased, the importance of performing fatigue design came to be claimed on steel plate deck where welding is used abundantly. In applying fatigue design, it is necessary to know the value and number of repetition of stress imposed during the expected life of bridge. From the point of view of fatigue, the effect of random wheel loads with different weights and numbers of repetition on steel plate deck may be evaluated by means of "equivalent number of repetition" of design live load stress due to design wheel load (8 ton), denoted by the following expression:

$$N_{eq} = K_1 \cdot K_2 \cdot N_t \qquad (1)$$

Where N_{eq} : Equivalent number of repetition of design live load stress

N_t : Number of total passing wheel loads during the expected life of the bridge

K_1, K_2: Coefficients

K_1 in Equation (1) is the coefficient used for converting the wheel load with certain weight into design wheel load of 8 ton, which may be expressed as Equation (2):

$$K_1 = \sum P(T) \left(\frac{T}{8}\right)^{\frac{1}{k}} \cdot \Delta T \qquad (2)$$

Where T : Weight of wheel load

P(T): Probability of occurrence of T

k : Coefficient determined from S-N diagram (the slope of S-N diagram in logarithmic sclae.)

The position where wheel loads pass in certain traffic lane is not stationary. Fig. 7, illustrated as an example, shows that the distribution of passing positions of wheel loads in a traffic lane may be regarded as a normal distribution with the standard deviation of approximately 35 cm. Fig. 7 was obtained as the result of observation at 20 different points on national highways with two or four lanes, all over Japan. K_2 in Equation (1) is the coefficient to be multiplied with the number of repetition determined on the assumption that the all wheel loads pass on a fixed position, and is given from the following equation:

$$K_2 = \sum \left(\frac{R(x)}{R_o}\right)^{\frac{1}{k}} \cdot P(x) \cdot \Delta(x) \qquad (3)$$

Where Ro : Design live load stress

R(x): Stress of member under the design wheel load passing on certain position, x

P(x): Probability of occurrence of R(x)

The value of K_2 for the longitudinal rib of steel plate deck which is commonly used in Japan, is approximately 0.2.

P(T) in Equation (2) is given by Fig. 6, and P(x) in Equation (3), by Fig. 7. Such data, actually observed concerning the weight and the passing position of wheel load are indispensable for the fatigue design.

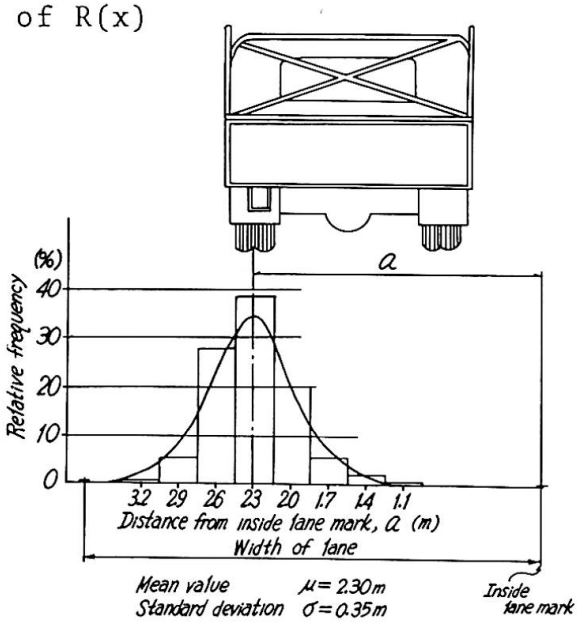

Fig. 7 Distribution of passing position of wheel

4. Actual status of vehicle row load[2),3)]

L-load, shown in Fig. 2, depends upon the vehicle row load such as shown in Fig. 8.

In order to ascertain the magnitude of actual vehicle row

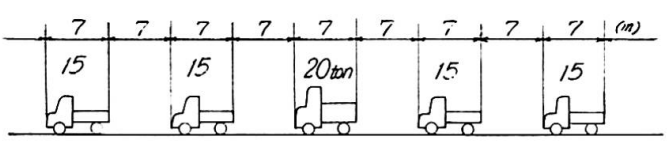

Fig. 8 Basic traffic pattern of L - load

Number of lanes	Number of points
2	25
4	40
6	8
	73

Table 2. Number of traffic pattern survey points

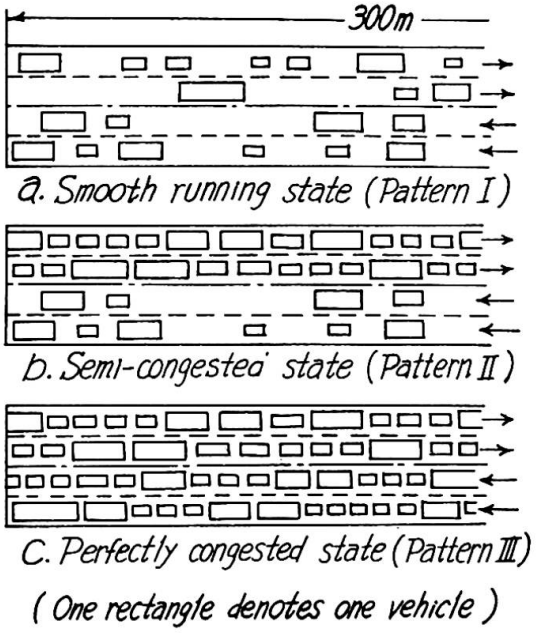

Fig. 9 Traffic patterns

load in comparison with the above design L-load, a survey on traffic pattern was carried out in the following procedure:

1) 73 survey points were selected (Table 2). These points are the places on the main national highways where the traffic is crowded and apt to be congested including a lot of large size vehicles.

2) At each survey point, traffic pattern extending over 300 m on the roadway was photographed intending to take as many heavy trucks as possible in the overlooked picture. Ten times of the photographing was carried out, and selected one case of pictures which appeared to be most congested in traffic, as they were assumed to represent the maximum of vehicle row load at the point.

3) Distinguishing the loading condition of each vehicle with or without cargo, as well as the type of each vehicle from the photograph, the figure of traffic pattern (Pattern I), as illustrated in Fig. 9a, which shows exactly same arrangement of vehicles as on the photograph was prepared. For the weight of different types of vehicles and different loading conditions, corresponding average values were established referring to the table of size and weight of motor vehicles in Japan.

4) On the basis of Pattern I, hypothetic pattern such as Fig. 9b (Pattern II) in which the half of traffic lanes is congested, while the opposite half lanes is smooth, and Fig. 9c (Pattern III) in which the whole lanes are perfectly congested, were prepared. In this case, the clear distance between two consective vehicles in the congested state was taken as 1 m, with reference to the vehicle distance observed on highways actually at the time of congested. Pattern II is the state which is usually observed in Japan, and Pattern III is the state which is very rarely observed.

5) In regard to Pattern I, II and III, the maximum bending moment Mo and maximum shear force So, which are imposed in a simply supported girder under each loading pattern, were calculated by means of electronic computer. In this case, Mo and So were obtained for nine cases of the span length of 20, 40, 60, 80, 100, 150, 200, 250 and 300 meters.

6) M/MD and So/SD were calculated, which are the ratio of Mo and So due to "actual vehicle load" obtained in 5), to beinding moment MD and shear force SD due to "design load" showed in Fig. 2.

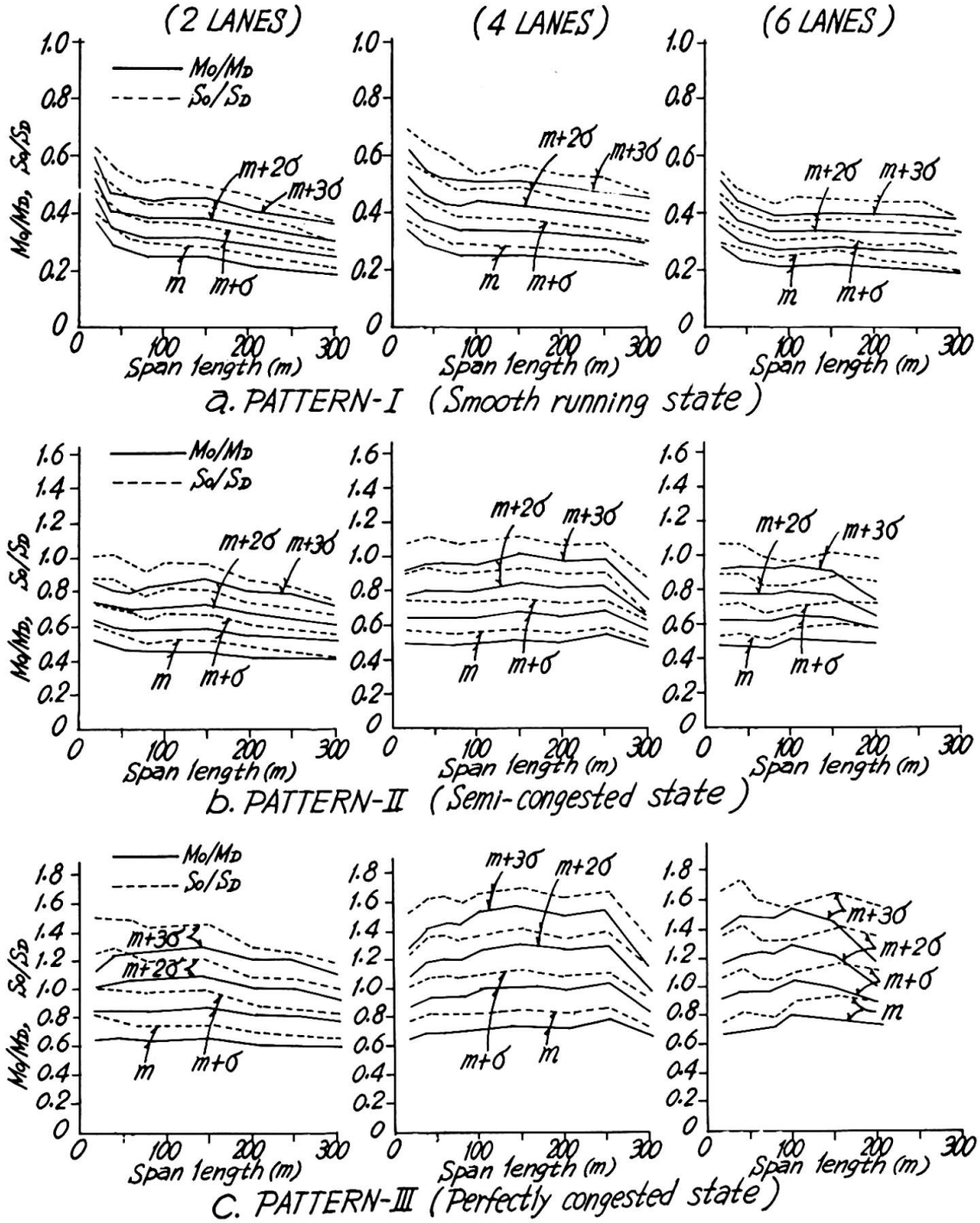

Fig. 10 Ratio of measured value to calculated value due to design load

The values of M_O/M_D and S_O/S_D thus obtained for all of observed points were gathered up for different number of lanes, and a histogram of M_O/M_D and S_O/S_D was drawn. The histogram showed that the form of distribution of M_O/M_D and S_O/S_D may be regarded as the normal distribution. Thereupon, the mean value "m" and the standard deviation "σ" of the values of M_O/M_D and S_O/S_D for different numbers of traffic lane and for different span lengths were calculated, then the relation between different expected magnitudes of the vehicle row load and their frequencies was presumed.

Fig. 10 was obtained in this way, indicating the features of magnitude of actual vehicles load in Japan. From Fig. 10, the following facts may be understood:

1) The magnitude of vehicle row load under normal traffic condition (Pattern I) is considerably low, the average value of the loading effects (moment and shear) in main girder is equal to 30%, at most, of those due to design live load regardless of the number of traffic lane and of span length, and even at the level of $(m+3\sigma)$, it is only 60%, at most, of the loading effects due to design live load.

2) Under the semi-congested state of traffic (Pattern II), that is usally occured in Japan, the average value of the loading effect imposed in main girder ranges from 40 to 60% of that due to design live load, and the level of $(m+3\sigma)$,corresponds approximately to the level of design live load.

3) When vehicles are congested with clear distance of 1 m over the whole lanes (Pattern III), the average value of loading effect imposed in main girder is presumed to be 60 to 80% of that due to design live load, and the level of $(m+\sigma)$ corresponds approximately to the level of design live load.

4) S_O/S_D is usually larger than M_O/M_D. Namely, the current design live load in Japan is not well-balanced between bending moment and shearing force in main girder.

Fig. 11, comparison of loading effects due to design live load of well-known HS 20 Loading of AASHO (1969) and "Brücken Klasse 60" of DIN 1072 (1967) to those due to Japanese design live load, may facilitate understanding the consideration made in this report.

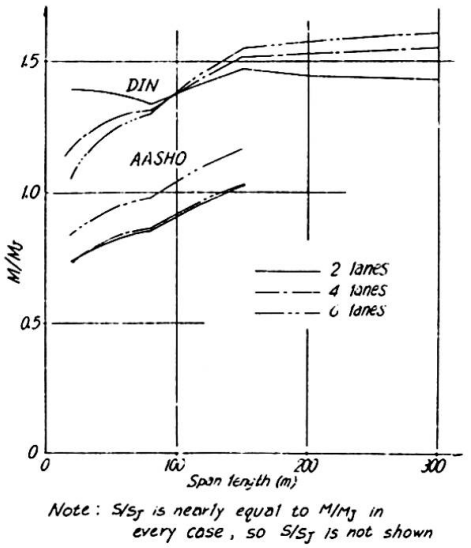

Fig. 11 Comparison of design loading effect in various countries

5. Conclusion

The following conclusion may be introduced concerning the load on highway bridges in Japan, on the basis of the results measured on the stress levels in bridge members, and on the wheel load and vehicle row load:

1) The live load stress imposed in main girder and main truss under usual traffic condition is 300 kg/cm^2 or so at most, which is considerably small as compared with the calculated design live load stress.

2) Vehicle row load under normal traffic condition is in considerably lower level as compared with the current design vehicle row load, but under the state in which the whole lanes are perfectly congested, there is a little chance that the vehicle row load may reach to the level of design load. Considering the fact that semi-congested state of traffic in which the half of traffic lanes are congested while the opposite half lanes are smooth is usually observed wherever in Japan, it seems to be suitable to determine the design load for main girder on the basis of such loading condition.

3) The relation between the weight and frequency of vehicle wheel load shows fairly big divergence according to area, but nearly constant trend on the same point. Generally speaking, the actual condition of wheel load is that it has no such allowance to design load as is seen in the vehicle row load, and the existence of such heavy wheel load exceeding design wheel load is amounting to a number which may not be ignored.

4) Since vehicle wheel load (single vehicle load) is in the severer condition than in the case of vehicle row load in comparison with the current design load, considerable unbalance of load carring capacity between main girder and floor system has been arisen. In order to design a bridge of which each member is well balanced in strength, it will be necessary, so long as the current design load is employed, to use larger safety factor for the floor system than that for main girder.

References

1) Tetsuo Kunihiro, Minoru Ohta: "A Study on Stress Levels on Highway Bridges", Annual Meeting of Civil Engineering, Ministry of Construction, 1968 and 1969. (In Japanese)

2) Tetsuo Kunihiro, Minoru Ohta: "A Study on the Actual Condition of Traffic Load and its Effect on Highway Bridges", Report of Public Works Research Institute, Ministry of Construction, No. 626, Oct. 1970.(In Japanese)

3) Tetsuo Kunihoro, Hajime Asakura and Keiichi Inoue: "Study on Design Live Load", Report of Public Works Research Institute, Ministry of Construction, No. 701, Nov. 1971. (In Japanese)

Summary

As the result of our surveys of wheel load, row load of vehicles and of stress in bridge members, it was made clear that the magnitude of vehicle row load or corresponding stress in main girder has considerable allowance in comparison with the current design live load and corresponding stress, under any traffic loading condition except perfectly congested states, while the single vehicle load sometimes exceeds the design load and poses a problem in relation to the safety of slab and floor system.

Mesure des variations de réactions d'appuis d'ouvrages hyperstatiques en béton précontraint ou mixtes

Messungen von Variationen von Auflagerreaktionen bei statisch unbestimmten, vorgespannten oder Verbundbauwerken

Measuring of Variations of Support Reactions at Undetermined Prestressed or Mixed Structures

S. BRETONNIÈRE M. DIRUY
Laboratoire Central des Ponts et Chaussées
Paris, France

1. INTRODUCTION

L'étude expérimentale du comportement à long terme des ouvrages présente nombre de difficultés, eu égard aux techniques délicates de mesures in situ qu'elle implique. En ce qui concerne les ouvrages hyperstatiques, la mesure permanente des réactions d'appuis constitue un puissant moyen d'étude de la redistribution des contraintes due aux phénomènes à long terme imputables à la nature des matériaux constituants, à leur rhéologie (retrait et fluage du béton, relaxation des câbles de précontrainte) ainsi qu'aux variations climatiques environnantes (hygrométrie, température, ensoleillement).

De telles mesures nécessitent des capteurs devant répondre à des critères très particuliers :

- grande sensibilité, les variations de force à mesurer étant parfois très faibles par rapport à la charge permanente,
- absence totale de dérive, l'évolution des réactions devant pouvoir être suivie à très long terme,
- insensibilité aux sollicitations diverses d'ordre thermique ou mécanique (mouvements relatifs tablier-appui).

Les dynamomètres à déformation élastique présentent une dérive due au fluage du corps d'épreuve qui ne peut être éliminée que par une reprise périodique du zéro du capteur. Cette opération dans le cas des appuis de pont nécessite le déchargement du dynamomètre par un dispositif spécial reprenant les efforts. L'influence des sollicitations perturbatrices, mécaniques ou thermiques, est également difficile à éliminer d'où la mise au point d'un nouveau procédé qui utilise une cellule de charge ayant les qualités requises.

2. PRINCIPE DE LA CELLULE DE CHARGE

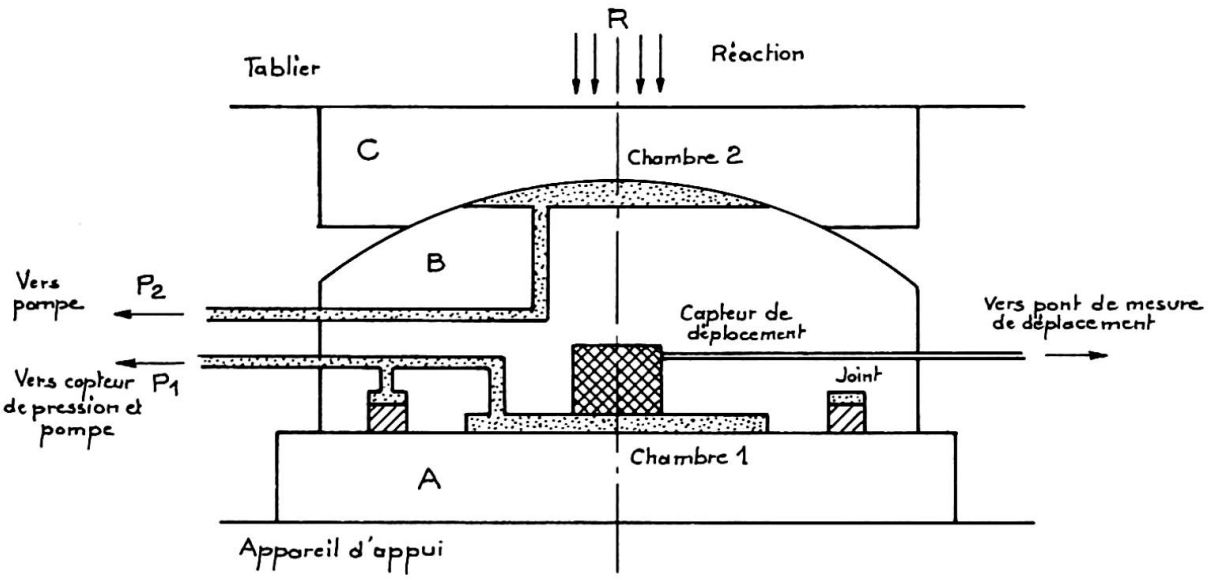

Fig. 1 - Schéma de fonctionnement

La cellule de charge directement interposée entre l'appui de l'ouvrage et le tablier, est constituée par 3 blocs rigides superposés (voir fig. 1 ci-dessus).

Ces blocs sont en contact par des faces planes rectifiées (A et B) ou par des surfaces sphériques (B et C). Deux chambres ménagées dans B peuvent être alimentées indépendamment sous pression d'huile au moyen d'une petite pompe à main.

La pression dans la chambre 1, développe à partir d'une certaine valeur une force qui équilibre la réaction d'appui et entraîne le soulèvement de B. Le déplacement relatif "d" de A et B, mesuré par un capteur incorporé à la cellule, est fonction de la pression hydraulique mesurée par un capteur indépendant de la cellule. Il faut atteindre un écartement de 50 à 60 μ pour éliminer tout contact entre B et C et obtenir, pour des déplacements inférieurs à 120 μ, une variation linéaire de p en fonction de d. La pente (α) de cette droite, traduisant la rigidité de l'ouvrage, est obtenue par des mesures de p de 10 μ en 10 μ. La pression p_o pour d = 0, obtenue par extrapolation, fournit d'après la courbe d'étalonnage la valeur de la réaction d'appui.

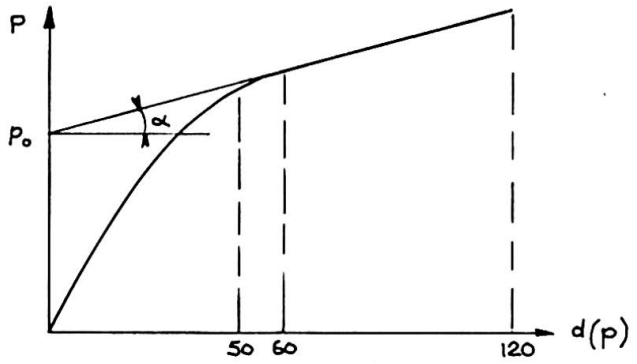

Fig. 2 - p = f (d)

Toutefois le fonctionnement correct du dynamomètre n'est assuré que si la réaction d'appui R est centrée sur la chambre 1 sans aucun moment entre les blocs A et B. Dans ce but, avant toute mesure, la chambre 2 est mise sous pression d'huile pour permettre à l'élément C de rotuler sans frottement sur coussin d'huile.

3. CARACTERISTIQUES METROLOGIQUES

La force maximum mesurable avec une cellule de charge est fonction de la pression admissible dans la chambre et de sa surface.

La pression normale de service est de 250 bars et peut atteindre exceptionnellement 400 bars, ce qui permet de réaliser des cellules pour des forces de plusieurs centaines de tonnes.

Les erreurs de linéarité dues à la cellule de charge proviennent des variations possibles de la surface efficace de la chambre 1 ; le montage particulier du joint d'étanchéité permet de limiter cette erreur à 0,2 % pour des variations de pression comprises entre 2 bars et 400 bars.

La fidélité est très bonne et le pouvoir de résolution inférieur à 5.10^{-4} de la force mesurée. La cellule ne présente aucune hystérésis mesurable (vérifié lors d'étalonnage au 1/1000è près en laboratoire sur des cellules de force 100 KN).

Des variations de température entraînent des modifications de la section efficace de la chambre de l'ordre de 0,1 % pour $\Delta T = 40°C$.

La précision des mesures est étroitement liée aux caractéristiques de la chaîne de mesure de pression qui peut être réétalonnée fréquemment. Pour des domaines de variation de force très étendus pouvant entraîner des variations de pression comprises entre 1 bar et 400 bars, il est nécessaire d'utiliser plusieurs capteurs d'étendues de mesure différentes. Dans le cas des réactions d'appuis les variations excèdent rarement $\pm$ 15 % et la pression nominale du capteur est donnée en conséquence.

Ce procédé peut fournir la valeur des réactions d'appui avec une précision inférieure à $\pm$ 0,2 % à condition de disposer des moyens d'étalonnage en force.

4. UTILISATION PRATIQUE

Pour effectuer les mesures deux opérateurs sont nécessaires, l'un pour imposer la pression d'huile en fonction des déplacements désirés, l'autre pour mesurer cette pression grâce à un capteur à jauges de déformation et un pont de mesure statique de haute précision.

Pour les mesures de réactions d'appui, où chaque extrémité de travée est équipée de deux cellules de charge, on relève successivement les valeurs. Dans ces conditions la pente de la partie linéaire de la courbe $p = f(d)$ est surtout liée à la rigidité de torsion de l'ouvrage, la rigidité de flexion intervenant très peu.

5. APPLICATIONS

5.1 Modèle de pont mixte

Une ossature mixte acier-béton a fait l'objet d'une étude récente comportant notamment une série de mesures à moyen terme (quelques mois) ayant pour but une meilleure connaissance des effets du retrait de la dalle de béton sur le comportement de l'ouvrage. Ce dernier, construit dans le hall d'essais du Laboratoire Central des Ponts & Chaussées comportait 2 travées de 9,5 m (voir schéma fig. 3). Il reposait sur 6 appuis par l'intermédiaire de 6 pesons hydrauliques de capacité 100 KN (10 T) (photo de la fig. 3). Plusieurs sections étaient en outre équipées par divers moyens de mesures : jauges à fil résistant, extensomètres mécaniques et optiques, sondes de température, dispositifs optiques de mesure des flèches. Des dalles témoins constituées du même béton que celui du modèle devaient permettre de mesurer le retrait libre du matériau pris seul. Les mesures ont débuté en même temps que le coulage de la dalle. Les courbes de la fig. 4 résument les mesures de réactions d'appuis effectuées d'abord à intervalle très rapproché (1 h pendant la prise du béton) puis quotidiennement, ceci pendant 3 mois. La température et l'hygrométrie ambiantes furent maintenues sensiblement constantes pendant toute cette période ($t = 21° \pm 2$ $H_r = 60\ \% \pm 10\ \%$). Les pesons étaient disposés de la façon suivante :

pesons 1 et 4 - appui extrémité gauche

pesons 5 et 6 - " " droite

pesons 2 et 3 - " central

On pouvait vérifier le poids du modèle (constant aux pertes d'eau du béton près) en faisant la somme des réactions d'appuis après chaque mesure.

Le calcul des réactions hyperstatiques effectué à partir des mesures extensométriques est en parfaite concordance avec les réactions mesurées à l'aide des pesons hydrauliques. On remarque pendant la prise du béton l'influence des phénomènes thermiques différentiels sur les réactions d'appuis. La perte de poids due au décoffrage apparaît également ainsi que les charges additionnelles qui furent ensuite ajoutées aux extrémités de l'ouvrage pour compenser un délestage trop important de ces appuis dû au retrait, et qui risquait d'annuler les réactions d'extrémité.

Par exploitation conjointe des valeurs des réactions d'appuis et des déformations mesurées, on a pu suivre l'évolution de divers paramètres, notamment celle du coefficient d'équivalence $\left(n = \frac{E_A}{E_B} \right)$ et du retrait libre (ε_r).

A la suite de ces essais il a été procédé à une dénivellation de l'appui central et à l'étude du fluage-relaxation consécutif. L'interprétation des mesures est en cours.

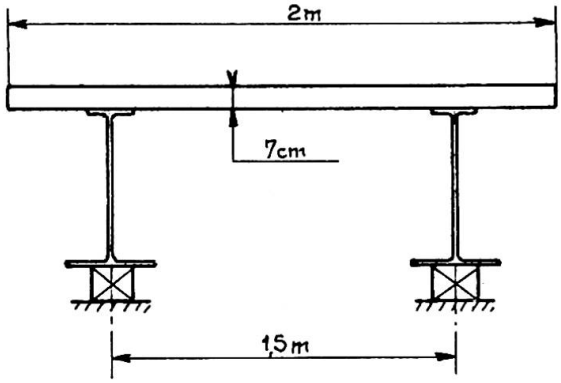

coupe transversale

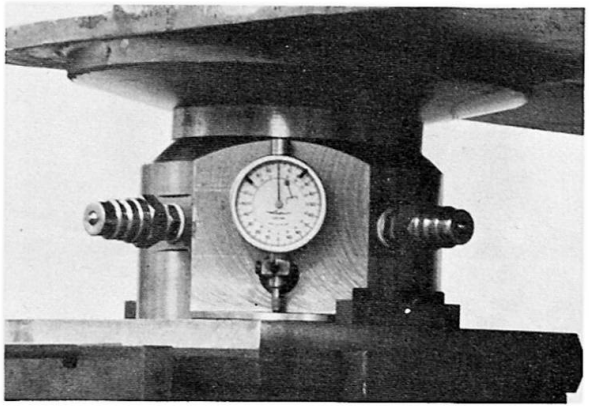

peson de 100 KN

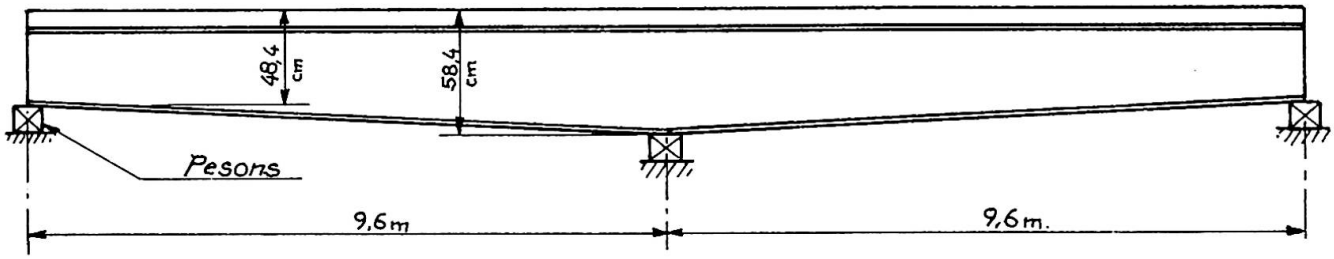

vue longitudinale

Fig. 3 - Essais d'une ossature mixte acier-béton

5.2 Ponts hyperstatiques en béton précontraint

5.2.1 Pont de Champigny-sur-Yonne

Ouvrage à 3 travées continues de 35 - 70 - 35 m de hauteur constante (voir fig. 5). Fin de construction : Avril 1970. Les culées de cet ouvrage ont été équipées chacune par 2 pesons hydrauliques de capacité 1000 KN (100 T), situés entre le tablier et les appuis néoprène-téflon. Les mesures qui ont été entreprises aussitôt après construction et sont poursuivies actuellement ont pour but principal de contribuer à l'étude de la redistribution des contraintes dues aux phénomènes de retrait-fluage-relaxation dans l'ouvrage. Elles sont effectuées une fois par mois environ. Les variations des réactions d'appuis mesurées sont modulées par les variations journalières de la température du béton. Celles-ci sont surtout dues à l'ensoleillement qui provoque un gradient thermique entre les parties supérieure et inférieure du tablier ; ce gradient amène une déformation différentielle des fibres longitudinales des hourdis et des âmes d'où variations de courbure de l'ouvrage et redistribution des réactions entre les piles et les culées. Le calcul des variations de réactions imputables à ce phénomène thermique est possible si l'on connaît la distribution des températures dans une section. On a donc placé convenablement des sondes thermiques qui renseignent à chaque instant sur la température du béton et permettent d'établir des corrections aux mesures de réactions sur culées.

Les courbes de la fig. 5 résument les mesures déjà effectuées. Après correction les courbes présentent une allure assez régulière

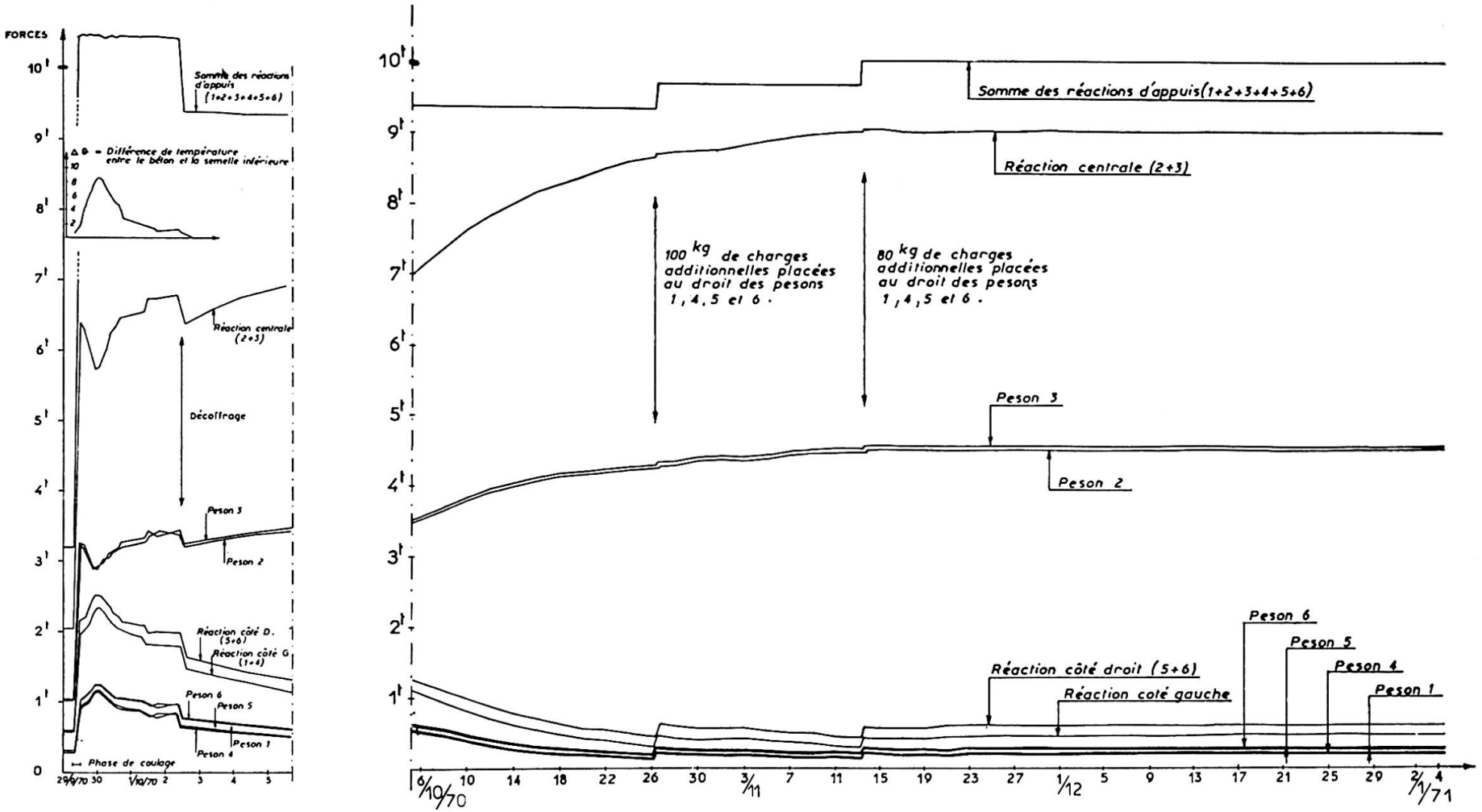

. fig 4. Modele de pont mixte - Etude du retrait

Evolution des reactions d'appuis

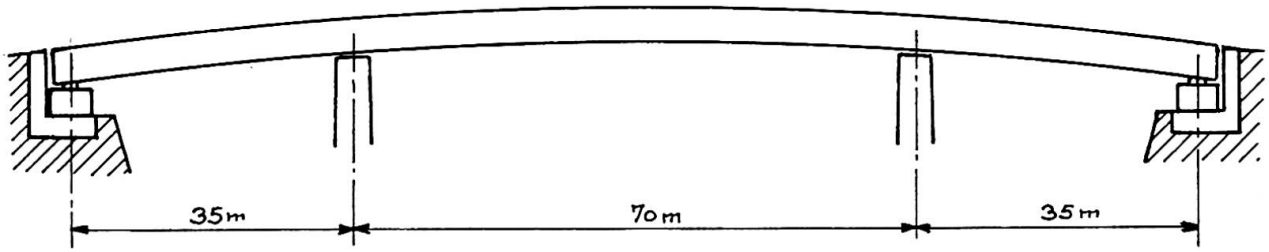

vue longitudinale

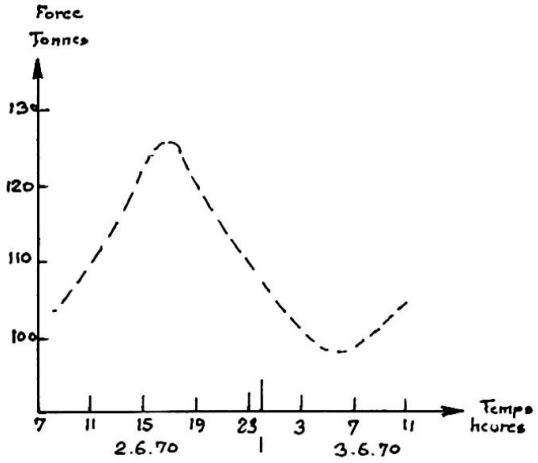

effet de l'ensoleillement

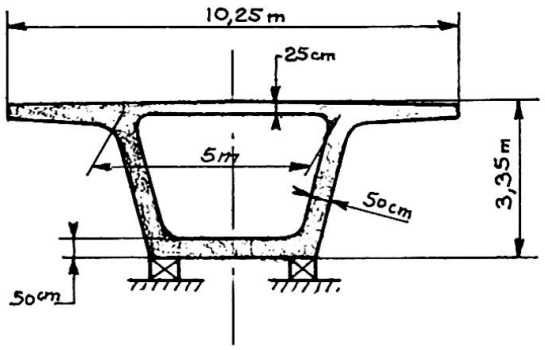

coupe transversale
du tablier

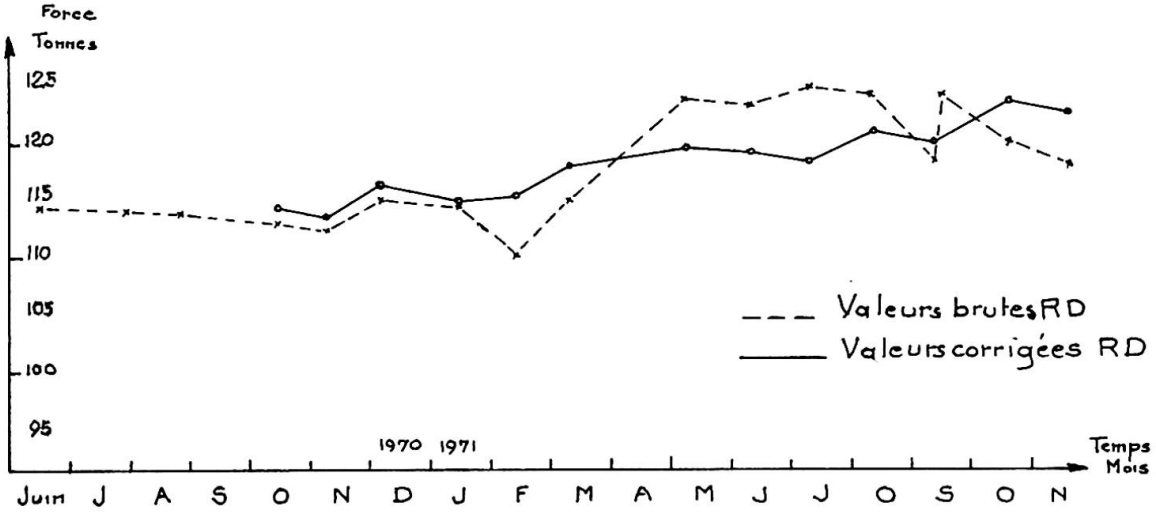

évolution des réactions d'appuis rive droite

Fig. 5 - PONT DE CHAMPIGNY S/YONNE

ascendante (8 tonnes pour 1 an) qui peut être due à l'adaptation de l'ouvrage par fluage relaxation. L'interprétation de ces résultats ne fait que débuter et ne sera sérieusement engagée que lorsque les mesures auront été faites sur un laps de temps suffisant (2 ans environ).

Parallèlement, l'influence de l'ensoleillement sur l'ouvrage a été étudiée par des campagnes de mesures continues s'étendant sur 24 heures au moins. Au cours de l'une de ces campagnes des variations de 24 % de la réaction sur culée ont été constatées (fig. 5). Il s'agit probablement d'un cas extrême pour cet ouvrage mais des variations journalières de 15 ou 20 % sont courantes l'été. De telles constatations incitent assurément à la réflexion car l'ouvrage de Champigny n'est pas exceptionnel par sa situation géographique et nombre d'ouvrages de même type doivent subir des conditions climatiques plus sévères.

5.2.2 Pont de Tourville (sur la Seine)

Une étude analogue à celle concernant le pont de Champigny a été récemment entreprise sur un ouvrage en Béton Précontraint à 3 travées continues de 60 – 90 – 60 m , mais d'inertie variable.

Des pesons hydrauliques sont disposés sur les culées et la réaction par culée est de l'ordre de 2000 KN. Les mesures ont débuté en Mai 1971 et il est trop tôt pour en donner des résultats intéressants.

RESUME

Un dynamomètre hydraulique très sensible, sans dérive, et de haute fiabilité a été mis au point pour les mesures de réactions d'appuis des ouvrages.

Deux types d'applications en ont été faites :

1) Modèle de Pont Mixte étudié en hall d'essais -

   Etude du retrait de la dalle de béton et des effets d'une dénivellation d'appuis.

2) Ouvrages en béton précontraint : Champigny-sur-Yonne et Tourville.
   Etude de la redistribution des réactions d'appuis due à l'adaptation par fluage-relaxation de l'ouvrage.

   Etude de l'influence des gradients thermiques sur la valeur des réactions d'appuis.

Aerodynamic Behaviour of the Cable Stayed Bridge Toyosato Ohhashi

Comportement aérodynamique du pont haubané de Toyosato Ohhashi

Aerodynamisches Verhalten der seilabgespannten Toyosato-Ohhashi-Brücke

I. KONISHI
Prof. Dr.
Department of Civil Engineering
Kyoto University, Japan

S. KOMATSU
Prof. Dr.
Department of Civil Engineering
Osaka University, Japan

H. INOUE
Chief of Bridge Department
Osaka City, Japan

Abstract

This paper describes the aerodynamic behavior of a cable-stayed girder bridge. The wind tunnel experiment was conducted at relatively large Reynolds numbers by using a sectional model, which was 1/20 scale of a prototype.

The results show that the cable-stayed girder bridge with a trapezoidal closed cross section is always stable against a horizontal wind. However, some restricted motions could occur in an inclined wind to a horizontal direction with a comparatively low wind velocity and not so large amplitudes.

To make clear the aerodynamic behavior of the prototype in turbulent flow, the observation of atmospheric turbulences at the site where the prototype was constructed has been continued. By analyzing the structures in the atmospheric turbulence, it was recognized that the restricted motions, which had been observed in the wind tunnel experiment by using a smooth flow, would not occur in the prototype which was subjected to a natural wind fluctuating at random.

1 Introduction

The authers have been concerned about the response of flexible structures to a wind. Such structures as suspension bridges, tall stacks and cable-stayed girder bridges are known to be vulnerable to the effect of a wind. It has been known that a large number of bridges and stacks were damaged or destroyed by winds. Especially, the failure of the Tacoma Narrows Bridge which is a suspension bridge having a main span 853 meters long is known to be a remarkable accident. This bridge was destroyed by twisting vibrations which occurred at a relatively low wind speed of 19 m/s. After this accident, many treaties on aerodynamic behaviors of suspension bridges were presented.

F. Bleich[1] suggested that the aerodynamic instability of suspension bridges showed a flutter as experienced with the wings, and applied to the suspension bridges the general theory previously applied to an aeroplane by Theodorsen and others. Many studies have been done since Bleich presented his report. According to the fact that in most cases suspension bridges have complex cross sectional shapes compared with wings, experimental values can not agree well with the theoretical results.

Recently, G. V. Parkinson[2] has suggested that a galloping oscilation of a

prismatic bar is to be considered as a nonlinear self-exited oscilation. And he stated that this theory well fit the experimental result for bluff cross section like The Tacoma Narrow Bridge.

The above-mentioned studies are mainly concerned with the aerodynamic stability of suspension bridges in a smooth flow. On the contrary, it has been pointed out that the effect of a turbulence of a natural wind must be considered. A. C. Davenport[3] has applied a noise theory to determine the response of a suspension bridge in a turbulent flow.

The aerodynamic behavior of a bridge is different from each other, because it has different cross sectional shape, dimensions and dynamic characteristics. So, none can predict exactly its behavior without carrying out a wind tunnel experiment.

The authers conducted a wind tunnel experiment to investigate the aerodynamic stability of a cable-stayed girder bridge, Toyosato Ohhashi Bridge. (Fig. 1). Catastrophic motions and restricted motions were observed in this experiment. It was concluded that the formers appeared at so high wind velocities and the latters would not occur in a natural wind.

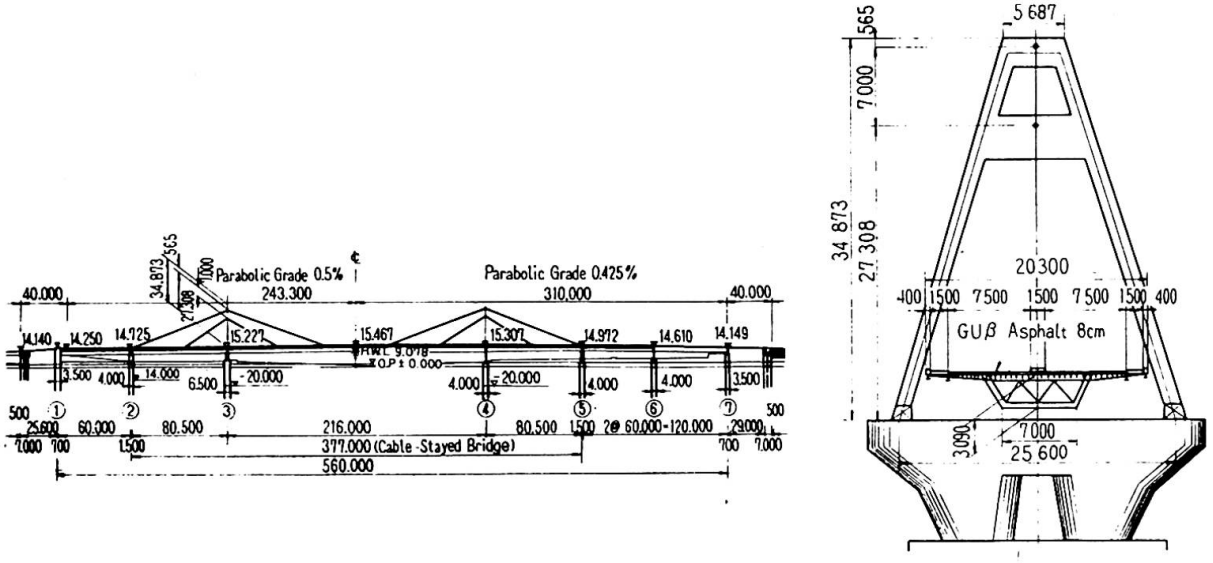

(a) Elevation (b) Section

Fig. 1 General view of Toyosato Ohhashi Bridge

2. Wind Tunnel Experiment

2.1 Model

To perform a wind tunnel experiment, such a sectional model as indicated in Fig. 2 was selected. The model was reduced to 1/20 of the prototype. It consists of two kinds of parts, one is the moving model of 2.5 meters long (4 in Fig. 2). It has a supporting shaft along the center axis of the model (2 in Fig. 2). The other parts are end plates and dummy models of 0.1 meter long (1 and 3 respectively in Fig. 2). The existence of the end plates and dummy models will be useful for eliminating three-dimensional effects of a wind stream.

The model was manufactured minutely so that it might resemble the prototype in detail, and its weight and moment of inatia were 68.8kg and 65.8kg.cm. sec. respectively.

2.2 Test Procedures

The model was supported horizontally in the wind tunnel by using eight coil springs so as to move vertically in the plane of the tunnel cross section and

rotate about the supporting shaft and fixed by piano wires not to move windward. Natural frequency of the vertical vibration of the model was varied by changing a spring constant, and natural frequency of the rotational vibration was varied by changing a distance between the opposite springs. Structural damping of the model was varied by using magnet dumpers, changing an intencity of magnetic forces and a location of the dampers, and damping coefficients of the both of vertical and rotational vibration were controlled freely.

Accelerations and displacements of the vibrating model were measured by accelerometers of wire strain gauge type and linear transformers, respectively. Wind pressures were measured by an alcohl manometer.

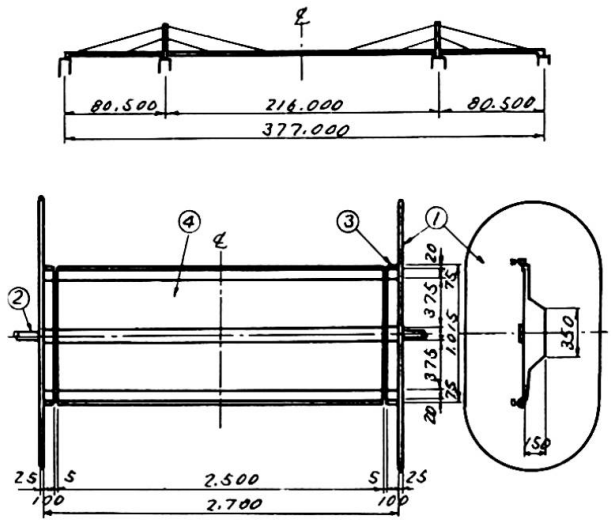

Fig.2 Prototype and its wind tunnel model.

The tests were conducted at Reynold's numbers of $1.0\times10^5/2.0\times10^6$, which were considerably higher than at ordinary dynamic tests.

Static tests were conducted at constant Reynold's numbers of 6.7×10^5 and 1.0×10^6.

The typical examples of the dynamic tests are shown in Table 1.

2.3 Test Results

(a) Static Tests

The drag, lift and moment coefficients of air forces were calculated with measured data. There are no significant differences among each coefficient which is obtained at the different Reynold's number. These coefficients of the air forces are compared with the other types of models, namely a truss type and a wing type as indicated in Fig. 3.

(b) Dynamic Tests

i) Catastrophic Vibrations

When an angle of attack for the model is zero degree, no catastrophic vibration can be observed in all the range of wind velocity, corresponding test numbers are A-1, 2, 3 in Table 1. When the angle of attack exists, catastrophic vibrations occur at relatively low wind velocities, corresponding test numbers are B-1, 2 and C-1, 2, 3, 4 in Table 1.

ii) Restricted Vibrations

When the model has a positive angle of attack, vibrations are observed at lower wind velocities than the velocity at which the catastrophic vibrations occur. These vibrations disappear when the wind velocity increases to some more high values. These phenomena are so cal-

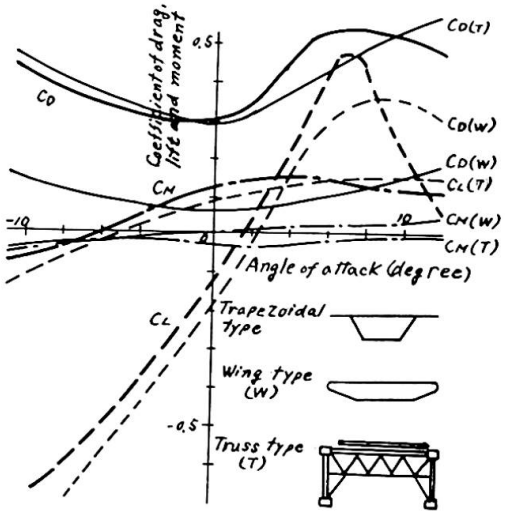

Fig.3 Coefficients of air forces compared with the other types of bridge sections.

led "restricted vibrations". Amplitude response curves of these phenomena are shown in Fig. 4 (a) and Fig. 4 (b).

Table 1. Summary of tests and results

Test number	α deg.	N_z c/s	N_θ c/s	Vc m/s	V_z m/s	T_z sec	V_θ m/s	T_θ sec	S_z	S_θ
A - 1	0	4.28	5.25	119	-	-	-	-	-	-
A - 2	0	3.08	3.82	108	-	-	-	-	-	-
A - 3	0	3.11	3.27	200	-	-	-	-	-	-
B - 1	3	4.25	5.25	67	4.3	480	24	100	0.18	0.17
B - 2	3	5.00	5.22	52	4.1	480	17	105	0.18	0.17
C - 1	5	1.30	2.66	72	4.6	169	30	55	0.11	0.15
C - 2	5	3.07	3.83	59	4.0	250	31	-	0.11	0.14
C - 3	5	3.08	3.16	46	4.1	244	38	51	0.11	0.15
C - 4	5	3.10	2.57	86	4.8	185	31	-	0.11	0.19

Note: N_z, N_θ : Frequency of model.
Vc : Critical Velocity for catastrophic vibration.
V_z, V_θ : Wind Velocity at which restricted vibration occur.
T_z, T_θ : Time during which amplitude of restricted vibration is growing.
S_z, S_θ : Strouhal number of model.
Suffixes z and θ indicate vertical and rotational vibrations respectively.

It is well known that in case of the catastrophic vibration, the amplitudes grow rapidly in a short time to catastrophic magnitude from a rest position. On the contrary, the restricted vibrations observed in these tests were mild. It took a very long time to attain to stationary amplitudes.

The vertical or rotational vibration appeared independently with proper natural frequency. In some cases the both vibrations were observed at the same time, each frequency of the both vibrations were near its natural frequency and not combined together.

The damping coefficients of the model were changed and the corresponding response curves are shown in Fig.4 (a). The amplitudes decrease as the damping coefficients increase, but no strong relation between the amplitudes and the damping coefficient can be found in these tests.

The wind velocity at which the restricted vibration attains its maximum stationary amplitude is different in each test which has a different natural frequency and angle of attack. If the Strouhal numbers of the vibrating model are defined as follows: S=Nh/V, where N is vertical or rotational natural frequency

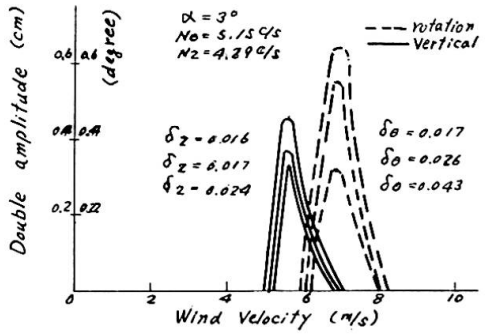

Fig.4 (a) Amplitude response curves

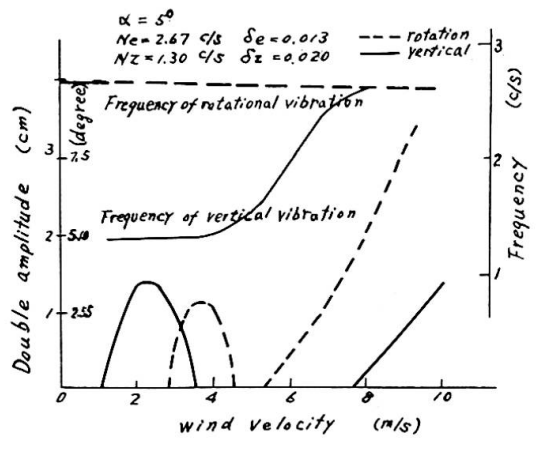

Fig.4 (b) Amplitude response curves

of the model, h shows horizontal projection of a height of the model and V is wind velocity at which the amplitude response attains the muximum value. In cases of angle of attack $\alpha = 5^{\circ}$, corresponding test numbers are C-1, 2, 3, in Table 1, the Strouhal numbers are S ≒ 0.17 for the rotational vibrations and S ≒ 0.11 for the vertical vibrations respectively. In cases of angle of attack $\alpha = 3^{\circ}$, corresponding test numbers are B-1, 2 in Table 1, the Strouhal numbers are S ≒ 0.17 for the both of the vertical and rotational vibrations.

K. Klöppel[4] and T. Yamaguchi[5] measured the Strouhal numbers of the models whose cross sectional shapes were similar to the model handled in this paper. They showed that the Strouhal numbers of the models were about S = 0.12. Their models were simply designed and made of wooden plates, on the contrary the model herein was closely resembled to a prototype having handrails, wheel guards, etc. According to the cross sectional shape of the models, the frequencies of wake voltices discharged from the models seem to be different from each other sensitively. Those of the model herein were slightly higher than those of their models, and the Strouhal numbers of the model herein were slightly enlarged.

3. Safety of Prototype

3.1 Critical Velocities for Catastrophic Vibrations

From the previous section the critical velocities at which the model caused catastrophic vibration were obtained. The models were arranged to satisfy the aerodynamic similarity, so the critical velocities of the model prototype could be calculated from those of the model. The critical velocities of the prototype are shown in Table 1. In cases of angle of attack $\alpha = 0^{\circ}$, the critical velocities are very high. If a safety factor for the critical velocity of a catastrophic vibration is assumed as f = 1.2*), the allowable maximum wind velocity is estimated from the critical velocity in Table 1 to be $Va = Vc/f = Vc/1.2$. In cases of angles of attack $\alpha = 3^{\circ}$ and $\alpha = 5^{\circ}$, the critical velocities are relatively low compared with a stormy wind velocity.

It will be necessary to examine if such critical velocities are dangerous for the prototype or not. It is useful to apply the relation[6] between angle of attack and velocity of a natural wind observed at the Severn Bridge in England and the Akashi Narrows Bridge in Japan to examin the above question. (Fig.5). According to the results of the above observations, the maximum wind velocity drops as the angle of attack increases, the maximum wind velocities are found to be 27 m/s and 10 m/s for the angles of attack of the wind $\alpha = 3^{\circ}$ and 5° respectively, where the velocities are the average values during 30 seconds.

The prototype has been constructed at an open field, so that the above-mentioned fact is applicable to this case. Namely, the prototype does not cause a catastrophic vibration corresponding to the model which has a positive angle of attack.

*) This value is specified at "Standard Specification for the design of the Honshu-Shikoku Renrakukyo (Long Span Suspension Bridge) against wind" 1967 (in Japanese).

3,2 Safety against restricted vibration

It has been studied that a restricted vibration appears at a very low wind velocity, for example a vertical vibration occurs at the wind velocity V = 4m/s if a natural wind flows having a positive angle of attack $\alpha = 5^{\circ}$.

The amplitudes of restricted vibrations of the prototype were predicted from the experimental data, using the theory by F. B. Farquarson[7]. The theory is based on the following assumption that the aerodynamic damping in the wind of a given velocity can be expressed by a power series equation of amplitude. The amplitudes of the prototype predicted with the above theory are shown in

Table 2. In this calculation a vibration mode of the prototype was assumed to be of the first mode. In cases of vertical vibrations the amplitudes of the maximum fiber stresses are not so large, and in cases of rotational vibrations the amplitudes of the maximum shearing stresses are relatively large, however the corresponding wind velocities at which the amplitudes attain the maximum values are higher than those of the vertical vibrations.

Table 2. Maximum amplitudes and stresses of prototype due to restricted vibrations and corresponding wind velocities.

Test number	α deg	Vertical Vibration			Rotational Vibration		
		η max cm	σ max kg/cm^2	V m/s	θ max deg	τ max kg/cm^2	V m/s
B - 1	3	2.6	32	4.2	0.36	359	30
B - 2	3	5.1	62	4.6	0.28	244	30
C - 1	5	14.5	177	7.6	0.80	700	34
C - 2	5	13.9	170	8.3	-	-	40
C - 3	5	11.0	134	8.1	0.38	311	37
C - 4	5	11.6	141	8.5	0.52	455	30

As indicated above, the vertical restricted vibrations occur at very low wind velocities when the wind has an angle of attack. It is doubtful if the prototype actually vibrates in a natural wind as indicated in the next section, because the natural wind flows horisontally in average for time and space at an open field, and has an angle of attack fluctuating positively and negatively at random with a relatively high frequency. On the other hand, the restricted vibrations grow very slowly, it takes more than 100 seconds long to attain the maximum stationary amplitude from the rest position in the cases of the vertical vibrations.

4. Aerodynamic Behavior of Prototype in Turbulent Flow

To see whether the above assumption is true or not, the observations of natural wind have been made at the point where the prototype was constructed, and at the same time the behavior of the bridge due to wind has been observed.

No restricted vibration has been able to be observed so far. Vertical components of the wind were analyzed with the observed data. One of these is shown in Fig.6, in which the full lines show the theoretical values calculated from the power spectrum of vertical component of a wind proposed by H. A. Panofsky and R. A. McCormic[8]. This figure shows the maximum angle of attack of a wind as a function of time during which an angle of attack is averaged. In this case the mean wind velocity is about 10 m/s. The angle of attack of a wind decreases as the time increases.

It can be concluded that a wind does not continue to flow in the constant direction at negative or positive angle of attack for a long time,

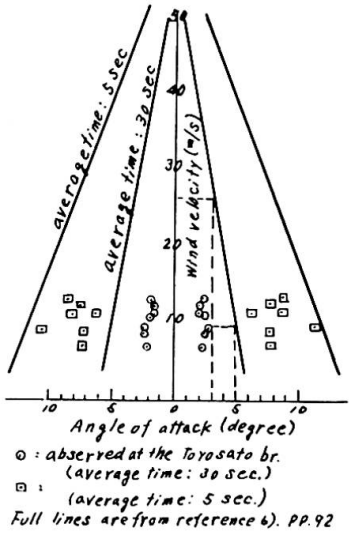

Fig.5. Wind velocity and angle of attack.

and such a wind can not develop a restricted vibration at all. That is to say, it is recognized that there is no natural wind which enables the prototype to cause the restricted vibration which was observed in the wind tunnel experiment.

5. Conclusions

The following results could be obtained from the wind tunnel experiment concerning to the cable-stayed girder bridge.

(1) When no angle of attack of a wind exists, this type of bridge is considerably stable in terms of an aerodynamic stability.

(2) When a positive angle of attack of stationary wind exists the model gives rise to the restricted vibrations at very low wind velocities.

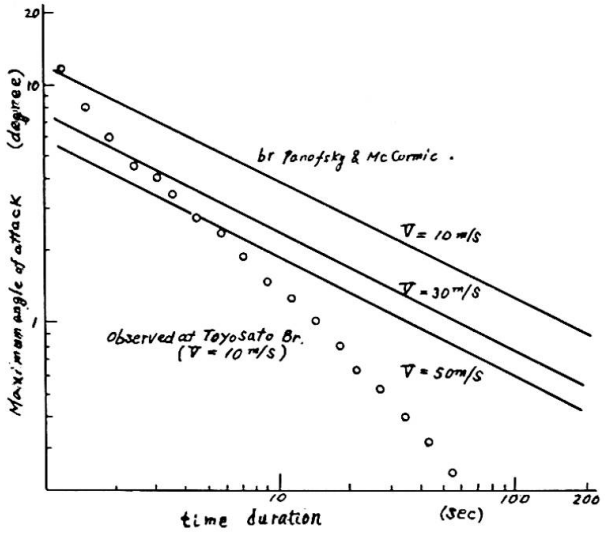

Fig.6 Maximum angle of attack of natural wind.

(3) Both vertical and rotational amplitudes of the restricted vibrations of the prototype in the stationary wind were predicted. As a result, it was found that these amplitudes would not grow to a significant quantity.

(4) It takes more than 100 seconds for the vibration to attain a maximum stationary amplitude from its rest position in case of vertical vibration of the prototype.

(5) From the field measurements, it was found that a natural wind could not cause the restricted vibrations. Besides, no vibration of the prototype has been observed up to now.

Acknowledgment

Particular thanks are due to Mr. A. Matsukawa and H. Kobayashi who cooperated with us throughout this study.

References

(1) F. Bleich, Trans. ASCE, Vol. 114, No.2385 (1949).
(2) G. V. Perkinson and N. P. H. Brooks, Trans. ASME, Vol. 83 (1961) pp. 252--258.
(3) A. G. Davenport, Proc. ICE, Vol.19 (1961) pp.449--472.
(4) K. Klöppel and F. Thiele, Der Stahlbau, H-12 (1967) pp.353--365.
(5) T. Yamaguchi, et al, Mitsubishi Heavy Industries Tech. Review, Vol. 7, No.7 (1970), (in Japanese).
(6) K. Aoki, et al, "Supplementary Note to First Rep. of Tech. Investigation on the Honshu-Shikoku Br." JSCE, Tokyo, Japan (1964), (in Japanese) pp.91--92.
(7) F. B. Farquarson, et al, Bull. Univ. Washington, Eng. Station, No.116, Part V (1949--1954) pp.13--31.
(8) H. A. Panofsky and R. A. McCormic, Inst. Aero. Sci., Rep. Vol. 59, No.6 (1959).

Summary

Zu make clear the aerodynamic characteristics of a cable-stayed bridge (Toyosato Ohhashi Bridge) with trapezoidal cross section, the wind tunnel investigation has been carried out using two-dimensional model with linear scale of 1:20 in comparatively high Reynold's number.

The investigation has shown that the aerodynamic instability will not be induced in high wind which may be experienced at the site of actual bridge.

The small stationary amplitude vibrations, so-called restricted vibrations, grew up slowly in smooth airflow inclined upwards 5 degrees to horizontal. However, it is recognized from studying the three-dimensional effect of actual bridge that the restricted vibration may not be considered to occur in turbulent airflow such as natural wind which has been measured at the site.

VI b

Essais sur modèle en vue du dimensionnement

Modellversuche im Hinblick auf die Bemessung

Model Study for Design

Leere Seite
Blank page
Page vide

Hybridstatik – Computerberechnung von elastischen Tragwerken aufgrund experimentell gewonnener Einflussfunktionen

Hybrid Structural Analysis – Computer Aided Investigation of Elastic Structures Based on Experimentally Generated Influence Functions

Analyse hybride de structures – Calcul électronique des structures élastiques basé sur des fonctions d'influence obtenues par l'essai

W. SALATHÉ
Laboratorium H. Hossdorf
Basel, Schweiz

Das hier kurz skizzierte neue Verfahren zur Berechnung des Verhaltens komplexer Tragwerke im linear-elastischen Bereich stellt eine optimale Symbiose zwischen experimentellen Verfahren der ehemaligen Modellstatik und dem digitalen Computer dar. Daher die Bezeichnung "Hybridstatik". Die Verflechtung zwischen der nach wie vor aus dem Modell gewonnenen analogen Information mit der durch den Computer zusätzlich errechneten ist so eng, dass der Aussenstehende die Herkunft der Ergebnisse kaum mehr feststellen kann.

Der Computer wird sowohl als numerische Rechenmaschine als auch als Prozessrechner eingesetzt. Ihm werden die folgenden Aufgaben übertragen:

1. Er steuert den Versuchs- und Messablauf,

2. reinigt die Messdaten mit statistischen Methoden und rechnet die Werte aufgrund der Aehnlichkeitsgesetze in entsprechende statische Grössen am Tragwerk selbst um,

3. und führt mit Hilfe der so gewonnenen Information die statischen Berechnungen durch.

Vergleich Modellstatik - Hybridstatik

Die Formulierung des statischen Problems setzt sich immer aus den drei folgenden Schritten zusammen:

1. Wahl der geometrischen Form des Tragwerkes
2. Wahl der Lagerungsbedingungen
3. Wahl der anzuwendenden Lastfälle

In der reinen Modellstatik werden die geometrische Form des Modelles und seine Lagerungsbedingungen jeweils durch einen individuellen Versuchsablauf erfüllt. Die Ergebnisse für die einzelnen Lastfälle werden normalerweise durch mechanisches Aufbringen von spezifischen Lastanordnungen erzeugt. Diese Umstände lassen die Modellstatik als ein sehr schwerfälliges Werkzeug erscheinen, welches deshalb nur in Ausnahmefällen verwendet wird.

In der Hybridstatik wird nach wie vor ein Modell hergestellt. Es soll uns ja Auskunft über das elastische Verhalten des nicht exakt berechenbaren Körpers liefern. Die Verwendung eines Computers zur Steuerung des Versuchsablaufes und zur direkten Registrierung der Messdaten ermöglicht jedoch, das Modell in Verbindung mit einer hierfür entwickelten Versuchstechnik programmgesteuert beliebig zu belasten und Informationen allgemeinster Art über dessen Tragverhalten zu gewinnen. Für viele Modellpunkte werden Steifigkeits-, Flexibilitäts- und Einflusswerte gemessen. Man kann sich das Modell als grosses Finites Element mit sehr vielen Knoten vorstellen, welches überall belastet werden kann, wobei aber die Spannungsfunktion von Natur aus exakt erfüllt ist. Sind zusammengehörige Gruppen von Einflusswerten in genügend dichter Anordnung bekannt, so lassen sie sich numerisch als Funktionen (Einflusslinien, Einflussflächen) behandeln. Diese ortsabhängigen Beziehungen enthalten alle Verhaltensweisen des elastischen Körpers und damit sämtliche durch lineare Kombination errechenbaren Lösungen des gestellten Problems. Die verschiedenen, später zu berechnenden Lastfälle sind daher vollständig vom Modellversuch entkoppelt und die Versuchsauswertung wird weitgehend unabhängig von den bei der Messung

vorliegenden Lagerungsbedingungen. Durch diese Eigenschaften verliert die Hybridstatik die Schwerfälligkeit der reinen Modellstatik und wird zu einem Werkzeug für den entwerfenden Ingenieur, welches er mit ähnlicher Leichtigkeit für die Lösung täglicher Probleme einsetzen kann, wie die uns geläufigen Computerprogramme.

Versuchs- und Messtechnik

Die oben angedeuteten analytischen Operationen, welche mit der grossen Menge von Messwerten später durchgeführt werden sollen, setzen numerische Genauigkeiten der Grundwerte voraus, welche weit über die Forderungen der klassischen Modellstatik hinaus gehen. An die mechanische und elektrische Versuchstechnik werden daher ungewöhnlich hohe Ansprüche hinsichtlich Präzision und auch Geschwindigkeit gestellt.

Das Modell wird auf einem massiven Aufspannboden auf modularen mechanischen Elementen aufgebaut. Diese Elemente erfüllen klare, eindeutige Lagerungsbedingungen; ihre Modularität ermöglicht, alle denkbaren Auflagerbedingungen mühelos herzustellen. Alle Komponenten von räumlichen Kräften oder Verschiebungen, Aktionen genannt, werden durch programmgesteuerte Geräte auf das Modell aufgebracht. So wird das Modell beispielsweise in vertikaler Richtung durch ein über dem Aufspannboden montiertes, koordinatengesteuertes Gerät punktförmig belastet. Jedes Auflager wird abgesenkt, oder, im Falle eines Lagers mit komplexeren Auflagerbedingungen, werden die entsprechenden Verschiebungen als Aktionen ausgeführt. Solche Aktionen werden mit pneumatischen Zylindern programmgesteuert erzeugt.

Die jeder Aktion zugeordneten Reaktionen, Verschiebungen oder Dehnungen, als Effekte bezeichnet, werden mittels moderner elektronischer Messtechnik erfasst. In der Regel dienen Dehnungsmessstreifen zur Umwandlung der mechanischen Grössen in elektrische Spannungen. Während des Messablaufes registriert der Computer mit Hilfe eines Messstellenumschalters und eines hochauflösenden, integrie-

renden Digitalvoltmeters diese Spannungen. Die Abfragegeschwindigkeit beträgt dabei ca. 20 Kanäle pro Sekunde.

An allen Lagerstellen wird die Information gemessen, welche die spätere rechnerische Aenderung der Lagerbedingungen ermöglicht. Die Steifigkeit des Modelles am Ort eines vertikalen Auflagers, beispielsweise, wird durch die Messung der Auflagerkraft einerseits und der Auswirkung einer erzwungenen vertikalen Lagerverschiebung andrerseits ermittelt.

Da alle Lagerelemente mit Kraftmesszellen ausgerüstet sind, schwimmt das Modell auf lauter bekannten Kräften. Dies lässt eine einfache Kontrolle des Kräfte- und Momentengleichgewichtes zu. Daraus ergibt sich auch eine Möglichkeit, über die Fehler der Messungen etwas auszusagen; sie betragen zur Zeit ca. 1%.

Form der Daten

Für jede aufgebrachte Aktion werden jeweils die Werte der selben Messstellen abgefragt. Die Gesamtheit aller so aus dem Experiment gewonnenen Daten kann offenbar als Matrix dargestellt werden, wobei die Matrixspalten sämtliche gemessenen Effekte für eine Aktion und die Zeilen den gleichen Effekt für alle Aktionen (Einflusswerte) enthalten. Diese Matrix hält alle Eigenschaften des untersuchten Tragwerkes fest.

Sämtliche Lagerkräfte infolge jeder Aktion sind bekannt. Mit Hilfe eines Ausgleichsprogrammes, das die Methode der kleinsten Quadrate benützt, wird für diese, mit Messfehlern behafteten Kräfte, Gleichgewicht erzeugt. Ein bei diesem Vorgang hergestelltes Protokoll informiert den Benützer über die beim Hybridversuch vorhandenen Messfehler. Unter Berücksichtigung der Aehnlichkeitsgesetze wird aus den Modelldaten die Informationsmatrix für den Tragwerksprototyp erzeugt und auf Magnetband gespeichert. Diese Werte dienen als Grundlage für die statische Berechnung des Tragwerkes im Computer. Das physikalische Modell hat damit seinen Zweck erfüllt.

Statikprogramm

Für den Benützer erscheint das Statikprogramm als ein leicht handzuhabendes, flexibles Computerprogramm zur Berechnung des Tragwerkes, für das der experimentelle Versuch durchgeführt wurde.

Das Programm hat die Fähigkeit, die gewünschten Aufgaben in die korrekten linearen Operationen, die auf die Informationsmatrix angewandt werden müssen, umzuwandeln und sie durchzuführen. Dank der vorliegenden Daten lässt sich jedes statische Problem erster Ordnung auf diese Aufgabe reduzieren; deshalb kommt das Programm ohne jegliche Integration von infinitesimalen Elastizitätsbeziehungen aus.

Beispielsweise lässt sich jede Lastgruppe an beliebigen Stellen des Tragwerkes als Summe von geeignet gewichteten Punktlasten an den Orten, wo eine senkrechte Einheitslast am Modell als Aktion angebracht wurde, darstellen.

Da, wie einleitend erwähnt, linear-elastische Tragwerke betrachtet werden, gilt das Superpositionsgesetz. In Matrizenform geschrieben, kann das Ergebnis infolge eines Lastfalles als Produkt aus der Informationsmatrix und der als Vektor geschriebenen Lastgruppe verstanden werden.

Die üblichen Möglichkeiten, die das Statikprogramm bietet, können in drei Gruppen eingeteilt werden:

1. Erweiterung der Informationsmatrix

   Die Informationsmatrix kann durch Einflussfunktionen von zusätzlichen Effekten, wie Schnittkräften an beliebigen Stellen von stabartigen Tragwerken, erweitert werden. Ebenso können Spannungen in gewünschten Richtungen oder Verschiebungs- und Verdrehungseffekte erzeugt werden, soweit sie sich aus der ursprünglichen Matrix errechnen lassen.

2. Modifikation des statischen Systems

Das ursprüngliche beim Modellaufbau verwendete statische System kann auf drei verschiedene Arten modifiziert werden:

a) Die Einflussmatrizen für einen Teils des betrachteten Tragwerkes können erzeugt werden. Dazu wird die ursprüngliche Informationsmatrix so transformiert, dass die Schnittkräfte an den Schnittflächen des Teiltragwerkes identisch verschwinden. Bauzustände lassen sich damit einfach behandeln.

b) Tragwerksteile können zu einer monolithischen Gesamtstruktur verbunden werden. Auf die Konsequenzen dieser Möglichkeit wird später eingegangen.

c) Die Lagerungsbedingungen lassen sich weitgehend verändern. So können Auflager neu eingeführt, entfernt, verschoben oder elastisch gemacht werden. Bei räumlichen Lagern kann auch der Einspanngrad gewählt werden.

3. Berechnung der Lastfälle

Die geläufigen Lastfälle können in problemorientierter Sprache mit Leichtigkeit behandelt werden. So lassen sich Ergebnisse für Einzel-, Linien- und Flächenlasten, von erzwungenen Verschiebungen und von gleichmässigen und ungleichmässigen Temperatureinflüssen berechnen. Für Flächenlasten und längs frei wählbarer Linien sich bewegender Lastenzüge können zusätzlich Grenzwerte abgefragt werden. Bei der Vorspannung räumlich gekrümmter Kabel wird die Reibung und das Spannprogramm berücksichtigt. Schliesslich können alle so gerechneten Lastfälle, mit Proportionalitätskonstanten versehen, zu neuen Ergebnissen kombiniert werden.

Die Berechnung der Wirkung von vorgespannten auch räumlich gekrümmten Kabeln wird dank der zur Verfügung stehenden Daten äusserst einfach. Der Einfluss der Vorspannung wird auf Umlenk- und Reibungskräfte, die einzig von der Kabelgeometrie abhängig sind, und auf einen Normalspannungsanteil reduziert. Diese rein rechnerisch bestimmten Kräfte werden dann wie alle übrigen Lastfälle behandelt;

deshalb kann die Kabelgeometrie beliebig vorgegeben werden.

Alle Matrizen von modifizierten Strukturen und Ergebnisse der Lastfälle werden auf Magnetband gespeichert. Deshalb können mit geringem Aufwand jederzeit zusätzliche Lastfälle untersucht werden.

Wie aus dem bisher gesagten hervorgeht, bestehen die Elemente der Informationsmatrix aus statisch sinnvollen Zahlenwerten, welche sich ausschliesslich auf das zu untersuchende Tragwerk beziehen und von der ursprünglichen Quelle, dem Modell, völlig unabhängig geworden sind. Sie haben genau die Form und Werte, welche aus einer rein numerischen Berechnung des elastischen Körpers hervorgegangen wären, falls diese möglich gewesen wäre.

Diese Tatsache eröffnet der Hybridstatik eine weitere Möglichkeit, welche der Modellstatik bisher verschlossen blieb. Die Fähigkeit des Programmsystems, verschiedene Teiltragwerke an Nahtstellen, wo die Steifigkeitswerte bekannt sind, analytisch zu monolithischen Gesamtstrukturen zusammenzufügen, ermöglicht es nicht nur, modellstatisch untersuchte Tragwerksteile untereinander zu verbinden, sondern auch experimentell untersuchte Teiltragwerke mit rein analytisch berechneten Konstruktionen zu vereinigen. Damit ist ein weiterer Schritt zur "Entmaterialisierung" der Modellstatik unter Wahrung ihrer Vorzüge getan. Ein Modell wird nur für Tragwerksteile hergestellt, welche sich analytisch nicht befriedigend erfassen lassen. Deren Tragverhalten wird dann im Computer als Element mit bekannten statischen Eigenschaften in die Gesamtstruktur integriert.

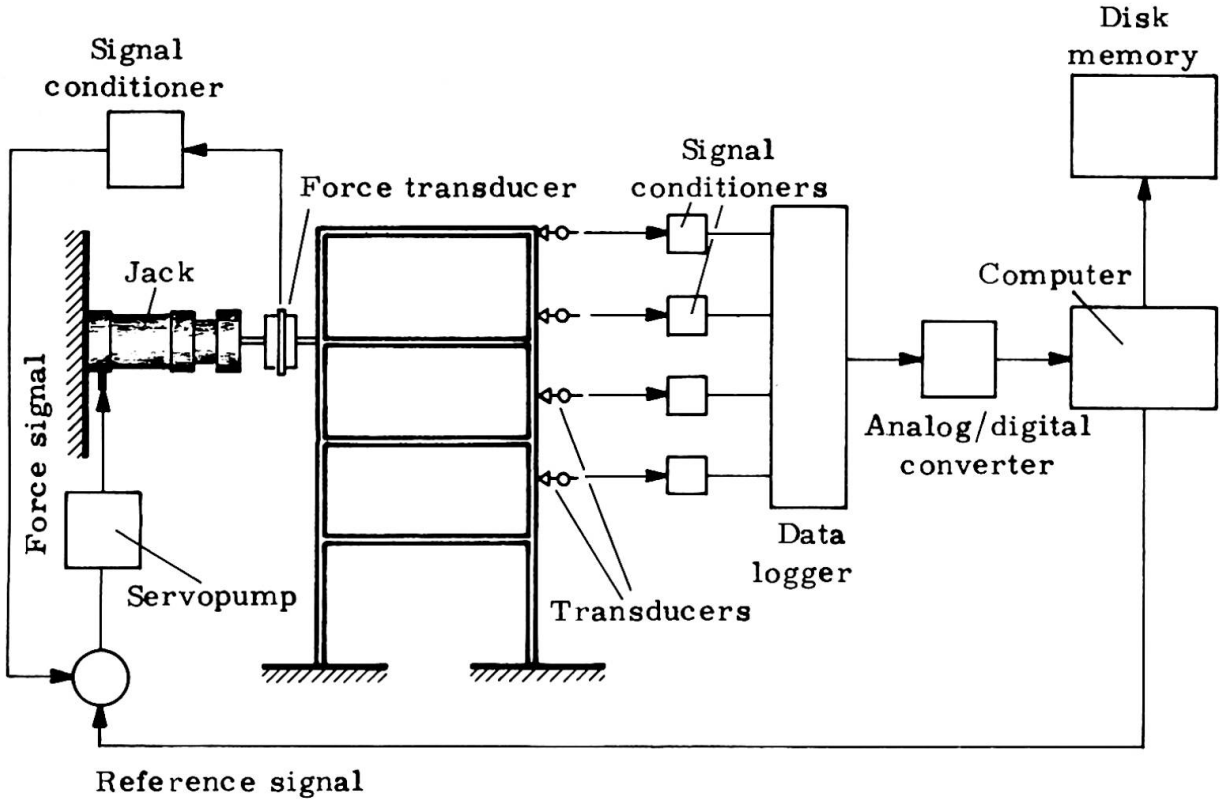

Fig. 1

Fig. 1 Ueberblick über die hybridstatische Versuchsanlage im Laboratorium H. Hossdorf.
Erkennbar ist die Computeranlage (Hewlett-Packard 2116B) mit Plattenspeicher und Magnetband, sowie die durch ihn gesteuerten Mess- und Versuchseinrichtungen, wie koordinatengesteuerte Belastungsmaschine, pneumatisch bewegte Verschiebungsgeber, die anwählbaren, elektrischen Messkanäle mit integrierendem Voltmeter (VIDAR 521B) als Analog-Digital-Wandler, u.s.f.

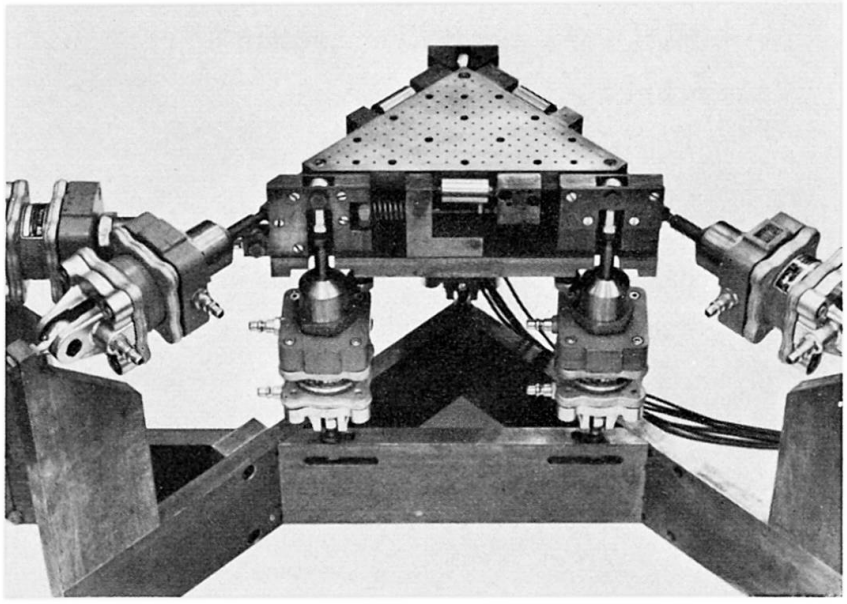

Fig. 2 Universelles räumliches (6-Komponenten-) Auflagerelement, mit welchem, in Verbindung mit dem Computer, die 36 Steifigkeitswerte an einem Strukturknoten experimentell bestimmt werden.

Ein Beispiel aus der Praxis

Hybridstatisch berechnetes, frei geformtes Brückentragwerk.

Eisenbahnbrücke in Killwangen, Schweiz

Bauherr: Schweiz. Bundesbahnen
Projekt: Ingenieurbüro Dr. H. Hugi und P. Schuler, Zürich

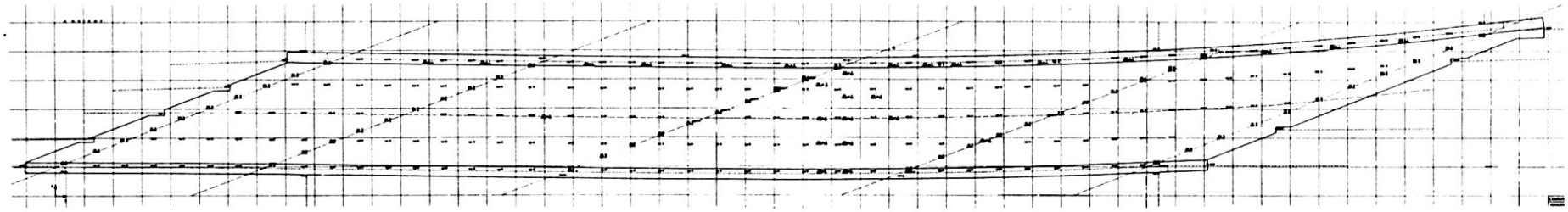

Fig. 3 In einem Modellplan werden die im Versuch verwendeten Aktionsvektoren (Kräfte, Verschiebungen), sowie die Effektvektoren und -tensoren festgehalten und relativ zu einem Koordinatensystem beschrieben. Damit wird dem Computer ermöglicht, Gleichgewichtsberechnungen durchzuführen und die ermittelten Einflusswerte als Ortsfunktionen (z.B. Einflussflächen) aufzufassen.

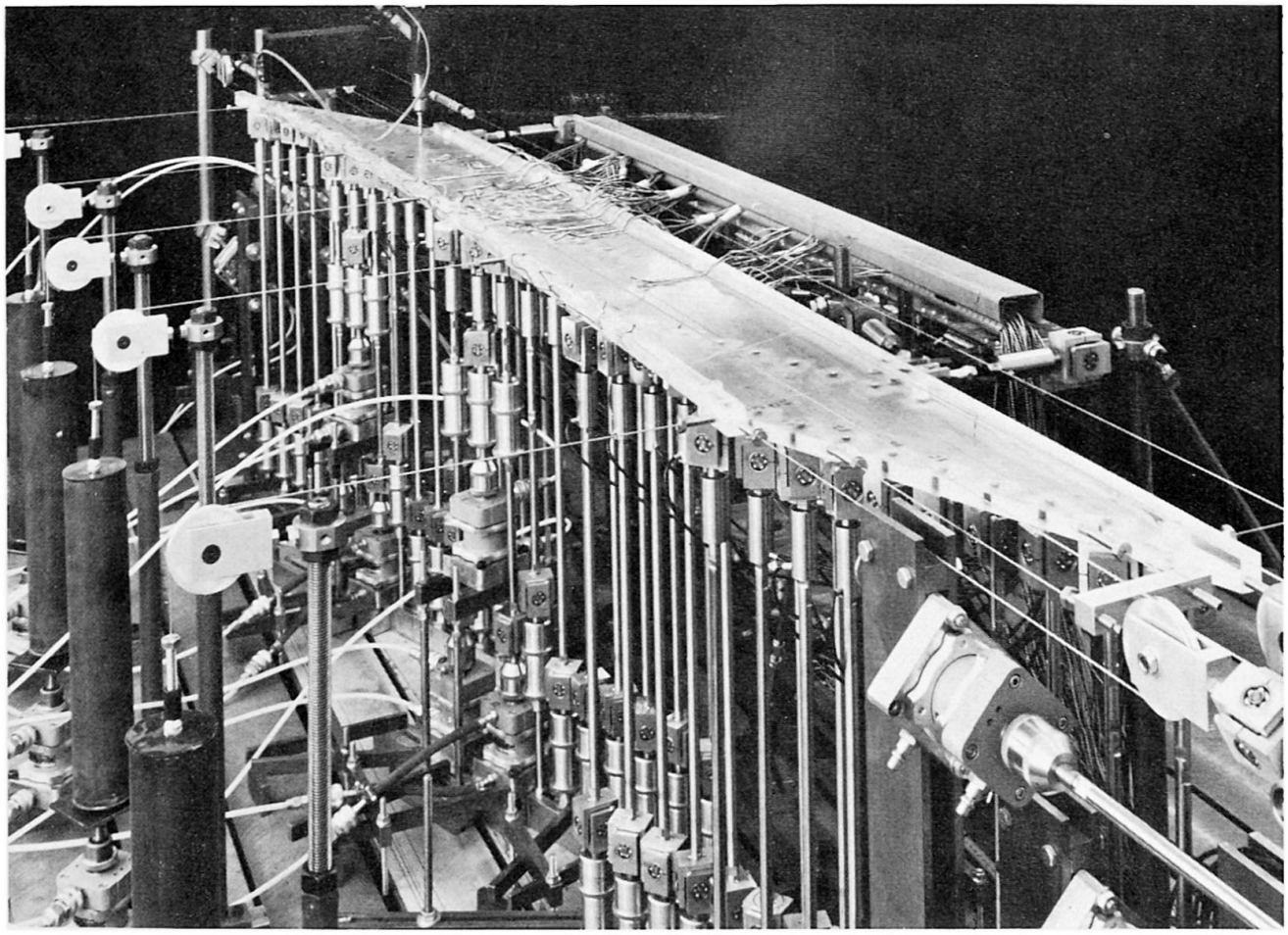

Fig. 4 Versuchsaufbau der Brücke Killwangen.
Der Aufbau der mechanischen Präzisionselemente auf einem massiven Aufspannboden garantieren die exakte Erfüllung der angenommenen Lagerungsbedingungen und die genaue Eintragung der Kraft- und Verschiebungsvektoren.
Aufgrund der an dieser Brücke gemessenen Einfluss- und Steifigkeitswerte (total ca. 40'000 Messwerte) wurden mit dem Programmsystem HYBRAN neben dem Lastfall Eigengewicht die Grenzwerte infolge von Normzügen auf zwei Geleisen, sowie der Lastfall Vorspannung (die Kabel sind hier räumlich gekrümmt) untersucht. Zudem wurde das Tragverhalten der Brücke unter modifizierten Randbedingungen (Entfernung von Stützen durch Anprall entgleisender Züge) nachgerechnet.

Literaturverzeichnis

Argyris, J. H.	Recent Advances in Matrix Methods of Structural Analysis	Pergamon Press, London, 1964
Fenves, S. J. Branin, F. H. Jr.	A Network Topological Formulation of Structural Analysis	J. Struct. Div. ASCE, ST4, 483, 1963
Hossdorf, H.	Eine programmgesteuerte, vollautomatische Modellmess- und Datenauswertungsanlage	Schweiz. Bauzeitung Nr. 39, 1955
Hossdorf, H.	Modellstatik	Bauverlag Wiesbaden, 1971
Langhaar, H. L.	Dimensional Analysis and Theory of Models	John Wiley & Sons, Inc., New York, 1962
Reinschmidt, K. F.	Datalink An On-line Computer System for Structural Laboratory Research	M.I.T. Press, 1965
Zienkiewicz, O. C. Cheung, Y. K.	The Finite Element Method in Structural and Continuum Mechanics	McGraw-Hill Publishing Company Ltd., New York, 1968

Zusammenfassung

In der Hybridstatik liefert das analoge Modell, in Verbindung mit einer prozessgesteuerten, präzisen Versuchstechnik, Einflussfunktionen, Flexibilitäts- und Steifigkeitswerte von geometrisch beliebig komplizierten elastischen Körpern. Aufgrund dieser Information lassen sich für die Praxis leistungsfähige Computerprogramme entwickeln, welche sich um die schwierige Integration der infinitesimalen Elastizitätsbeziehungen nicht mehr zu kümmern brauchen und so die Computerkapazität wesentlich wirkungsvoller ausschöpfen.

Leere Seite
Blank page
Page vide

New Trends in Model Research on Large Structures

Nouvelles tendances dans la recherche sur modèle pour grandes structures

Neue Tendenzen in Modelluntersuchungen für grosse Bauwerke

GUIDO OBERTI
Prof. Ing.
Polytechnic Institute, Turin
Technical Adviser, ISMES, Bergamo
F. ASCE

ALDO CASTOLDI
Dr. Ing.
Manager, Dynamic Department, ISMES
Italy

1. FOREWORD

The design of a civil engineering structure of importance usually goes through two successive stages.

In the first stage, the basic choice of the structural scheme to be adopted in relation to the technical problem under consideration is carried out, so as to set then roughly up the sizes of the structure. The designer, at this time, thus operates on a structure that is set up only along general lines and is, therefore, likely to be changed and improved in its component parts.

Thereafter, a detailed check of the behavior of the structure up to determining, if possible, its factor of safety is performed on one or several alternative designs already well defined on the basis of the above study.

At the outset, therefore, only mathematical analysis and especially personal experience are available to the designer. In fact, quite obviously a model study, though useful, is at this stage rather costly (both in time and money) and is seldom appropriate in the design of a structure which is still undergoing modification.

Instead, it is during the second stage that experimentation is profitably associated with the most refined mathematical methods.

Recently both experimentation and mathematical analysis have greatly advanced. In fact, on the one hand, efficient calculation procedures based on the finite elements method and made possible by the advent of the new digital computers have been developed. On the other hand, the introduction of the modern electronic techniques has enormously improved the measurement accuracy, while the use of small process computers has made possible the handling of large quantities of data.

It seems, therefore, appropriate to try to define, even in so rapidly an evolving situation, the perspectives and application field of the experimental method as compared with the analytical one by both summarizing the oper-

ational techniques and available facilities, and illustrating two recent model studies carried out at the ISMES.

2. TESTING EQUIPMENT

A thorough understanding of the possibilities and also present-day limitations of the experimental techniques requires at first a description, though a brief one, of the equipment presently available to the experimenter.

The criterion followed below consists in mentioning, on the basis of their functions, the various component parts used. We thus have:

Loading equipment

The loading is applied, using a conventional technique, by one or more oil-controlled jacks.

However, it is today possible to have an automatic control of the loading by means of a force transducer inserted between the structure and the jack. The transducer generates a feedback signal which, compared with a reference one, then acts on a servopump that controls the pressure of the oil and, hence, the load value.

The accuracy of this system is nowadays enormous; suffice it to consider the performances of the materials testing machinery operating in a like manner.

Data acquisition instrumentation

Data acquisition instruments (transducers) of any type, size and characteristics are presently available in commerce. Their accuracy is very high (about 1%).

For example, the displacement measurement problems are solved by using capacitance or inductance type transducers. Strains are easily measured by various types of extensometers (foil grid strain gages for a great stability or semiconductor strain gages for a large sensitivity).

Moreover, a wide variety of electrical instruments sensitive to different mechanical quantities (force, pressure, moment, etc.) is based on the use of extensometers.

In the dynamic field, the use of materials with piezoelectric properties has brought about lightweight accelerometers, force pickups, etc., working very well in any environment (in water, under pressure, at high temperature or in the presence of radiation).

Each transducer then is connected to a data logger by means of a signal--conditioning device whose task it is to raise the level of the electric signal of the transducer to a value that is sufficient for the following processing and datum acquisition phases.

The data logger commutates the various signals at the input of a digital reading instrument which furnishes a numerical indication of the performed measurement.

The data acquisition time substantially depends on the adopted scanning method, on the reading system and on the type of instrumentation available for the data storage. It generally ranges from a few points per second to a few hundred ones.

Data processing instrumentation

The operator who elaborated a few data has now been replaced by the process computer.

This computer is charged with all the test control operations. In particular, it regulates the various loading cycles, it controls the data logger in the commutation phase (with possible selection of the gage point), it orders the measuring system to read the datum and, finally, it commits the indication to memory.

3. EXPERIMENTAL TECHNIQUES ON ELASTIC MODELS

a) Test criteria in the static field

In elastic range tests, the conventional procedure usually required a complicated equipment capable of reproducing simultaneously over the entire structure a certain loading condition (e.g., dead load, working loads, live load, wind effect, etc.). This equipment, made up of a reacting frame and a series of jacks, was constructed to be used on a model of a given size and shape, and necessarily had to be redesigned if the model under study was changed and sometimes even when the type of loading applied varied.

It is, therefore, obvious that under such conditions the number of tests was kept as low as possible and, likewise, the cost of a manual data elaboration limited the number of instruments used.

The present trend, sponsored by Hossdorf,is rather to use a more general method consisting in determining appropriate influence coefficients. When these coefficients are known, it is simple to calculate the "response" of the structure to any system of acting forces.

The method can be summarized as follows.

A series of n points capable of describing accurately enough the state of deformation (or stress) of the structure is chosen. The structure is then loaded only by one jack in the position i, while the measuring equipment reads, for all the n points, the value of the quantity δ_i under study (displacement, strain, moment, shearing stress, etc.). The influence coefficients

$$\delta_{ji} = \frac{\delta_j}{F_i} \qquad (j = 1, n)$$

are thus obtained.

The jack is then applied to each of the remaining points.

The set of n · x values of δ_{ji} forms the matrix $[\delta]$ of the influence coefficients for the given quantity. The values $\{x\}$ of this quantity for a certain loading condition P is then given by

$$\{x\} = [\delta] \cdot \{P\} \tag{1}$$

Quite clearly, this investigation method is very efficient, especially when the rapidity with which the testing equipment can determine the matrix $[\delta]$ is taken into account.

However, it seems appropriate to point out some disadvantages which in practice may limit its use.

1) The method makes use of the principle of superposition of effects and is, therefore, applicable only to structures with a linear behavior. It cannot rigorously be used in all those cases where, though the stress remains in the elastic range, the strain is not proportional to the acting load because of the geometry of the structure (e.g., suspension bridges).

2) For a number of massive structures (such as dams, nuclear reactor vessels, etc.) the possibility of measuring accurately enough the influence coefficients depends on the possibility of increasing the applied load without locally damaging the model. This possibility is determined solely by the elastic properties of the model material and frequently does not exist.
Difficulties in evaluating the influence coefficients appear also in all the cases where it is necessary to measure a mechanical quantity that is superposed by an undesired quantity of the same type having a very high value. Such cases are found, for instance, when it is necessary

to measure the displacement in a certain direction while a large displacement exists in the orthogonal direction (case of a diverted flexure or a flexure accompanied by torsion) or when the axial stress in a cross-section loaded also by a large moment is to be found.

3) The final result of the analysis is always obtained, on the basis of equation (1), as the sum of the results of numerous independent measurements. Quite obviously, this sum contains the errors of all the measurements made and, therefore, this method is intrinsically less accurate than the conventional one.

b) Test criteria in the dynamic field

The experimental study of the dynamic behavior of a structure is correctly made when the dynamic actions on the prototype (or the anticipated ones) are applied to a model faithfully simulating all the essential details.

In such a study, the difficulty of having an excitation equipment reproducing the characteristics of utmost interest (spectral density function, probability density function, r.m.s. value) of the dynamic actions is added to the difficulty of manufacturing a model responding to the similitude laws.

The instruments available at present (shaking tables, electrodynamic or electrohydraulic exciters, etc.) have partly met the request but are very expensive and require skilled operators.

On the other hand, modal analysis theory shows that the dynamic behavior of a structure in the elastic range is entirely known when its vibration modes (i.e., natural frequency, shape and damping of each mode) are determined. It is, therefore, natural that the experimenter prefers to look for the principal vibration modes and then obtain by calculation the response of the structure to any excitation, rather than simulate such an excitation on the structure.

The evaluation of the principal "modes" is presently based on the following considerations.

The oscillations of a structure, produced by a system of external forces, can always be expressed as the sum of the oscillations relative to the various modes. It is also obvious that a particular choice of the excitation forces can render negligible or even nullify the contribution of a single mode to the response of the structure.

Therefore, the problem of exciting a dynamic system according to one only vibration mode is reduced to determining the particular force system for which the response of all the modes, except the desired one, is nil.

The problem cannot be solved directly because it would require an advance knowledge of the frequency and shape of the mode under examination. Nevertheless, a technique has been developed, based on an iterative process which permits at each successive step to render ever more negligible the response of the undesired modes.

In practice, each iteration permits, on the basis of the results obtained in the previous test, to apply a certain number of exciters (capable of gener

ating sinusoidal forces having a frequency equal to the one of the supposedly known desired mode) to the most suitable points of the structure, and, at the same time, to regulate the value of the force generated by them. It should be:

$$\{F\}^{(i)} = [m] \cdot \{\ddot{x}\}^{(i-1)}$$

where $\{\ddot{x}\}^{(i-1)}$ are the accelerations resulting in the (i - 1)th iteration.

Although extremely efficient, this method requires complex equipment and is not too easily applicable, especially when the higher vibration modes are also to be determined.

At present, in this field, too, the advent of the test techniques described under point 3 a) has produced a considerable simplification and a cost reduction.

Suffice it to observe that the influence coefficients for the displacement are but the coefficients of the structure's flexibility matrix. Therefore, when the structure is considered as a lump system of springs and masses (concentrated in the points chosen for the experimentation), the problem of the mode determination is turned into the rather simple problem of calculating the eigenvalues and eigenvectors relevant to the matrix $[m] \cdot [\delta]$, where $[\delta]$ is not affected by calculation or schematization errors as it has been obtained experimentally.

The dynamic problem has thus been changed into a statical one and, therefore, can be handled by numerous laboratories.

Some limitations of this type of analysis will be pointed out here, too. They are:

1) the structure has to be schematized by a lump system of masses. This involves inevitable errors which experience alone can reduce to a minimum;

2) the number of masses (or degrees of freedom) of the system chosen to schematize the structure must be fixed in function of the modes which one wishes to derive. An accurate description of the modes may, therefore, require a large number of masses, and this very much increases the amount of work necessary to determine the flexibility matrix;

3) the flexibility matrix must be known very accurately. In fact, the errors affecting the coefficients greatly influence the calculation of the higher modes.

4. TEST CRITERIA BEYOND THE ELASTIC RANGE UP TO FAILURE

The superiority of the experimental method over the analytical one is unquestionable when the structure's behavior has to be checked beyond the elastic range until determining its factor of safety. However, serious problems still exist about the construction of a model reproducing the prototype with complete faithfulness. In this case, the data acquisition

and processing techniques have not basically changed the testing scheme in a way similar to the one of experimentation in the elastic range.

The main reason is that, because of the impossibility of applying the principle of superposition of effects, the operator is not free to choose the type and value of the loadings, which must be the same as those predicted for the prototype.

Nevertheless, the computer can in this case, too, be of a very great use, mainly because the rapid elaboration on line of the acquired data enables it to readily indicate the arising of yielding zones, fractures, etc.

However, the greatest developments of the experimental technique are to be expected in the modeling field by producing materials most responding to the similitude laws.

5. EXAMPLES

The above techniques are illustrated below by two examples, one high-rise building and one suspension bridge, recently tested at the ISMES in the elastic range under seismic action.

a) Parque Central building, Caracas, Venezuela

Fig. 2 shows the 1 : 40 scale resin model. The number of gage points chosen was 32, and the model was successively loaded in each of them so as to furnish a series of deformed surfaces (fig. 4). Simultaneously with the displacements, recordings were made also of the indications of numerous strain gages applied to the base.

The results obtained permitted to calculate the vibration modes (fig. 3), and these were later found experimentally by placing the model on a shake table excited in resonance.

At this point it was possible to check the seismic performance of the structure by calculating the response of each mode to the design earthquake and determining the resulting distribution of the forces of inertia. Having thus obtained the system of horizontal forces P equivalent in its effect to the earthquake, it was easy to also calculate the stresses at the base as a superposition of effects.

b) Bosphorus suspension bridge

A 1 : 200 scale resin model was made, using appropriate artifices for a correct reproduction of all the parameters of interest (fig. 5).

As the influence coefficient method could not be applied to this structure, a first test was made to determine the importance of the nonlinearity of behavior. The conclusion was that in this case, too, the load-deformation curve, for loads of not too great a magnitude, could in a first approximation be assimilated to a straight line.

The above-described criteria were, therefore, used by determining at first the deformed surfaces of the deck (fig. 6) and also of the cables for different positions and directions of the load and, hence, the natural vibration modes (fig. 7).

7. CONCLUSIONS

In concluding the above considerations, a comparison between the experimental and analytical investigation methods can be attempted.

As is known, the analytical method deals with a structure whose behavior has been schematized by well-defined mathematical laws. In general, both by the conventional solution methods and the one of the finite elements, one arrives at a system of linear algebraic equations which in a matrix form is of the type:

$$[K] \cdot \{x\} = \{B\} \tag{2}$$

System (2) contains the following three matrices:

1) "column matrix" $\{x\}$ whose elements form the unknowns of the problem (sometimes the displacements and sometimes the forces);

2) matrix $[K]$ whose coefficients depend on the geometry of the structure and the elastic properties of the material;

3) column matrix $\{B\}$ of the known terms containing the data of the problem (external loads, restraint settlements, temperature variations, etc.).

The solution of system (2) leads to the relation

$$\{x\} = [K]^{-1} \cdot \{B\} \tag{3}$$

Relation (3) shows that the investigation of the unknowns is, in any case, directly or indirectly connected with the problem of inverting the matrix $[K]$.

The detailed description of the solution procedure shows that the most serious and significant problems are as follows:

a) Formation of matrix $[K]$

The calculation of the coefficients of the matrix $[K]$ can in the simplest cases (beams, plane or space frames, etc.) be easily set up. It is more complicated for three-dimensional structures, and the simplifications which must be introduced make frequently the results little reliable.

b) Inversion error

As was already mentioned, there is, explicitly or implicitly, the problem of inverting a matrix.
However, as the number of unknowns increases, this inversion may become too laborious even with computers of great power. This is so because the propagation of the rounding-off errors, when the direct solution methods are used, or the "cutoff errors" when the "iterative methods" are resorted to, make in any case the final error sometimes so appreciable as to annul the advantage of a better schematization.
The attempt to obviate these inconveniences by conducting the calculations with a great number of significant figures can lead to economi cally almost prohibitive computation times.

c) Cost

The treatment of complex problems in which an accurate description of the structure requires a large number of unknowns involves not only solution difficulties but also great cost increases in using the computer for both forming and inverting the matrix [K] .
It should also be pointed out that, in the case of unusual structures, very heavy economic problems may arise in adapting existing programs (especially as regards the input and output of the data) and in checking the quality of the adopted schematizations.

In the experimental method, the construction of the model is the equivalent of the matrix [K]. It should, however, be observed that, at least in the elastic range, no particular difficulties exist and the similitude laws can easily be complied with when a suitable material and geometric scale are chosen.

Of utmost importance is, moreover, the fact that, in this case, there is no matrix inversion problem.

The model functions as an analogic computer and furnishes the exact solution (if the model is exact) with no approximations of any kind.

The cost of the model test is rather high even in simple cases despite the fact that the new data acquisition equipment has appreciably reduced the time required.

Likewise expensive is still the construction of the model, on whose accuracy and fidelity of operation depends the quality of the results.

In view of all the above, we may conclude that the experimental and analytical methods have complementary fields of employment. The problems relating to structures that are plane or symmetrical with respect to their axis, and to plane or space frames will advantageously be studied on a computer, whereas recourse to model testing will be more economical (and accurate) for complex structures.

SUMMARY

Some general considerations on the usefulness of model studies in both the design and verification stages of large tridimensional structures are first outlined.

The new testing techniques in both the static and dynamic fields, based on the use of modern data acquisition systems in association with a computer, are then analyzed. As regards the dynamic field, emphasis is placed on the considerable simplification of the excitation equipment with consequent cost reduction.

In this connection, the results of some elastic model tests conducted at ISMES, Bergamo, Italy, by using the above criteria are illustrated.

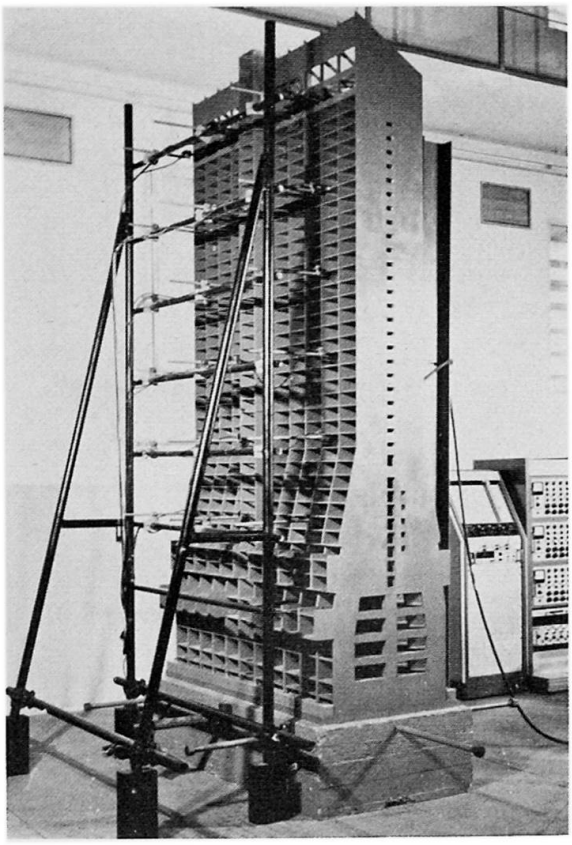

Fig. 2

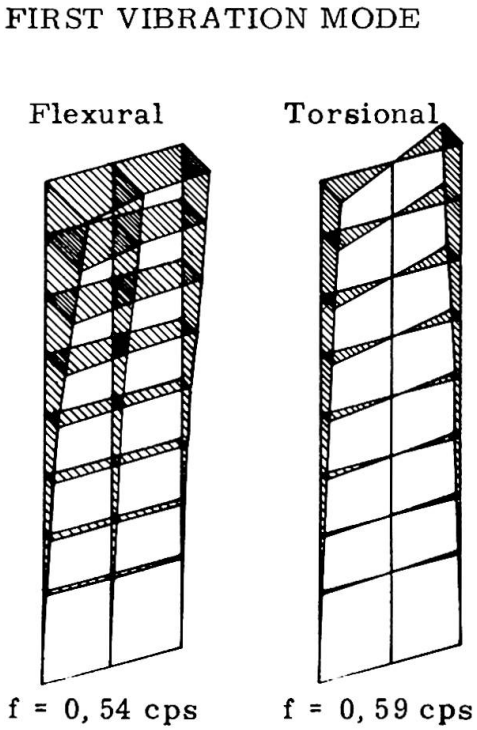

Fig. 3

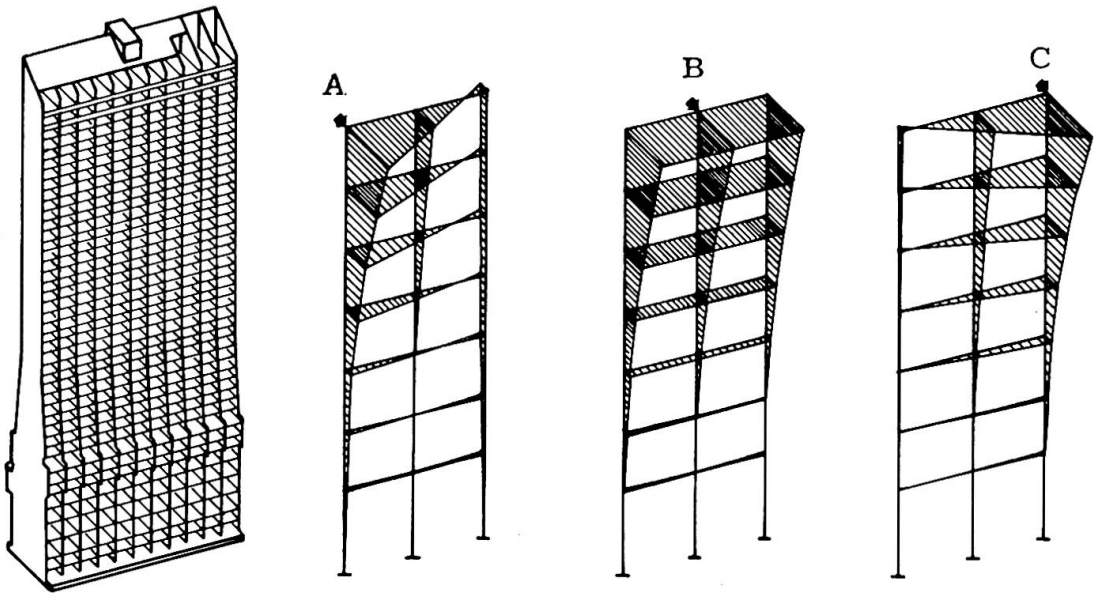

Fig. 4

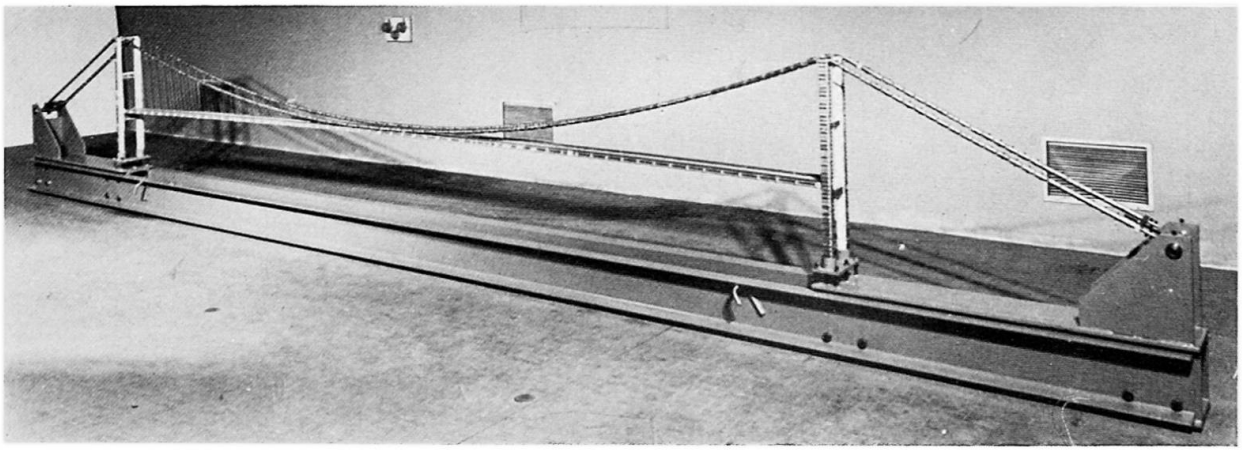

Fig. 5

DECK DEFORMATIONS FOR VERTICAL LOADS

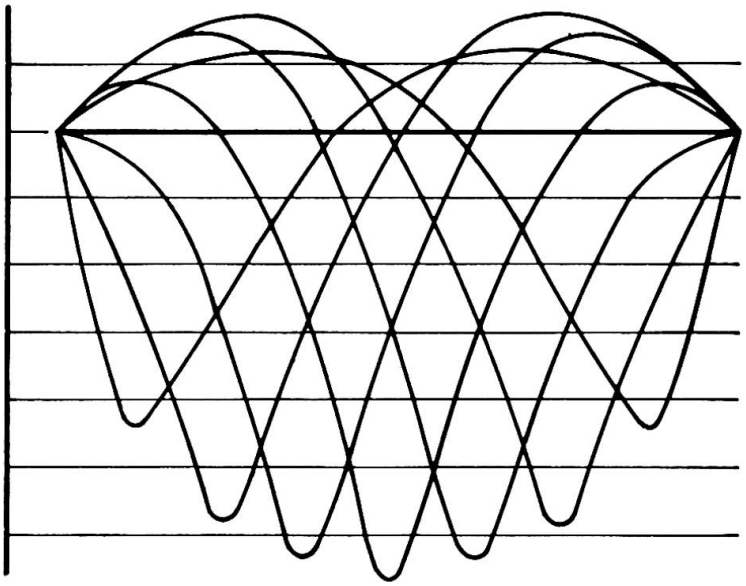

Fig. 6

VIBRATION MODES

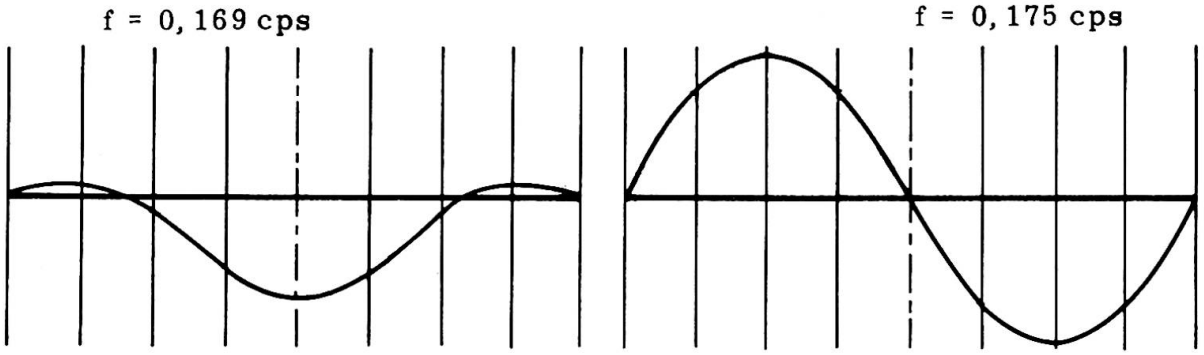

Fig. 7

Leere Seite
Blank page
Page vide

Etude de systèmes physiques par analogie avec un réseau électrique purement réactif Application au comportement statique et dynamique des structures mécaniques

Untersuchung physikalischer Analogsysteme mit einem rein reaktiven Elektrizitätsnetz Anwendung auf das statische und dynamische Verhalten von mechanischen Bauwerken

Analysis of Physical Systems by Means of Analogy with a Purely Reactif Electric Network Application to the Static and Dynamic Behaviour of Mecanical Structures

PIERRE ALAIS
Professeur
Faculté des Sciences de Paris

GILBERT LAMBOLEY
Ingénieur
Ecole Polytechnique

Paris, France

1 - INTRODUCTION

Plusieurs tentatives ont été faites pour résoudre par un procédé d'analogies électriques des systèmes d'équations linéaires sans tenir compte de leur origine (V) et (VI). Le but de la présente étude est de résoudre, par de semblables analogies, les systèmes d'équations linéaires qui interviennent dans le calcul du comportement de nombreux systèmes physiques, en s'attachant à développer un modèle analogique qui suive d'aussi près que possible la structure même de l'exemple physique proposé: la construction d'une maquette simulatrice est ainsi substituée à l'écriture, toujours laborieuse pour un ensemble complexe, des équations du problème. Un tel dispositif élimine de ce fait tous les phénomènes d'instabilité parasites qui peuvent éventuellement résulter, même lorsque le système physique est parfaitement régulier, des transformations effectuées sur les équations dans les procédés classiques de résolution. D'intéressants travaux (I), (II), (III), (IV) ont d'ailleurs été menés avec ce souci concernant le problème particulier des structures hyperstatiques, sans toutefois fournir à notre avis un outil définitif, adapté aux diverses hypothèses effectuées classiquement en résistance des matériaux ainsi qu'à une géométrie quelconque d'ossature.

Bien que les matrices inhérentes aux systèmes envisagés soient en général, et pour des raisons physiques évidentes, définies positives et symétriques et qu'il soit possible par conséquent de rendre tous leurs coefficients positifs dans un système de coordonnées approprié, l'usage des variables naturelles a été jugé, dans ce travail, préférable: outre l'intérêt que le technicien peut avoir à ne manipuler que des grandeurs directement transposées de celles auxquelles il est habitué dans les systèmes réels, on évite ainsi tout changement artificiel et parfois dangereux de variables et toute écriture d'équation, c'est à dire pratiquement tout travail d'attention fastidieux et source d'erreur. En contrepartie de ces avantages, on est cependant tenu de faire face à certaines difficultés; d'une part, il faut surmonter le problème en acceptant des coefficients des deux signes dans la matrice correspondante, ce qui conduit à utiliser pour constituer les réseaux analogiques, non plus des résistances passives auxquelles devraient nécessairement être associés des dispositifs à résistances négatives, de réalisation délicate et coûteuse, mais des selfs et des capacités alimentées par une source alternative à fréquence stabilisée: nous pensons montrer clairement dans ce qui suit que ce type de réseau, très peu employé

jusqu'à présent en calcul analogique, donne d'excellents résultats. D'autre part, les coordonnées naturelles présentent en général l'inconvénient de ne pas être indépendantes, mais liées par des relations linéaires homogènes inhérentes à certaines propriétés internes des systèmes physiques: la traduction analogique de cette dépendance s'acquiert aisément à l'aide d'un réseau complémentaire superposé au réseau constitutif proprement dit. Ces deux difficultés résolues dans leur généralité, on appréciera les avantages résultant de la simulation fidèle du modèle physique; en particulier, l'édification du réseau général à l'image de la construction réelle à partir des éléments analogiques de chaque barre, permet des montages très rapides et une analyse poussée des phénomènes.

2 - PRINCIPE DE L'ANALOGIE

Le comportement d'un réseau de conductances électriques linéaires excité harmoniquement à la pulsation ω est caractérisé par la matrice symétrique d'admittance C_{ij} ($C_{ij} = C_{ji}$) reliant les potentiels φ_i de ses noeuds aux intensités d'excitation I_i imposées de l'extérieur selon les relations:

$$(1) \quad I_i = C_{ij}\,\varphi_j$$

Réciproquement, toute matrice symétrique C_{ij} peut conduire à l'élaboration d'un réseau électrique vérifiant les relations (1) de la manière suivante:

- chaque couple de coefficients non diagonaux C_{ij} et $C_{ji} = C_{ij}$ est représenté par le réseau élémentaire

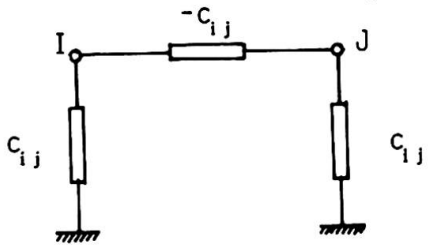

- chaque coefficient diagonal C_{ii} est représenté par la conductance C_{ii} reliant le noeud I à la masse.

Le réseau obtenu est ainsi composé des conductances $\Gamma_i = \Sigma_i C_{ij}$ reliant chaque noeud I à la masse et des conductances $\Gamma_{ij} = -C_{ij}$ reliant les noeuds I et J.

De même tout système physique discret linéaire excité statiquement ou harmoniquement voit son comportement décrit par des relations du type (1) et est donc susceptible d'être simulé électriquement par un réseau élaboré comme il vient d'être dit à la condition de disposer des conductances Γ_i et Γ_{ij} imposées par le problème à un arbitraire d'échelle près. Les composants électriques classiques se réduisent aux résistances, aux selfs et aux capacités et ne permettent, quelle que soit leur combinaison que la réalisation d'admittances à partie réelle positive, ce qui semble une entrave au procédé, la réalisation de conductances à partie réelle négative étant possible grâce à l'utilisation de circuits actifs mais compliquée et onéreuse. Toute une classe de systèmes échappe cependant à cette limitation: il s'agit en l'occurence des systèmes linéaires statiques, lesquels sont décrits par une matrice symétrique à coefficients réels, laquelle peut être toujours représentée par un réseau purement réactif de capacités et de selfs si on convient d'adopter un coefficient d'échelle analogique imaginaire pur reliant les composantes matricielles C_{ij} fournies par le système réel étudié et les admittances réactives de simulation utilisées, ceci se traduisant par un simple déphasage de $\Pi/2$ entre intensités et potentiels électriques. De même, les systèmes physiques en oscillation harmonique libre ou forcée sans pertes peuvent être directement simulés par un réseau purement réactif (§ 4). Enfin, tout système linéaire discret en oscillation forcée avec pertes peut être simulé mais le formalisme retenu, c'est-à-dire le choix des variables s'identifiant aux potentiels du réseau simulateur doit être effectué de manière que le réseau associé ne comporte que des conductances Γ_i et Γ_{ij} à partie réelle positive (§5)

3 - CARACTERISATION ET SIMULATION D'UN SYSTEME DISCRET LINEAIRE (VIII)

Une ossature hyperstatique chargée statiquement.

- La description d'un tel système conduit au choix d'une collection de n variables naturelles φ_i permettant par exemple d'atteindre les déplacements et rotations des noeuds.
- Si nous supposons provisoirement que les effets extérieurs ne sont exercés qu'au niveau des noeuds, l'énergie élastique de la structure somme des énergies de chaque élément constituant s'écrit selon la forme quadratique

$$(2) \qquad W = \frac{1}{2} A_{ij} \varphi_i \varphi_j$$

ce qui permet d'associer aux variables de position φ_i les variables de tension

$$(3) \qquad A_i = A_{ij} \varphi_j$$

la matrice symétrique A_{ij} s'exprimant sans ambiguité à partir de la forme quadratique (2).

Les charges sont caractérisées par le travail élémentaire qu'elles développent dans la déformation élémentaire $\varphi_i \to \varphi_i + d\varphi_i$

$$(4) \qquad dW = B_i \, d\varphi_i$$

Ce travail s'identifie à la différentielle de l'expression (2), soit compte tenu de la symétrie des A_{ij} :

$$dW = \frac{1}{2} A_{ij} (\varphi_j \, d\varphi_j + \varphi_j \, d\varphi_i) = A_i \, d\varphi_i$$

soit encore

$$(5) \qquad (B_i - A_i) \, d\varphi_i = 0$$

Deux cas se présentent alors:

- les φ_i sont indépendantes et $B_i = A_i$ les équations

$$(6) \qquad B_i = A_{ij} \varphi_j$$

constituent la relation matricielle caractéristique du système.

- cas beaucoup plus fréquent, la collection de variables φ_i est surabondante et celles-ci sont reliées par p relations de dépendance linéaires homogènes

$$(7) \qquad \alpha_{li} \varphi_i = 0 \qquad l = 1, \ldots . \; p < n$$

le système ne possédant en fait que $n - p$ degrés de liberté.

On ne peut plus alors identifier les données de charge B_i aux variables A_i conjuguées des φ_i mais l'introduction de p paramètres de Lagrange φ_l permet d'écrire compte tenu de (5) et (7): $(B_i - A_{ij} \varphi_j - \alpha_{il} \varphi_l) \, d\varphi_i = 0$

et d'aboutir aux $(n + p)$ équations $B_i = A_{ij} \varphi_j + \alpha_{il} \varphi_l \quad , \; 0 = \alpha_{il} \varphi_l$

lesquelles constituent la correspondance matricielle symétrique caractéristique du système

$$\begin{vmatrix} B_i \\ 0 \end{vmatrix} = \left|\begin{array}{c|c} A_{ij} & \alpha_{il} \\ \hline \alpha_{li} & 0 \end{array}\right| \begin{vmatrix} \varphi_i \\ \varphi_l \end{vmatrix}$$

La simulation des A_{ij} conduit à l'élaboration du réseau constitutif dont l'énergie associée ou la puissance dissipée, pour parler en termes de conductances réelles, s'identifie à l'énergie élastique de la structure. Naturellement, la construction de ce réseau peut s'effectuer à partir de l'assemblage de réseaux plus élémentaires représentatifs de chaque élément de la structure. La simulation des α_{il} conduit à l'élaboration du réseau de transmission auquel aucune énergie n'est associée. En termes de conductances réelles, ce réseau ne " dissipe rien " et se contente de transmettre au réseau constitutif les intensités A_i à partir des intensités B_i injectées au réseau total.

Charge équivalente - Si les charges exercées ne s'appliquent pas directement aux noeuds, ce qui est d'ailleurs le plus fréquent, on se ramène au cas précédent pour déterminer les φ_i en remplaçant les charges réelles par une charge équivalente appliquée aux noeuds, en ce sens qu'elle provoque la même déformation généralisée φ_i de la structure. Un raisonnement élémentaire n'invoquant que la linéarité de la réponse de la structure à la charge exercée montre qu'une telle charge équivalente est constituée par les efforts opposés aux efforts de blocage qu'il faut développer pour annuler toute déformation généralisée en présence de la charge réelle. Cette charge équivalente se détermine ensuite à partir de chaque élément chargé supposé bloqué à ses extrémités.

4 - L'ANALOGIE DU POINT DE VUE ENERGETIQUE

Nous venons de montrer que dans le cas très général où la représentation est surabondante, les dépendances linéaires homogènes reliant les variables utilisées sont traduites par le réseau de transmission. A chaque relation $\alpha_{li}\,\varphi_i = 0$ est associée une étoile de conductances:

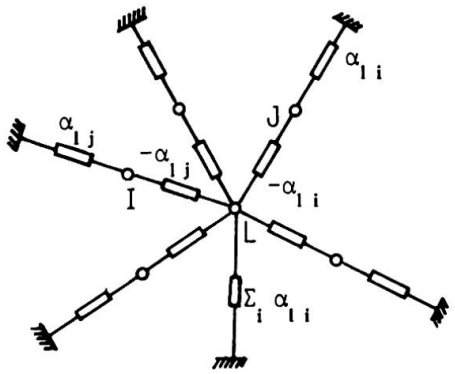

Souvent ces relations sont de la forme simple $\varphi_a - \varphi_b = \alpha\,(\varphi_c - \varphi_d)$ et peuvent être imposées alors par un transformateur de rapport α qui se substitue à l'étoile. Un tel circuit de transmission, étoile ou transformation, est caractérisé essentiellement par le fait que, retenant toujours le langage des conductances réelles, il ne " dissipe " aucune énergie. Ainsi dans le cas de l'étoile:

$$P_l \doteq \sum_i \left(\alpha_{li}\,\varphi_l^{\,2} - \alpha_{li}\,(\varphi_i - \varphi_l)^2\right) + \left(\sum_i \alpha_{li}\right)\varphi_l^{\,2} = 2\,\varphi_l \sum_i \alpha_{li}\,\varphi_i = 0$$

Cette propriété essentielle du réseau de transmission fait que l'analogie est préservée entre la puissance dissipée par le réseau constitutif.

$$P = \sum_{i<j}\left(-A_{ij}\,(\varphi_i - \varphi_j)^2\right) + \sum_i \varphi_i^{\,2}\left(\sum_j A_{ij}\right) = 2\sum_{i<j} A_{ij}\,\varphi_i\,\varphi_j = A_{ij}\,\varphi_i\,\varphi_j$$

et l'énergie W associée au système réel simulé.

Il faut remarquer que, si pour un système statique la définition de l'énergie W ne prête à aucune confusion (en l'occurence, pour un système hyperstatique déformé, il s'agit de l'énergie élastique emmagasinée par le système), elle est moins évidente pour un système dynamique oscillant sans pertes (IX). Dans ce dernier cas au moins deux types d'énergie réactive participent à l'oscillation, par exemple l'énergie élastique et l'énergie cinétique pour une ossature vibrante. En pareil cas l'énergie W caractéristique du système est celle transférée par l'excitation extérieure au système dans le quart de période pendant lequel les variables φ_i passent de la valeur nulle à la valeur extrêmale. On vérifie d'ailleurs élémentairement que cette définition est en accord, dans le cas du réseau électrique simulateur lui-même réellement utilisé, avec la notion de puissance dissipée par le réseau fictif de conductances réelles positives et négatives. L'énergie W ne représente pas la somme des énergies réactives mais en fait la différence des énergies des deux types. Ainsi, dans le cas du réseau, l'énergie selfique et l'énergie capacitive apparaissent avec des signes opposés fixés conventionnellement. Lorsque le système oscille selon un mode propre, le bilan énergétique associé s'annule: W = 0

Pour les systèmes discrets implicitement considérés jusqu'à maintenant, les considérations énergétiques qui précèdent ne sont pas indispensables quoique fort commodes dans la pratique. Elles sont par contre essentielles dans la représentation des systèmes continus tels que plaques ou coques. Pour de tels systèmes c'est l'énergie (cinétique ou élastique) qui est la plus directement accessible quel que soit le mode de représentation retenu. La méthode de simulation par un réseau

consiste à choisir une représentation discrète φ_i permettant de représenter l'énergie ou le bilan énergétique W associé au problème de façon approchée par une forme quadratique reposant sur les φ_i et à bâtir le réseau associé. La connaissance de l'énergie W suffit donc, ou encore celle de la densité volumique ou surfacique d'énergie pour la représentation d'un massif ou d'une plaque. De même la traduction des conditions aux limites ne pose pas de difficultés de principe puisqu'elles ont toujours une interprétation énergétique, qu'il s'agisse d'encastrement, de bord ou d'extrémité libre ou encore d'appui élastique. Les couplages ou raccordements de systèmes continus à des systèmes naturellement discrets tels que coques et ossatures se font également simplement, l'élaboration du réseau global se faisant comme la construction du système réel envisagé. Il faut toutefois remarquer que, dans le cas d'une étude dynamique, le bilan énergétique W est une forme quadratique des φ_i dont les coefficients A_{ij} sont des fonctions de la pulsation ω de l'oscillation du système, ce qui exige modification du réseau simulateur quand on varie ω ce qui peut rendre la méthode inadéquate s'il faut varier trop de conductances. Un cas idéal est celui où la variation de la pulsation ω' de l'excitation du réseau électrique entraîne la modification souhaitée. On peut alors dire qu'il y a analogie forte et identification totale du système réel et du système électrique simulateur. Une telle circonstance ne se rencontre malheureusement que dans la simulation d'autres phénomènes électriques tels que le rayonnement électromagnétique d'une antenne ou de systèmes mécaniques de ressorts-masses, par exemple représentatifs de systèmes atomiques. Dans la plupart des calculs intéressant l'ingénieur, la représentation de l'énergie élastique interdit l'analogie forte. Restent cependant les cas assez nombreux où une représentation approchée ou encore la simplicité de la structure permettent de ne varier qu'un nombre réduit de conductances, ce qui autorise alors l'étude des fonctions de transfert du système.

5 - ETUDE DES SYSTEMES DYNAMIQUES OSCILLANT AVEC PERTES (XII)

Les systèmes considérés précédemment c'est-à-dire statiques ou vibrant sans pertes ne relèvent finalement que de la connaissance du scalaire W en fonction de la représentation φ_i choisie, laquelle est réelle puisque tous les points d'un système sans pertes vibrent en phase ou en antiphase (à la condition évidente de ne considérer, à chaque calcul, qu'une excitation également en phase). Il n'en est plus de même pour un système présentant des pertes. Pour un tel système, la représentation doit être complexe, chaque variable devant caractériser l'amplitude et le déphasage de la vibration en un point, et il n'est plus possible de faire appel à un scalaire donnant comme précédemment toutes les informations. Par contre il est toujours possible de traduire la relation matricielle inhérente au système sans nécessairement écrire les équations, ce, toujours par des considérations énergétiques. Il suffit en effet d'élaborer le réseau en représentant à un coefficient d'échelle arbitraire près la puissance reçue de l'extérieur par le système sous forme réactive des deux types et sous forme dissipative.

FORMULATION GENERALE DE L'ANALOGIE

L'état du système considéré oscillant à la pulsation forcée étant caractérisé selon la notation complexe habituelle par les vecteurs généralisés de rang n de position et vitesse respectives $x_i = X_i e^{j\omega t}$; $v_i = V_i e^{j\omega t} = j\omega x_i$, le problème est posé par la donnée:

a) de la puissance acceptée à l'instant $t = o$ par le système sous la forme

$$(8) \quad pm = < P_{ij} V_j , V_i > \quad \text{ou} \quad < A, B > = R_e A . R_e B$$

c'est à dire la donnée de l'impédance P_{ij} propre au système dans la représentation choisie x_i ou v_i

b) des p couplages linéaires homogènes liant éventuellement les variables de représentation

$$(9) \quad \alpha_{li} V_i = 0 \qquad l = 1, \ldots, p < n$$

les α_{ii} étant tous réels et adimensionnels;
c) de la puissance fournie à l'instant $t = o$ par le système extérieur sous la forme

$$(10) \qquad pm = < F_i , V_i >$$

c'est à dire par la donnée des composantes généralisées $f_i = F_i e^{j\omega t}$ de l'excitation extérieure. La conservation de l'énergie exige naturellement d'égaler les puissances (8) et (9), mais l'existance des couplages (9) interdit en général d'identifier les amplitudes F_i de l'excitation aux variables $A_i = P_{ij} V_j$ conjuguées des variables de représentation. Cependant, calquant le raisonnement déjà invoqué en (2), on peut dire que les données (8), (9), (10) posent correctement le problème car elles permettent théoriquement de choisir une nouvelle représentation du système à $n - p$ variables indépendantes V_s et l'identification alors possible des nouvelles composantes de l'excitation aux variables conjuguées des V_s conduit à l'équation

$$(11) \qquad F_s = A_s = P_{lk} V_k$$

qui fournit une solution unique V_s si la matrice P_{lk} n'est pas singulière, ce qui est toujours vérifié, si on exclut naturellement le cas très particulier des résonances propres d'un système isolé sans pertes.

L'analogie consiste à associer aux V_i les amplitudes des potentiels $\varphi_i = \Phi_i e^{j\omega t}$ de n noeuds électriques I selon la correspondance

$$(12) \qquad \Phi_i = \alpha V_i$$

et le réseau construit sur ces noeuds et excité à la pulsation ω' est élaboré de manière à admettre au temps $t = o$ la puissance

$$(13) \qquad pe = < \Gamma_{ij} (\omega') \Phi_j , \Phi_i > = \frac{1}{\eta} < P_{ij} V_j , V_i > = \frac{1}{\eta} pm$$

quels que soient les V_i ou les $\Phi_i = \alpha V_i$ ce qui impose que l'admittance du réseau s'exprime selon

$$(14) \qquad \Gamma_{ij} (\omega') = \frac{1}{\eta \alpha^2} P_{ij} (\omega)$$

Un tel réseau est construit comme ceux purement réactifs déjà étudiés en reliant les noeuds I et J par les conductances $C_{ij} (\omega') = - P_{ij} (\omega)/\eta\alpha^2$ ainsi que les noeuds I à la masse par les conductances $(\frac{1}{\eta\alpha^2}) \Sigma P_{ij} (\omega)$. Ceci n'est réalisable simplement à l'aide d'inductances, de capacités et de résistances que si les éléments non diagonaux de P ont une composante réelle négative et si la somme des éléments de chaque ligne ou colonne possède une composante réelle positive, l'usage systématique des résistances négatives étant interdit par l'encombrement et le coût de ces dernières: le choix de la représentation, toujours effectué en vue d'obtenir la plus grande simplicité possible du réseau, sera affecté par ces dernières restrictions. La donnée (8) étant ainsi traduite analogiquement, les relations (9) peuvent être imposées aux Φ_i comme aux V_i, à l'aide de circuits purement réactifs n'absorbant pas globalement de puissance et se contentant de transmettre cette dernière de manière à ne pas perturber la simulation énergétique. Ces circuits peuvent être constitués par des réseaux en étoile déjà décrits ou par des transformateurs créant des pertes négligeables, compensés de manière à n'emmagasiner qu'une énergie réactive faible en regard de celle qui affecte les autres composants. Enfin la donnée (10) est traduite en harmonie avec la correspondance (6) grâce à l'injection aux noeuds I d'intensités d'amplitude $I_i = F_i/\alpha\eta$. Le comportement en phase et en amplitude du réseau permet alors d'atteindre la solution unique satisfaisant aux données (8), (9) et (10).

On remarquera que la pulsation ω' d'excitation du réseau n'a aucune espèce d'importance dans la mesure où la correspondance (14) reste satisfaite: or, dans certains cas, la loi de variation $P_{ij} (\omega)$ peut être traduite en conservant les éléments du réseau et en variant la pulsation ω' selon une loi $\omega' = f(\omega)$ qui se trouve être dans le cas le plus fréquent une simple proportionnalité. Cette situation confère alors un avantage incontestable au calcul analogique dans la

recherche des fréquences propres des variations continues de toute grandeur en fonction de la fréquence, etc...; ce cas se présente effectivement dans l'étude approchée par une représentation discrète de la propagation à symétrie de révolution ou à caractère bidimensionnel d'un champ électromagnétique en intéraction avec un milieu, homogène ou non, diélectrique ou conducteur à conductibilité réelle ou complexe comme l'est un plasma (XI).
Enfin, il est évident qu'on peut traiter dans l'analogie les données, conjuguées dans le plan complexe, des données (8) et (10), ce qui a pour effet simplement d'inverser les phases relatives. Cette simulation " imaginaire conjuguée " permet d'intervertir le rôle des capacités et des inductances et peut être intéressante pour réduire le nombre de ces dernières.

Tout ce qui précède suppose le choix de la représentation X_i ou V_i effectuée et la connaissance de l'impédance généralisée P_{ij} correspondante. Or, les considérations énergétiques qui viennent d'être effectuées permettent d'envisager une façon plus naturelle et plus physique de procéder.
Elle consiste d'abord à détailler les diverses formes E_l d'énergie qui participent réellement à un échange dans l'oscillation, à la l fois suivant la forme d'énergie et suivant l'élément du système, si ce dernier en comporte plusieurs. Le bilan énergétique du système s'écrit en sommant les puissances associées à chaque forme d'énergie E_l et exprimées à partir des grandeurs conjuguées apparaissant naturellement associées à E_l, soit $pm = \Sigma_l < A_l , B_l >$
Les amplitudes A_l et B_l peuvent être de nature vectorielle et reliées entre elles par une impédance (ou une admittance selon la terminologie adoptée) matricielle, auquel cas le choix de la représentation reste affaire de cas particulier; mais le plus souvent ce sont des scalaires liés par une impédance (ou admittance) scalaire A = CB ou B = C'A. On conçoit alors que le seul impératif dans le choix de la représentation est de pouvoir traduire ou la grandeur A ou la grandeur conjuguée B par une amplitude de potentiel Φ_i ou une différence $\Phi_i - \Phi_j$ qui soit, par définition, en phase ou plus précisément lui corresponde, grâce à un coefficient α réel. Par exemple si $B = \alpha (\Phi_i - \Phi_j)$ la correspondance énergétique sera assurée si

$$pe = \langle C_{ij} (\Phi_i - \Phi_j),(\Phi_i - \Phi_j)\rangle = \frac{1}{\eta} < CB_i,B>$$

c'est à dire grâce à la conductance $C_{ij} (\omega') = C/\eta\alpha^2$ reliant les noeuds I et J du réseau. Le paragraphe suivant illustre cette manière de procéder pour un exemple de phénomène viscoélastique.

EXEMPLE : SIMULATION D'UN CHAMP BIDIMENSIONNEL DE DEFORMATIONS VISCOELASTIQUES D'UN MILIEU HOMOGENE

Nous traiterons le cas de déformations planes subies, à la pulsation ω imposée, par un massif vérifiant,ainsi que le système excitateur,l'invariance $\partial/\partial z = o$ dans un repère cartésien Oxyz. Les déplacements sont alors décrits par leurs seules composantes selon Ox et Oy, $u,v = U,V\, e^{j\omega t}$. Comme précédemment, nous ne retiendrons pour les diverses grandeurs que les amplitudes complexes et les puissances d'échange au temps $t = o$. La déformation est caractérisée par le champ tensoriel

$$(16) \qquad \tilde{\tilde{\varepsilon}}\ (x,y) = \begin{vmatrix} \frac{\partial U}{\partial x} & \frac{1}{2}\left(\frac{\partial U}{\partial y} + \frac{\partial V}{\partial x}\right) & 0 \\ \frac{1}{2}\left(\frac{\partial U}{\partial y} + \frac{\partial V}{\partial x}\right) & \frac{\partial U}{\partial y} & 0 \\ 0 & 0 & 0 \end{vmatrix}$$

et la contrainte par

$$(17) \qquad \tilde{\tilde{\sigma}} = 2\mu\tilde{\tilde{\varepsilon}} + \lambda\theta\tilde{\tilde{I}} \qquad \theta = \varepsilon_{ii} = \frac{\partial U}{\partial x} + \frac{\partial V}{\partial y}$$

où $\lambda = \lambda'(\omega) + j\lambda''(\omega)$, $\mu = \mu'(\omega) + j\mu''(\omega)$ sont les coefficients de Lamé complexes définissant les propriétés viscoélastiques du milieu à la pulsation ω

envisagée. La puissance associée à l'énergie viscoélastique s'écrit en densité volumique:

$$\pi = < \sigma_{ij} , j\omega\varepsilon_{ij} > = < \tilde{\sigma}, j\omega\tilde{\varepsilon}> = < 2\mu\tilde{\varepsilon}, j\omega\tilde{\varepsilon}> + < \lambda\theta, j\omega\theta >$$

$$= < 2\mu \frac{\partial U}{\partial x} , j\omega \frac{\partial U}{\partial x} > + <2\mu \frac{\partial V}{\partial y} , j\omega \frac{\partial V}{\partial y} >$$

$$+ < \frac{\mu}{2} (\frac{\partial U}{\partial y} + \frac{\partial V}{\partial y}), j\omega (\frac{\partial U}{\partial y} + \frac{\partial V}{\partial x}) > + < \lambda (\frac{\partial U}{\partial x} + \frac{\partial V}{\partial y}), j\omega (\frac{\partial U}{\partial x} + \frac{\partial V}{\partial y}) >$$

Le découpage du champ continu en volumes élémentaires reposant sur la surface élémentaire $\Delta x \Delta y$ et l'unité de longueur selon Oz conduit à expliciter de façon approchée la puissance associée à un tel volume à partir des accroissements Δx ou Δy de U,V selon Ox ou Oy sur les longueurs élémentaires Δx ou Δy;

$$(19) \quad \text{p elast.} = \Delta x \Delta y \Big\{ < 2\mu \frac{\Delta_x U}{\Delta x} , j\omega \frac{\Delta_x U}{\Delta x} > + < 2\mu \frac{\Delta_y V}{\Delta y} , j\omega \frac{\Delta_y V}{\Delta y} >$$

$$+ < \frac{\mu}{2} (\frac{\Delta_y U}{\Delta y} + \frac{\Delta_x V}{\Delta x}), j\omega (\frac{\Delta_y U}{\Delta y} + \frac{\Delta_x V}{\Delta x}) > + < \lambda (\frac{\Delta_x U}{\Delta x} + \frac{\Delta_y V}{\Delta y}), j\omega (\frac{\Delta_x U}{\Delta x} + \frac{\Delta_y V}{\Delta y}) > \Big\}$$

De même, la puissance associée à l'énergie cinétique du même volume peut s'écrire, ρ étant la masse volumique

$$(20) \quad \text{p cinet.} = \Delta x \Delta y \ (<-\rho\omega^2 U, j\omega U > + < -\rho\omega^2 V, j\omega V >)$$

ce qui conduit à choisir une représentation analogique par des potentiels associés aux vitesses des déplacements observés aux sommets d'un maillage $\Delta x \Delta y$ dans la co-correspondance

$$\Phi = \alpha \frac{j\omega U}{\Delta x} \qquad \Psi = \alpha \frac{j\omega V}{\Delta y} \qquad p_e = \frac{1}{\eta} (\text{p elast.} + \text{p cinét.})$$

La puissance associée à la maille fondamentale du réseau simulateur devant alors s'écrire, en posant $\gamma = \Delta x/\Delta y$

$$p_e = < \frac{2\mu\Delta x\Delta y}{j\omega\eta\alpha^2} \Delta_x\Phi, \Delta_x\Phi > + < \frac{2\mu\Delta x\Delta y}{j\omega\eta\alpha^2} \Delta_y\Psi, \Delta_y\Psi > + < \mu \frac{\Delta x\Delta y}{2j\omega\eta\alpha^2\gamma^2}$$

$$(\gamma^2\Delta_y\Phi + \Delta_x\Psi), (\gamma^2\Delta_y\Phi + \Delta_x\Psi) > + < \frac{\lambda\Delta x\Delta y}{j\omega\eta\alpha^2} (\Delta_x\Phi+\Delta_y\Psi),(\Delta_x\Phi+\Delta_y\Psi)>$$

$$+ < \frac{j\omega\rho\Delta x^3\Delta y}{\eta\alpha^2} \Phi,\Phi > + < \frac{j\omega\rho\Delta x\Delta y^3}{\eta\ \alpha^2} \Psi,\Psi >$$

On peut préférer utiliser la simulation conjuguée qui permet de réduire le nombre des inductances nécessaires, ce qui conduit au réseau de la figure 1. La représentation choisie permet manifestement de traduire sans difficultés les deux premiers et les deux derniers termes. Par contre, les deux autres exigent de faire appel aux potentiels

$\gamma^2\Delta_y\Phi + \Delta_x\Psi$ et $\Delta_x\Phi + \Delta_y\Psi$

dépendant de ceux déjà retenus et qui peuvent être établis à l'aide de transformateurs compensés. Cette situation justifie le décalage de $\Delta x/2$ et $\Delta y/2$ du maillage des Φ par rapport à celui des Ψ qu'on observe à la figure 1. Le tableau suivant précise la correspondance définissant les conductances et les valeurs des éléments avec lesquelles elles sont réalisées à la pulsation ω' d'excitation du réseau:

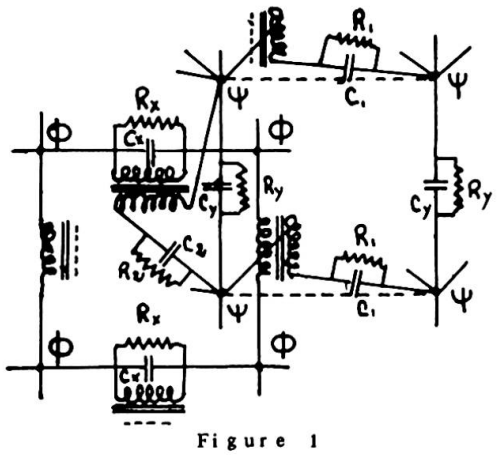

Figure 1

$$2 \frac{\Delta x\Delta y}{\eta\alpha^2} \frac{\mu'-j\mu''}{-j\omega} = jC_x\omega' + \frac{1}{R_x}$$

d'où l'on tire les valeurs de C_x et R_x

$$C_x = \frac{2\mu' \Delta x \Delta y}{\eta \alpha^2 \omega \omega'} \qquad R_x = \frac{\eta \alpha^2 \omega}{2\mu'' \Delta x \Delta y}$$

et de même $Cy = Cx$, $C_1 = \frac{1}{4}\gamma^2 C_x$, $C_2 = \frac{\lambda'}{2\mu' C_x}$

$$Ry = Rx \ , \quad R_1 = 4\gamma^2 R_x \quad R_2 = \frac{2\mu''}{\lambda'' R_x}$$

On peut de même envisager de traiter un champ bidimensionnel correspondant à un phénomène de révolution, par exemple l'attaque par une force oscillante normale à la surface d'un massif semi-infini à gradient d'inhomogénéité également normal à la surface, ce qui présente un grand intérêt pour l'interprétation des sondages acoustiques qu'on opère de cette façon, toutes les fois que les longueurs caractéristiques d'inhomogénéité sont de l'ordre des longueurs d'onde de propagation dans le solide ou inférieures, ce qui rend inopérente l'approximation analogue à celle de l'optique géométrique.

6 - BILAN DE NOS ETUDES CONCERNANT LES STRUCTURES

Nous avons recherché les modèles électriques d'un certain nombre de structures type; nous avons réalisé un certain nombre de ces modèles; nous avons vérifié leur fonctionnement correct; enfin, nous avons apprécié la précision des résultats sur des structures particulières susceptibles d'une analyse mathématique simple ou existant dans la littérature. Cette précision est excellente puisque le plus grand écart que nous ayons observé jusqu'à présent est de 3,4% sur le moment et la flèche au centre d'une plaque circulaire, appuyée sur sa circonférence et uniformément chargée.

Nous avons ainsi étudié un nombre important d'ouvrages actuellement construits. Ces ouvrages sont constitués d'assemblages divers de câbles,de poutres droites ou courbes et de plaques planes de forme quelconque. La disposition des appuis, les conditions d'appui et de chargement peuvent être absolument quelconques. Les modèles permettent la recherche rapide de l'ouvrage optimum, la représentation de la fondation (sol rigide, sol élastique, pieux), l'analyse du comportement en cours de construction (ouvrages en encorbellement), la recherche des réglages à effectuer (haubans, précontrainte, dénivellation d'appuis)...

Nous avons étudié à titre expérimental les vibrations d'une poutre Virendeel, des problèmes d'élasticité plane...

Nous avons étudié, sans réalisation des modèles correspondants, la représentation d'un solide en élasticité à trois dimensions, la représentation des coques, la représentation d'un massif viscoélastique soumis à une oscillation forcée de façon bidimensionnelle.

BIBLIOGRAPHIE

(I) - G. KRON - Tensorial analysis and equivalent circuits of elastic structures (J. Frankl. Inst.t. 238, n°6, 1944, p.399-452)

(II) - F.L. RYDER - The analysis of linear and non linear framed structures (Thesis, New York University, December 1950)

(III) - F.L. RYDER - Electrical analogs of statically loaded structures (Trans.Amer.Soc. Civ.Eng. t. 119, 1954, P. 1046)

(IV) - J. GOETHALS - Calcul analogique de structures hyperstatiques et application au calcul des tuyauteries en expansion thermique (Ann.Assoc.Intern.pour le calcul analogique,t.1,n°2,1958, p.64-74)

(V) - A. ROJAS-LAGARDE et J. SANGUINETTI - Resolucion de sistemas hiperestaticos mediante mediciones en circuitos electricos (Revista Electrotecnica, Buenos-Aires, Octobre 1958, p.389-392)

(VI) - L. MALAVARD et L. GYERGYEK - Calculateur analogique à éléments réactifs pour la résolution automatique des systèmes d'équations algébriques linéaires - (Actes des 3è journées Internationales de Calcul analogique. Presses académiques européennes BRUXELLES 1962, p. 46-51)

(VII) - P. ALAIS ET R. SIESTRUNCK - Sur la résolution analogique des assemblages continus plans de pièces droites. (C.R. Acad. Sc. t.252, 1961, p.1104-1106)

(VIII) - P. ALAIS - Calcul analogique de Systèmes Physiques linéaires. (Journ. de Mécan. Vol. II, n°3, Septembre 1963)

(IX) - P. ALAIS - Simulation du comportement dynamique de structures au moyen de réseaux de selfs et capacités. (Journ. de Mécan. Vol. III, Mars 1964)

(X) - Y. ROCARD - Dynamique des vibrations.

(XI) - P. ALAIS - Calcul analogique du rayonnement d'une antenne à symétrie de révolution en intéraction avec un plasma de rentrée. (Note technique intérieure ONERA)

R E S U M E

Une structure élastique en équilibre statique ou dynamique peut être représentée par un réseau électrique purement réactif; ce réseau est composé uniquement de capacités et de selfs; il est excité à fréquence invariable. Les intensités et les tensions électriques sont respectivement proportionnelles aux déformations et aux efforts subis par la structure représentée.

L'énergie réactive du réseau (énergie capacitive maximum - énergie selfique maximum) est proportionnelle à l'énergie de déformation de la structure (énergie élastique maximum - énergie cinétique maximum dans le cas dynamique).

Model Study of a Prestressed Concrete Box-Girder Bridge Under Thermal Loading

Etude sur modèle d'un pont en béton précontraint à section en caisson, soumis à des variations de température

Modellversuch einer vorgespannten Hohlkastenbetonbrücke unter Temperaturbelastung

M.J.N. PRIESTLEY
Dr.-Ing.
M.O.W. Central Laboratories
New Zealand

1. INTRODUCTION

Stresses are induced in bridge structures by diurnal temperature fluctuations. Although bridges have long been designed with expansion joints to cope with axial deformations due to temperature changes, effects of vertical and horizontal temperature gradients have largely been ignored, or dealt with by over-simplified theories.

The non-uniform temperature distribution induced in bridges by solar radiation has two main longitudinal effects. First, internal stresses are induced due to the non-linear vertical temperature gradient. Second, the increase in temperature of the bridge deck with respect to the soffit temperature results in an upwards hogging of the bridge. If the bridge is continuous, restraint of the upward deflection is provided at the internal supports, and the resulting reactions induce continuity stresses of appreciable magnitude.

Recent examples of distress, particularly in prestressed concrete box-girder bridges have forced engineers to investigate the problem in more detail. In New Zealand, damage to the Newmarket Viaduct, a large urban motorway bridge, caused by vertical temperature gradients, necessitated remedial action costing more than US$300,000. In consequence, considerable interest has been stimulated in New Zealand in thermal stress problems with the result that research projects have been initiated at the University of Auckland, and at the Ministry of Works Central Laboratories, specifically investigating thermal response of box-girder bridges.

Although some measurements made on concrete bridges have been reported (1,2,3) these have been limited in scope. Temperatures have been measured at comparatively few points, and correlations between stress and temperature, deflection and temperature, or theory and experiment do not appear to have been

made. The experimental programme described in this paper is aimed at producing a more comprehensive and cohesive body of data obtained under laboratory controlled conditions.

2. THEORY

Various simplified design methods exist for calculating thermal stresses in box-girder bridges. See References 4 and 5 for example. However, the temperature distributions used are over-simplified, and produce inaccurate results. Further, the simplifications made are unnecessary as consideration of basic equilibrium requirements leads to simple equations capable of handling any form of temperature distribution for any section shape.

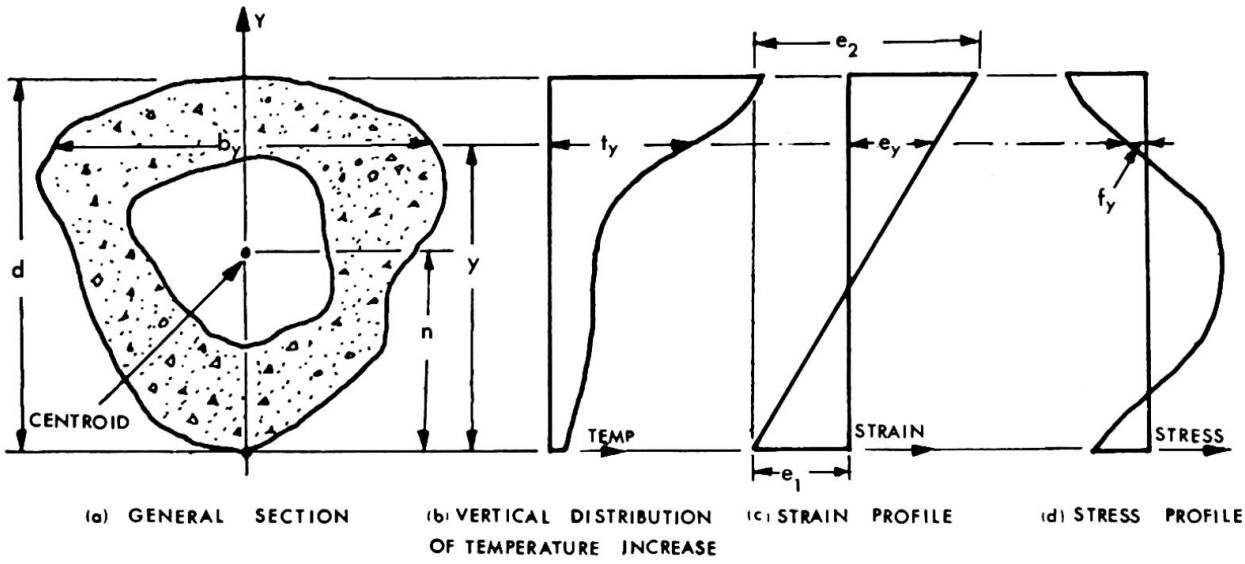

FIG 1. GENERAL SECTION WITH ARBITRARY VERTICAL DISTRIBUTION OF TEMPERATURE

Consider Fig.1 where an arbitrary section shape (Fig.1a) is subjected to an arbitrary vertical temperature distribution, (Fig.1b). Assuming the Euler-Bernoulli 'plane sections' hypothesis holds, the final vertical distribution of longitudinal strains will be of the form shown in Fig.1c. The stress induced by the temperature increase t_y will be given by

$$f_y = E(e_1 + e_2 \frac{y}{d} - \alpha.t_y) \quad \ldots\ldots\ldots\ldots\ldots\ldots \quad 1$$

Consideration of longitudinal force and moment equilibrium leads (6) to the following equations

$$e_1 + e_2 \frac{n}{d} = \frac{\alpha}{A} \int_0^d t_y.b_y.dy \quad \ldots\ldots\ldots\ldots\ldots\ldots \quad 2$$

$$\frac{e_2}{d} = \frac{\alpha}{I} \int_0^d t_y(y-n)b_y.dy \quad \ldots\ldots\ldots\ldots\ldots\ldots \quad 3$$

where α is the linear coefficient of thermal expansion, A is the

cross section area, and I is the moment of inertia about the horizontal axis through the centroid.

Solution of equation 3 directly yields the curvature of hogging. Substitution into equation 2 and solution provides the second unknown, e_1. Finally substitution of e_1 and e_2 into equation 1 produces the internal stresses. For a continuous bridge the additional stresses induced by continuity may be found by calculating (a) the notional deflections induced at the internal supports by the curvature e_2/d, (b) the forces necessary at the internal supports to reduce these notional deflections to zero and (c) the moments and stresses induced by these forces.

3. THE MODEL

3-1 MODEL DIMENSIONS

A model study offered the advantages over a full-scale prototype site investigation of a controlled rather than an unpredictable thermal input, an accelerated time scale, the separation of thermal effects from other load cases, reduced cost, and ease of instrumentation and data acquisition. A typical single-cell trapezoidal box-girder section was chosen for the model. The section, whose prototype dimensions are given in Fig.2, is typical of many urban motorway off-ramps in New Zealand.

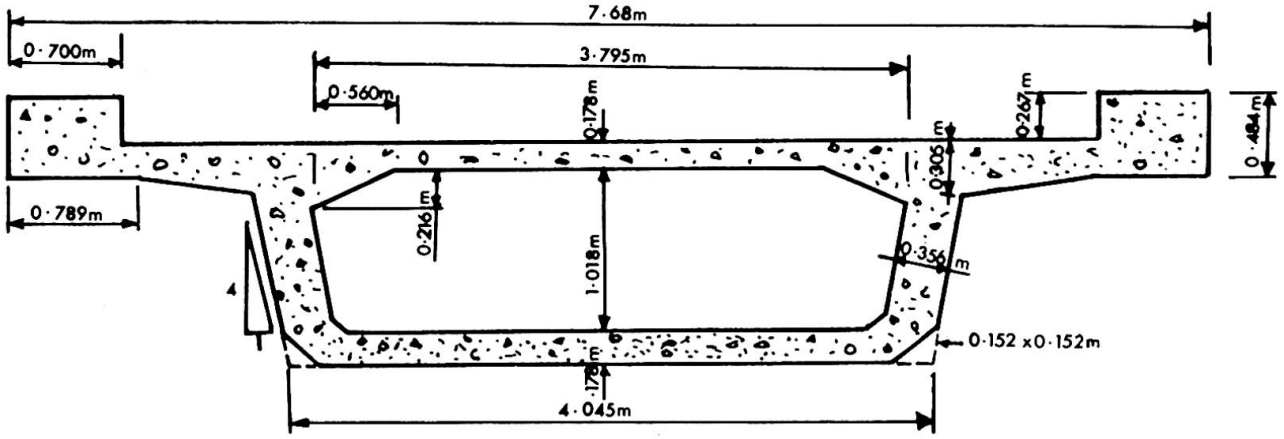

FIG.2. PROTOTYPE SECTION DIMENSIONS

A quarter-scale model representing a simply supported span of 30.5m was chosen. The scale was dictated by the physical size of the strong-floor testing area available, and by the availability of suitable steel to model mild-steel reinforcing. Fig.3 gives the overall model dimensions.

3-2 MODEL MATERIALS

The model was cast in six 1.22m segments with two solid 0.305m end diaphragms. This segmental form of construction was chosen to facilitate placing straingauges and temperature transducers. Each segment weighed about 570Kg. and was cast from a scaled concrete mix designed to have a 28 day cylinder crushing strength of $41.3 N/mm^2$. Maximum aggregate size was 4.75mm, and slump was between 50 and 75mm. Eighteen 300mm x 150mm dia. cylinders were cast with each segment and cured under the same conditions as the model, to provide sufficient control specimens

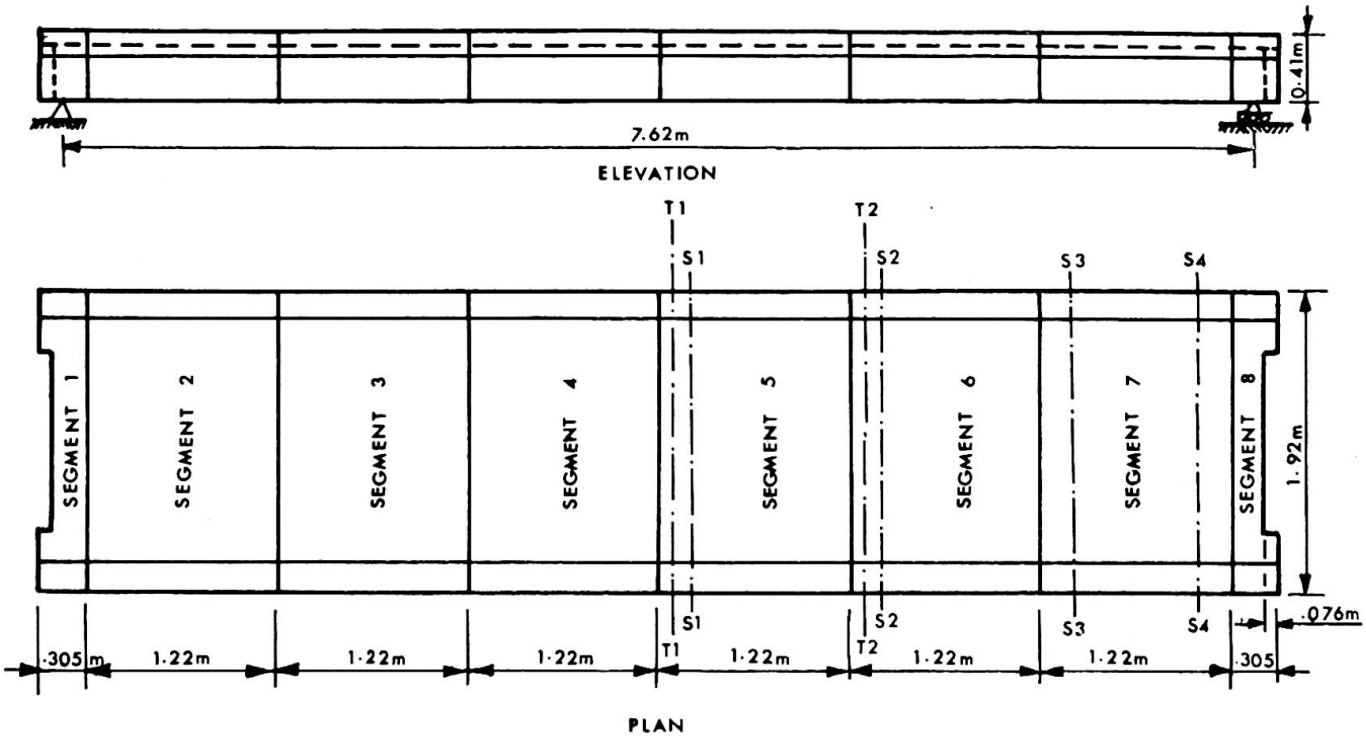

FIG 3. MODEL DIMENSIONS

for all stages of the testing programme.

Typical mild-steel reinforcing was included in the model by use of 4.83mm and 3.18mm dia. black annealed tie-wire, and 6.35mm dia. mild steel rod.

The model was prestressed by ten draped cables; five in each web. A BBR system was used which gave a cable force of 142N after transfer, and an average prestress of 4.16N/mm^2. At the centre of the bridge theoretical prestress stresses varied between 0.57N/mm^2 tension at the curbs to 10.23N/mm^2 compression at the soffit.

The eight precast concrete sections forming the model were glued together using an epoxy mortar. Requirements for this mortar were that it should have a high compression strength, a high modulus of elasticity, should gain strength rapidly, should stick to a vertical surface without slumping, should 'wet' the surface and should have a similar colour to the concrete. A mix based on CIBA's Araldite AW103/Hardener HY956 was adopted. Mix proportions were AW103:HY956:Silica Sand:Talc = 1.00:0.19:3.0:1.0. This mix produced 24 hr. cylinder strengths of about 40N/mm^2 with a 28 day cylinder strength in excess of 60N/mm^2. Modulus of elasticity exceeded 1.24 x 10^4N/mm^2 at 28 days.

3-3 INSTRUMENTATION

Electric resistance straingauges, resistance thermometers and thermocouples, and straingauged deflectometers were used to measure strain, temperature and deflection of the model. Because of symmetry it was only necessary to gauge one quarter of the bridge and use a few additional gauges to ensure that behaviour was in fact symmetrical. Fig.4a shows the distribution of straingauges at

each of sections S1 to S4 defined in Fig.3. In addition to these gauges, a large number were located in the vicinity of one end of the model to check the distribution of prestress stresses. These have been reported elsewhere (7).

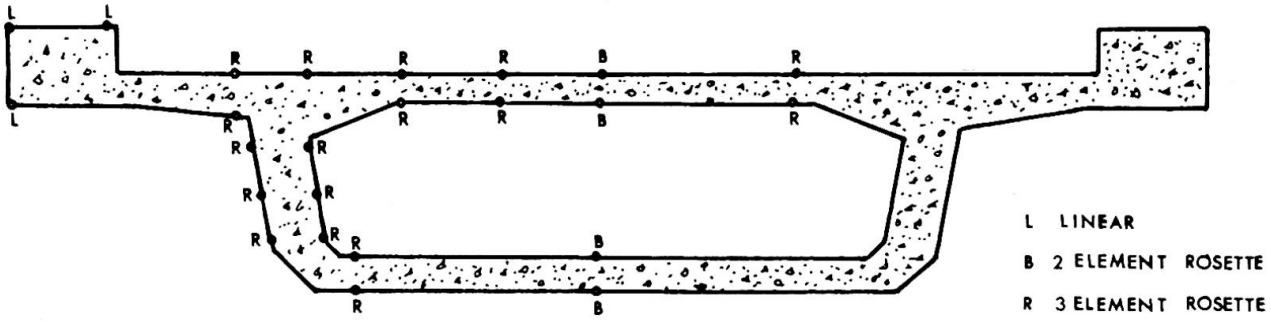

(a) STRAINGAUGE POSITIONS SECTIONS S1 TO S4

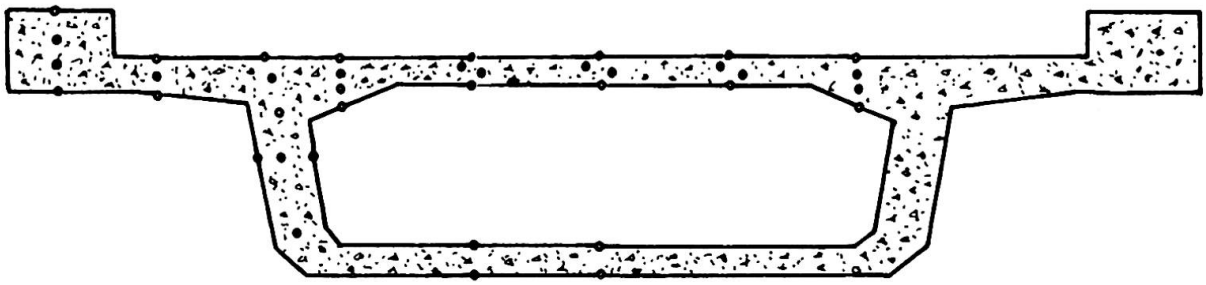

(b) THERMOMETER POSITIONS SECTIONS T1, T2

FIG 4. INSTRUMENTATION FOR THERMAL – LOAD TESTS

In Fig.4a L denotes a linear Kyowa KF-20-C8-11 foil straingauge, B denotes a two-element 90° Kyowa KP-20-B2-11 rosette and R denotes a three-element 90°-45° Kyowa KP-20-B3-11 rosette. All gauges had a gauge length of 20mm, and had transparent backings to ensure that gauge and concrete colours would be as close as possible, resulting in equal absorption of radiant energy. In all, 560 straingauge elements were fixed to the model.

Resistance thermometers and thermocouple positions at sections T1 and T2 of Fig.3 are shown in Fig.4b. The gauges were located in holes drilled 75mm into the ends of the segments prior to gluing. A mortar slurry was used to fill the holes after placing the gauges. Further thermocouples were distributed over the deckslab surface to provide a means for checking the uniformity of surface temperature.

Vertical deflections were measured by straingauged deflectometers on the soffit at nine points along the longitudinal centreline. All data was monitored by a 200 channel Dynamco Datalogger and recorded on paper tape at a rate of two channels/sec. Since the number of gauges greatly exceeded the capacity of the datalogger it was necessary to duplicate tests with different batches of gauges. Data reduction by computer required the minimum of control data and enabled data manipulation by matrix commands through free-format programming.

4. THERMAL LOADING

For the thermal load tests the model was enclosed within a controlled environment box consisting of sides and top of soft-board surfaced with insulating paper covered with aluminium foil. One hundred 375 watt infra-red light bulbs fixed to the ceiling of the box were connected into eight separate banks, each producing a uniform heat pattern on the deckslab of the model. Consequently the radiant intensity applied to the model could be controlled in a step-wise fashion. Convective cooling of the top surface was provided by two 457mm diameter propeller fans located at one end of the environment box, capable of producing a 3m/sec wind along the bridge deck. When forced cooling was required the end wall of the box opposite from the fans was removed and an exterior roller-door was opened, allowing the hot air contained by the box to be exhausted to atmosphere.

In all tests the model was subjected to a cycle representing four consecutive days of identical heat input and cooling. Heating and forced cooling were controlled for the first day to produce deckslab temperatures corresponding with surface temperature cycles recorded by Dickinson (8,9) on Australian bituminous concrete surfaces. This pattern of heating and cooling was then repeated for the next three days. Examination of the scaling laws for thermal loading (10) indicates that for identical prototype and model materials a model:prototype time scale equal to the square of the length scale is required to produce model: prototype temperatures and stress scales of unity. Consequently a prototype diurnal cycle required a model duration of 90 minutes, and the four-day cycles represented required only 6 hours continuous testing.

Fig.5 shows a photograph of the model within the environment box.

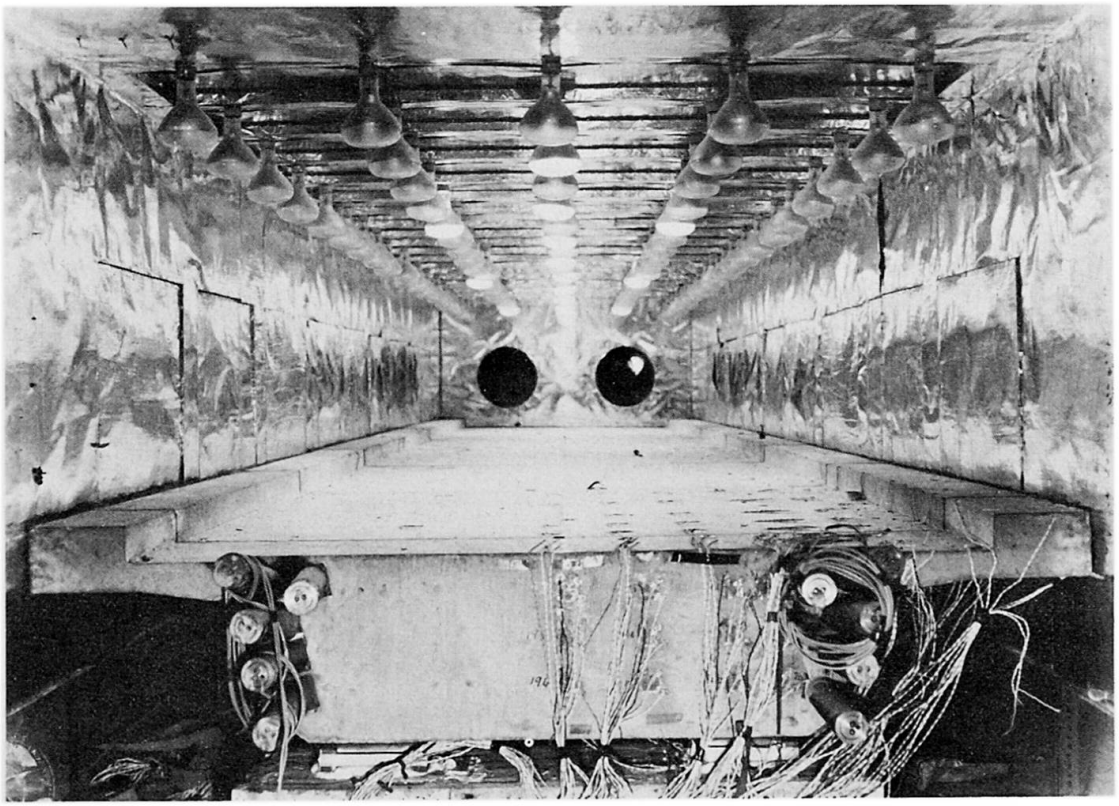

Fig.5 QUARTER SCALE MODEL IN ENVIRONMENT BOX

5. RESULTS

5-1 THERMAL RESPONSE OF MODEL

Fig.6 shows heat input:time and typical temperature:time curves in prototype time scale for a simulated four-day test cycle. As will be seen the heat input, which has only been expressed as a percentage of the maximum heat input was identical for the four days. Temperatures are all arbitrarily referred to a base of 20°C.

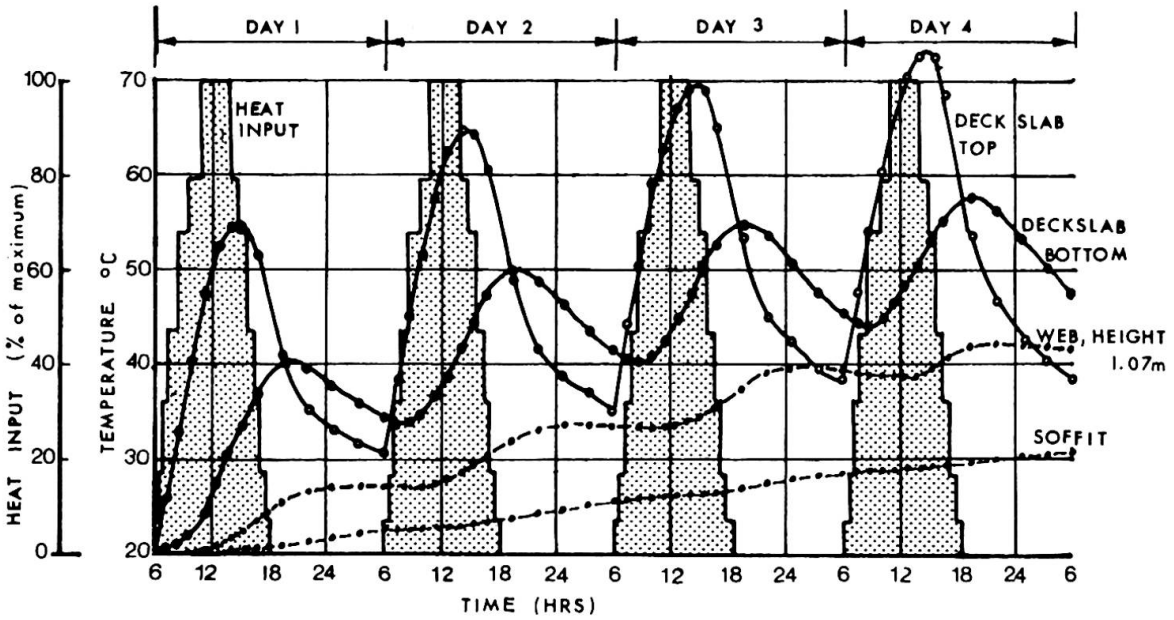

FIG. 6 TYPICAL THERMAL RESPONSE FOR 4-DAY CYCLE

Despite the convective cooling of the deckslab provided by the 3m/sec wind the peak temperatures continued to rise throughout the four-day cycle. This was particularly the case for the deckslab above the enclosed air cell where temperatures rose to higher values than in the concrete above the webs or in the cantilevered areas. The temperature above the enclosed air cell also dropped more slowly in the cooling periods, than in the other areas. This behaviour appears to result from the insulating behaviour of the entrapped air cell. There was more resistance to vertical heat flow from the bottom of the deckslab into the stagnant air mass than down the concrete webs, hence the higher temperatures above the air cell. Total heat stored will be similar in the volume below any given area of surface. In the cooling cycle heat could flow up and down the webs away from maximum temperature areas, whereas above the air mass heat flow would mainly be vertically up, away from the air mass, and therefore temperatures remained higher longer in the deckslab area above the air mass. This is illustrated by comparing the temperature profiles

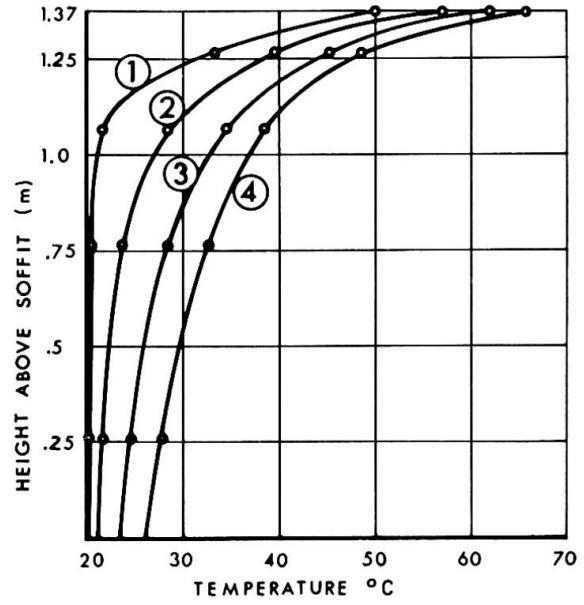

FIG. 7 TEMPERATURE PROFILES DOWN WEB AT 14:00 HRS ON 4 SUCCESSIVE DAYS

down the web, as shown in Fig.7, with the peak values in Fig.6. Fig.6 indicates a maximum deckslab temperature, above the air cell, of 73°C on the fourth day, in comparison with a peak of 66°C above the webs, as indicated in Fig.7.

5-2 COMPARISON BETWEEN THEORY AND EXPERIMENT

In order to compare experimental deflections and stresses with those predicted by Equation 1 to 3 above, temperatures measured at the positions shown in Fig.4b were used to define the temperature distribution t_y. The section of the model was considered to be divided into a number of different areas, each of

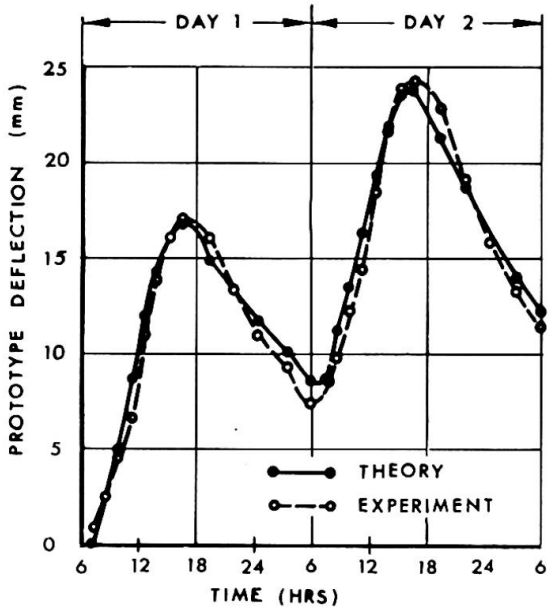

FIG. 8 CENTRAL DEFLECTION vs TIME

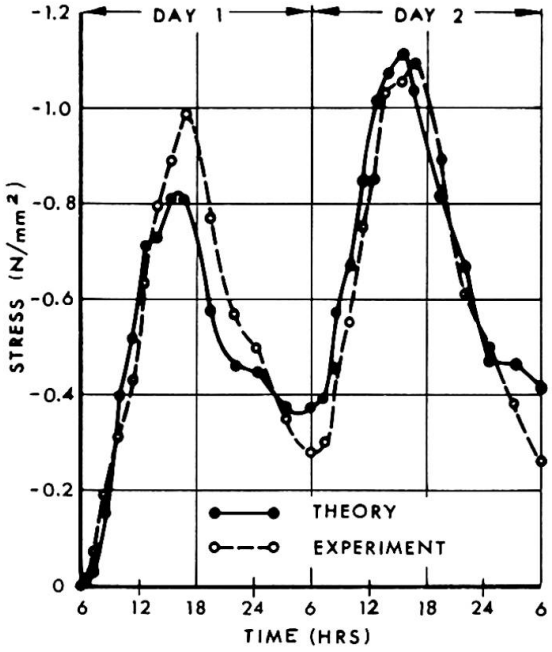

FIG. 9 SOFFIT STRESS vs TIME

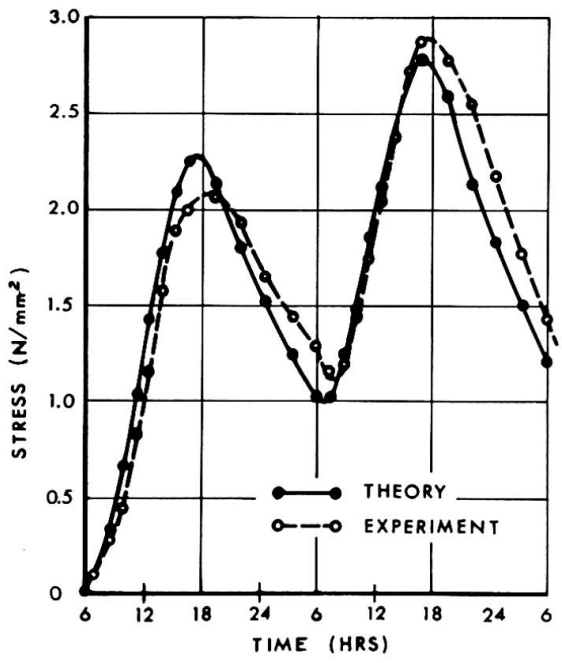

FIG. 10 WEB STRESS vs TIME at Height=870 mm

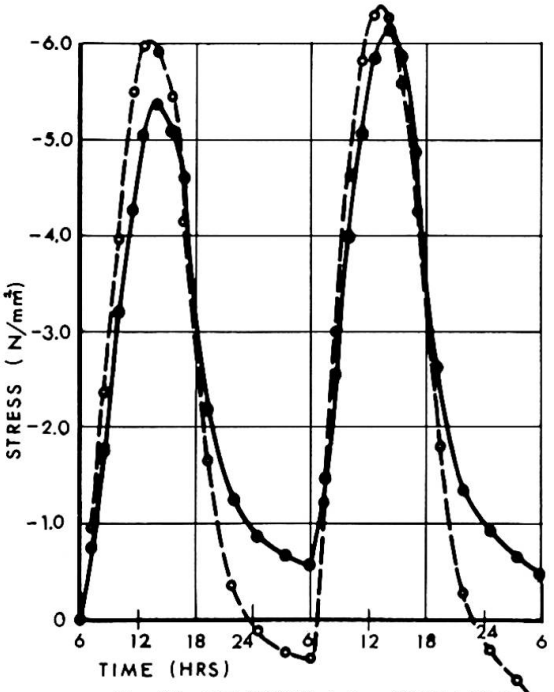

FIG. 11 DECKSLAB STRESS vs TIME

which contained a temperature transducer. At any given time the temperature indicated by a particular gauge was considered to be constant throughout the relevant area. Equations 1 to 3 were put into summation rather than integral form and solved by computer, which produced graphs of theoretical central deflection, and stress at salient points versus time, for the four-day cycles. These were then compared with experimental values.

In predicting the theoretical behaviour, experimentally obtained values for the coefficient of thermal expansion and modulus of elasticity of $10.65 \times 10^{-6}/^{\circ}C$ and $2.34 N/mm^2$ respectively, were used.

Figs. 8 to 11 show comparisons between theory and experiment for central deflection, soffit stress, deckslab stress, and web stress at a prototype height of 870mm above the soffit. In all cases only the first two days of the four-day cycle have been compared. Time is expressed in prototype scale, and the stress convention used is tension positive, compression negative.

Fig.8 indicates excellent agreement between theoretical and experimental deflections. The agreement between theoretical and experimental stress shown in Figs.9 to 11 is also good, and is in general within the expected experimental accuracy of $\pm 0.2 N/mm^2$. However, Fig.11, which shows deckslab stresses, exhibits much higher discrepancies, though experimental and theoretical curve shapes are very similar. It is thought that the discrepancy is largely due to the difficulties in obtaining accurate strain readings on the surface of the deckslab. Although the strain-gauges were compensated for a thermal coefficient of expansion of $10.8 \times 10^{-6}/^{\circ}C$, the differences in surface colour of the gauges and concrete deck may have induced artifically high temperatures in some gauges. Nevertheless, in all cases the predicted stresses exhibit satisfactory agreement with experimental values.

It is of interest to calculate the continuity stresses that would have been induced in the model if it had had a central support. At 16:30 hrs. on the second day of the thermal cycle, the central displacement was 24.2mm. If this displacement were restrained by an internal support, stresses of $3.40 N/mm^2$ compression at the top of the deckslab and $6.95 N/mm^2$ tension at the soffit would be induced. These should be added to the internal stresses indicated by Figs.9 and 11 to give final stresses of $7.60 N/mm^2$ compression at the deckslab and $6.15 N/mm^2$ tension at the soffit.

6. DISCUSSION AND CONCLUSIONS

The results presented above show that equations developed from consideration of simple statics accurately predict longitudinal stresses and curvatures in box-girder bridges. Transverse stresses resulting from restrained transverse expansion and hogging of the deckslab can also be of significant magnitude and should always be considered in design.

The temperatures induced in the model and reported herein represent extremely severe conditions. Although the surface temperatures sustained on the first day of the four-day cycle compare with those reported by Dickenson (8,9), the rather low wind velocities and the lack of forced cooling on the soffit during the cooling periods of each cycle will tend to make the

temperatures on the successive days artificially high.

At this stage of testing, the model has only been tested with a bare concrete deckslab. Further series of tests with a scaled bituminous wearing surface, and finally with a white painted surface will be carried out to investigate the influence of surface colour on thermal response. This model study is to be followed by a comprehensive prototype investigation into thermal stresses in a two-span three-cell prestressed box-girder bridge.

ACKNOWLEDGEMENTS

The permission of Mr J.Macky, Commissioner of Works and Mr J.H.H.Galloway, Laboratory Services Engineer, to publish this paper is acknowledged as is the advice and encouragement given by Mr J.B.S.Huizing, Chief Designing Engineer, M.O.W. Civil Engineering Division.

REFERENCES

1. CAPPS, M.W.R. 'The Thermal Behaviour of the Beachly Viaduct/ Wye Bridge', Road Research Laboratory. Report LR 234, 1968.
2. LEE,D.J. 'Western Avenue Extension - The Design of Section 5', The Structural Engineer, March 1970 No.3 v48.
3. New Zealand M.O.W. - Auckland District Testing Laboratory - Reports on Newmarket Viaduct Temperatures, 1970.
4. M.O.W. Civil Eng. Division - 'Bridge Design - Temperature Gradient' M.O.W. Head Office, March 1970.
5. MAHER, D.R.H. - 'The Effects of Differential Temperature on Continuous Prestressed Concrete Bridges', Institution of Eng. Aust. Concrete Conference 1969.
6. PRIESTLEY, M.J.N. 'Effects of Transverse Temperature Gradients On Bridges' M.O.W. Central Laboratories Report No.394, October 1971.
7. PRIESTLEY, M.J.N. 'Structural Model of a Prestressed Concrete Box Girder Bridge - Phase 1 : Manufacture and Prestressing', M.O.W. Central Laboratories Report No.388, July 1971.
8. DICKINSON, E.J. 'Temperature Conditions in Bituminous Concrete Surfacings - Melbourne', Aust.Road Research Vol.3 No.9. March 1969.
9. DICKINSON, E.J. 'Temperature Conditions in Bitumen Concrete Surfacings - Sydney' Aust. Road Research Vol.3 No.9, March 1969.
10. ROCHA,M 'Structural Model Techniques - Some Recent Developments', Memoria No.264, L.N.E.C. Lisbon 1965.

SUMMARY

A quarter scale prestressed concrete model of a single cell trapezoidal box-girder bridge is described. The principal aim of the study is the investigation of structural response to diurnal temperature fluctuations. Results of temperatures, stress and deflections induced by thermal loading are reported. Good agreement is obtained between experimental stresses and deflections and values predicted by a theory based on simple equilibrium criteria.

Roof Structure of the New Hangars by the International Fiumicino Airport (Rome) (Design, Model Tests)

La structure des nouveaux hangars à l'aéroport international de Fiumicino (Rome) (Projets, essais sur modèle)

Dachausbildung der neuen Hallen im internationalen Flughafen von Fiumicino (Rom) (Entwurf, Modellversuche)

RICCARDO MORANDI
Prof. Ing.

FRANCESCO PICCARRETA
Dott. Ing.

Istituto di Scienza delle Costruzioni
Facoltà di Ingegneria
Università degli Studi di Roma, Italy

1) DESIGN

1.1) General (Introduction)

The new structure, including workshops and stores, recently accomplished at the "Lennardo da Vinci" Airport in Fiumicino (Rome) is mainly developping all around the two main hangars designed for the housing and maintenance of the new jet Boeing 747. Actually the hangar shape and size perfectly cope with the shape of the aircrafts. This peculiarity guided the design towards the realization of large entrance openings, while on the opposite side the structures have been adequately reduced down to a large protruding "corridor" in which the bow of the aircrafts finds its place. Such solution has allowed the siting of shops, stores and operating centres in the back, also using the space resulting between the two corridors of both hangars.

As far as the vertical dimensions of the two hangar rooms are concerned, the great height of the B747 vertical rudder size has guided to a dissymmetric roof structure reaching its highest point at the entrance side, see in correspondence of the jet tail.

1.2) The Hangars

Each hangar consists of two adjacent rooms of different shape:

- one back room (the before mentioned "corridor") housing the aircraft bow, parallelepiped like, 45,00 m in length, 20,00 m in width and 16,40 m in height;
- one front room, housing the bow central and back part, the wings and tail; 78,25 m wide, 74,50 m long and varying in height from 20,00 m to a max of 30,00m.

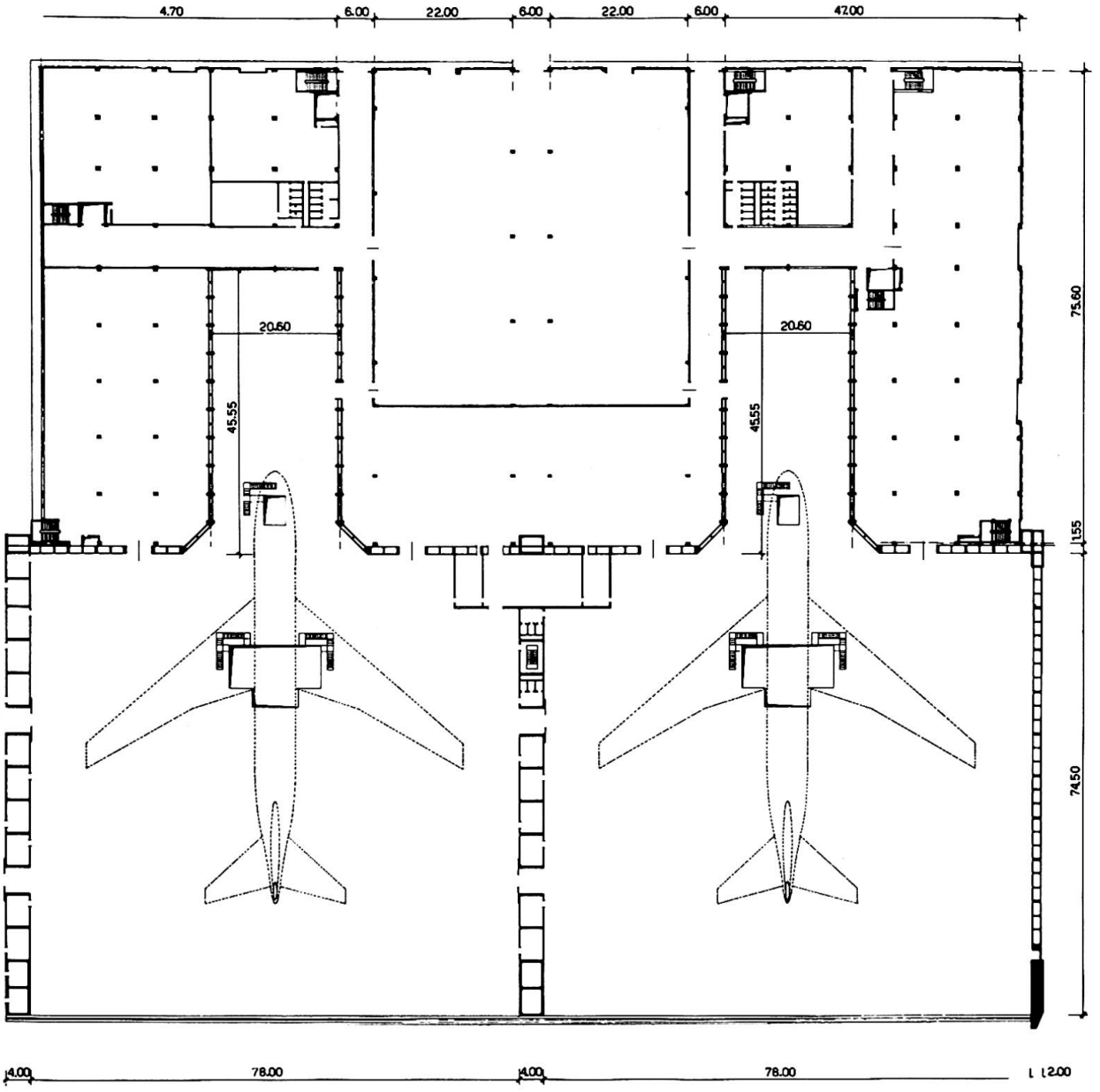

Fig. 2 Plan

The two rooms are closed all around by means of reinforced concrete walls, with exception of the entrance wall consisting of a large sliding door. The walls have also a static function: in effect they transfer to the foundations all actions originated by the roof.

The rear room has a flat ceiling consisting of a number of parallel prestressed concrete beams spaced 4,50 m and joined by precast concrete slabs.The main roof, on the contrary, is made by a steel concrete suspension structure anchored by

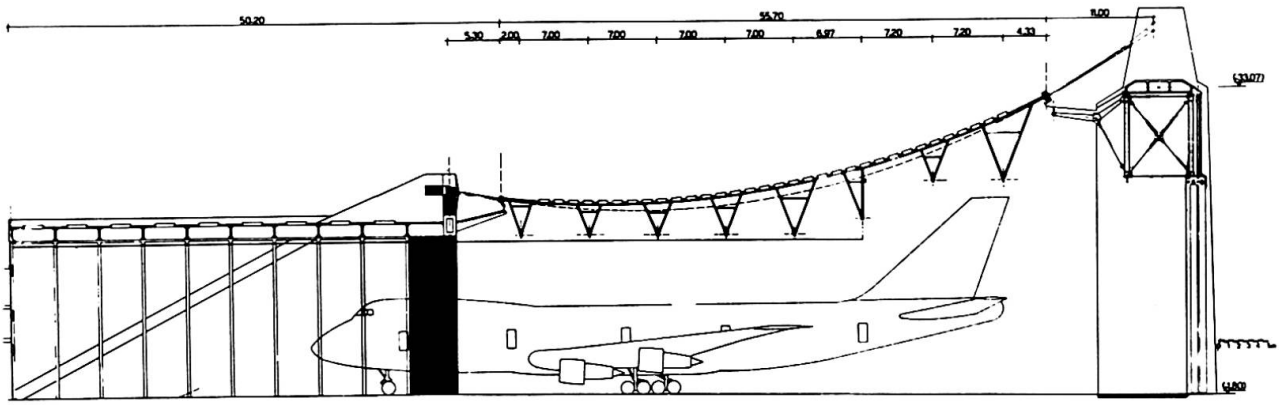

Fig. 3 Longitudinal section

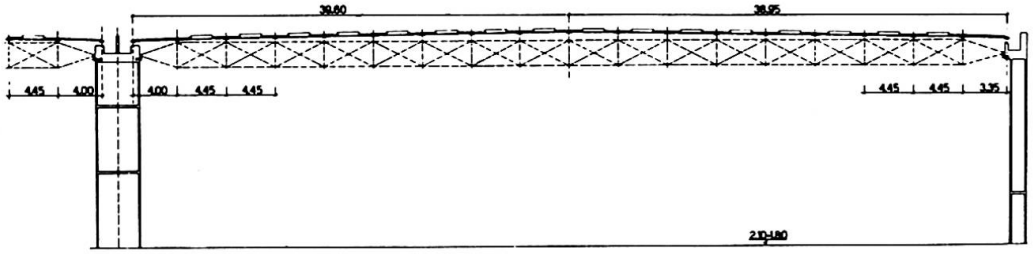

Fig. 4 Transversal section

means of ties to the walls at points A,B,C,F,G,H,(see Fig. 4 and 5).

In correspondence of these points are transmitted vertical and horizontal forces to the walls either longitudinally and transversally. All these forces are transferred to the foundations either through the walls themselves and through the transversal connections. In effect on the front plan are placed two connections: one at pavement level, consisting of a prestressed concrete beam resting on the ground; the other, at 31,00 m of height consists of a reinforced concrete box compression strut resting on a truss steel girder which, at the same time, gives support to the large sliding door.

In the back, the transversal connection is given partially by the rear concrete walls and partially by a reinforced box beam, placed between points C and F.

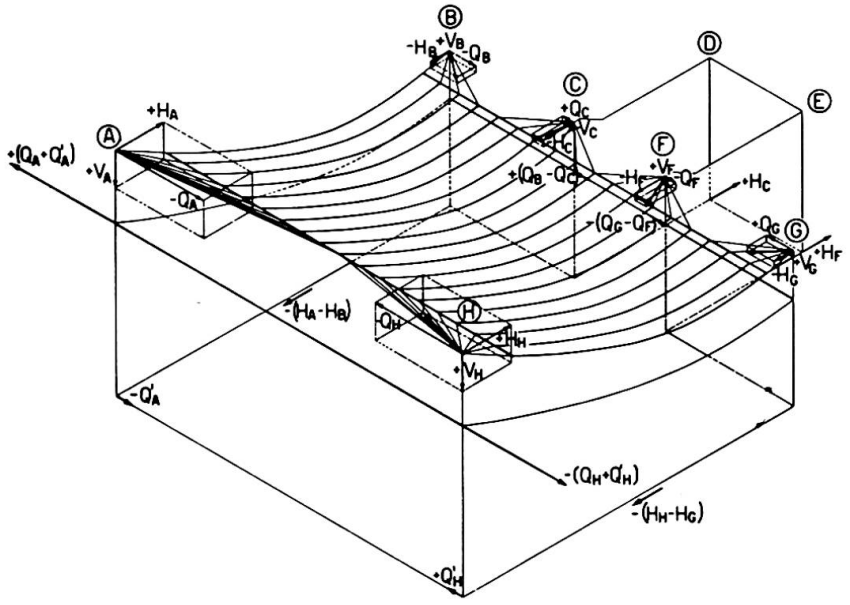

Fig. 5 Static schema of the structure.

1.3) The suspension roof

The roof structure of each hangar consists of 19 prestressed concrete cable-like members, directly supporting the roof plates and linked, at both ends, to two transverse beams also of prestressed concrete of variable cross section.

The resistant members and transverse beams are, then, linked to the walls by means of two series of prestressed concrete tendons fanning out from points A and H in the front, and from points B,C,F and G in the rear. The whole suspension structure, whose structural members are the cable-like members, the cross beams and the fans of tendons, is represented in Fig. 6.

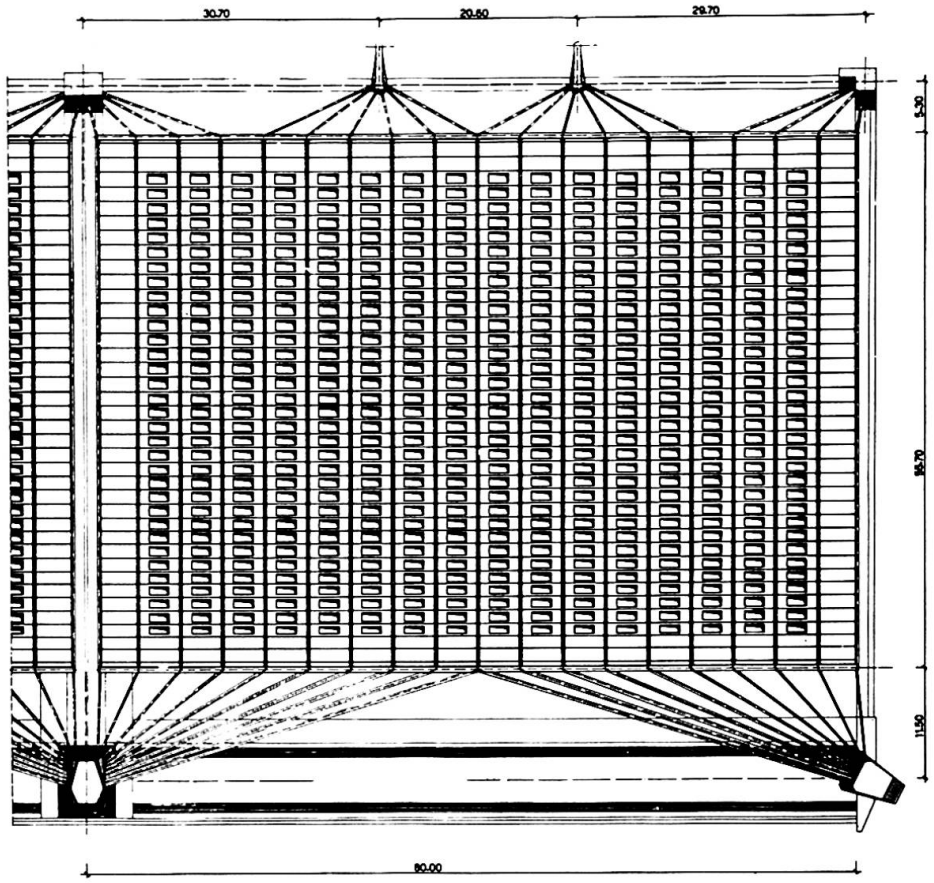

Fig. 6
Plan of the roof

The cable-like members (40x15 cm) are spaced 4,45 m and support the pre-cast roof plates. These plates allow also the light to pass through because of a central rectangular hole covered by a dome of acrylic resin. Each cable-like member is prestressed by means of three high tensile steel tendons consisting of eight 1/2" strands each. The fanning tendons are also of rectangular cross section: moreover, owing to the different values of the forces to which they are subjected, both the cross section and the number of prestressing cables are different from tendon to tendon.

The two end cross beams are sited in correspondence of the joints between cables and ties. Both beams are horizontal and present a rectangular section which is constant for the rear beam and variable for the front beam. Right more cross-beams are hanging from the roof. They are truss steel beams of triangular section with two upper and one lower chord; such beams are intended to distribute along the roof the heavy concentrated loads of the bridge cranes. The

ten cross beams provide a very efficient connecting action between the cable-like members of the roof.

The suspension structure is in the shape of the catenary of the dead load with different values of the tension in the various cable-like members. These members owing to their small thickness as referred to their length, can be considered perfectly flexible, that is, without flexural rigidity, and so they can undergo any change in their center-line curve.

It has to be pointed out that the structure is a one-way system of cables: therefore, the stability of the roof against the wind suction is due to the dead weight only, which is considerable because the plates of the actual roof are also made of concrete. Hereunder are given some values on the design loads:

- dead load of the roof including plates, cables, cross beams, crane beams, 230 kg/m^2;
- overload 120 kg/m^2;
- wind load 100 kg/m^2.

1.4) Construction techniques

It has been already told that the initial tensile structure is in the form of the dead load catenary, for given values of the stresses in the various members. For the erection was used a steel tube scaffolding, following the structure shape, which supports the whole roof. Then the prestressed elements have been subjected to tensioning beginning from the cable-like ones, then the cross and finally the fan-like tendons.

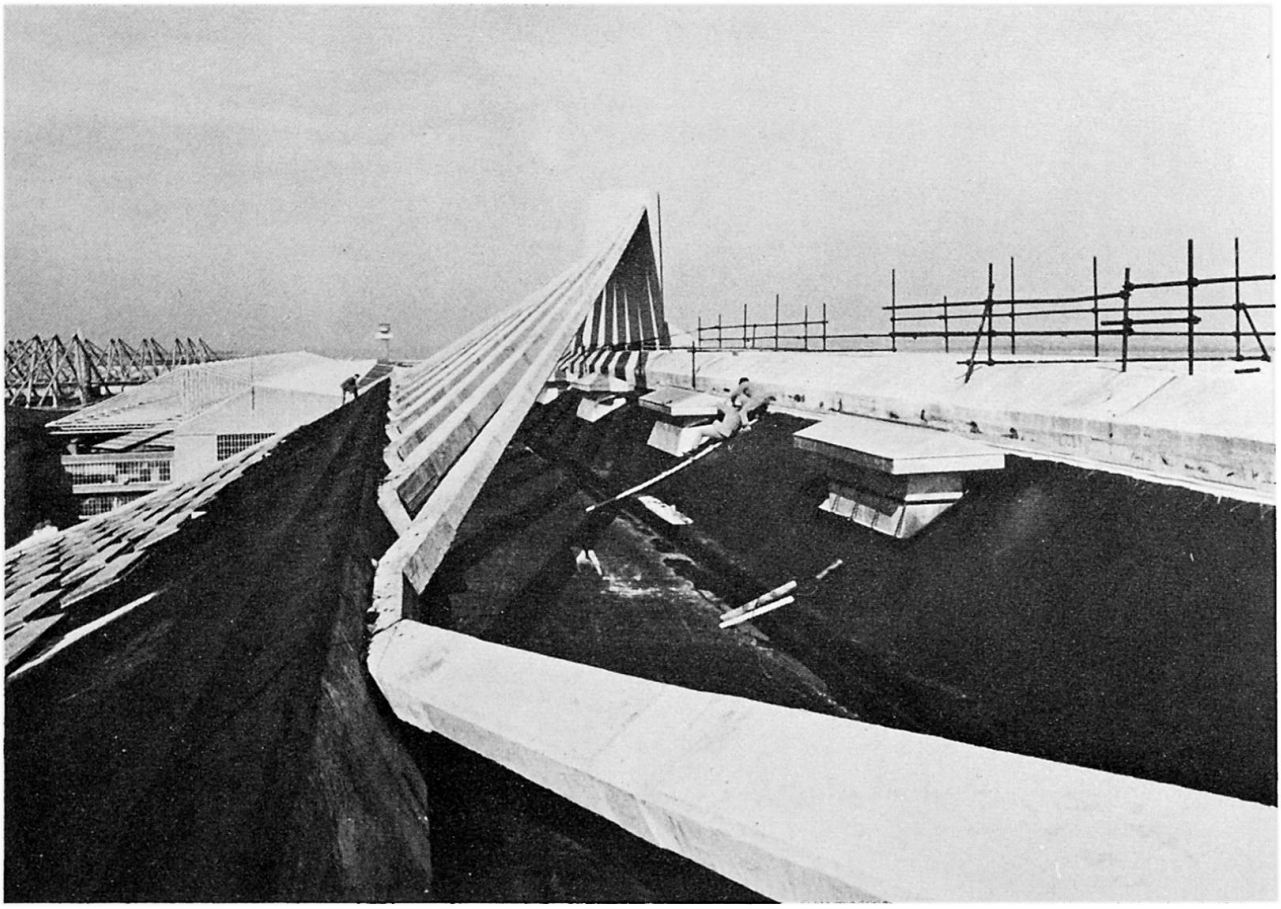

Fig. 7 View of the fan-like tendons.

2) TESTS ON MODEL

2.1) General characteristics

As it has been previously pointed out, the actual structure is composed of prestressed concrete members, precast concrete plates and steel trusses. In the model the corresponding elements were made respectively of steel, aluminium and an aluminium alloy called anticorodal.

The same alloy was used for the two cross beams.

The reasons of the heterogeneous choice of materials follows from the requirements due to the similitude laws, as well as the technical ones (assemblage) and the necessity of having, in the proper places, space enough for applying the straingauges.

In order to establish the sizes of the model various elements, following the mechanical similitude, it has been assumed the value 0.35×10^6 kg/cm^2 for concrete in the actual structure; 2.1×10^6 kg/cm^2 for the steel elements of the model, and $E = 0.7 \times 10^6$ kg/cm^2 for the aluminium ones. The anticorodal modulus of elasticity was determined by preliminary tests on the actual laminates which were to be employed in the model.

As far as the various structural member sizes are concerned, the mechanical similitude laws have been taken into account starting from the representative equations of the problem. If ϕ is the force-ratio and λ is the length one, we obtain the following relationships:

$$\sigma_m = \frac{1}{\lambda}\sigma^* \quad ; \quad A_m = \frac{1}{\phi}\frac{E^*}{E_m} A^* \quad \text{(tendons)}; \quad I_m = \frac{I}{\phi\lambda^2}\frac{E^*}{E_m} I^* \text{ (beams)}$$

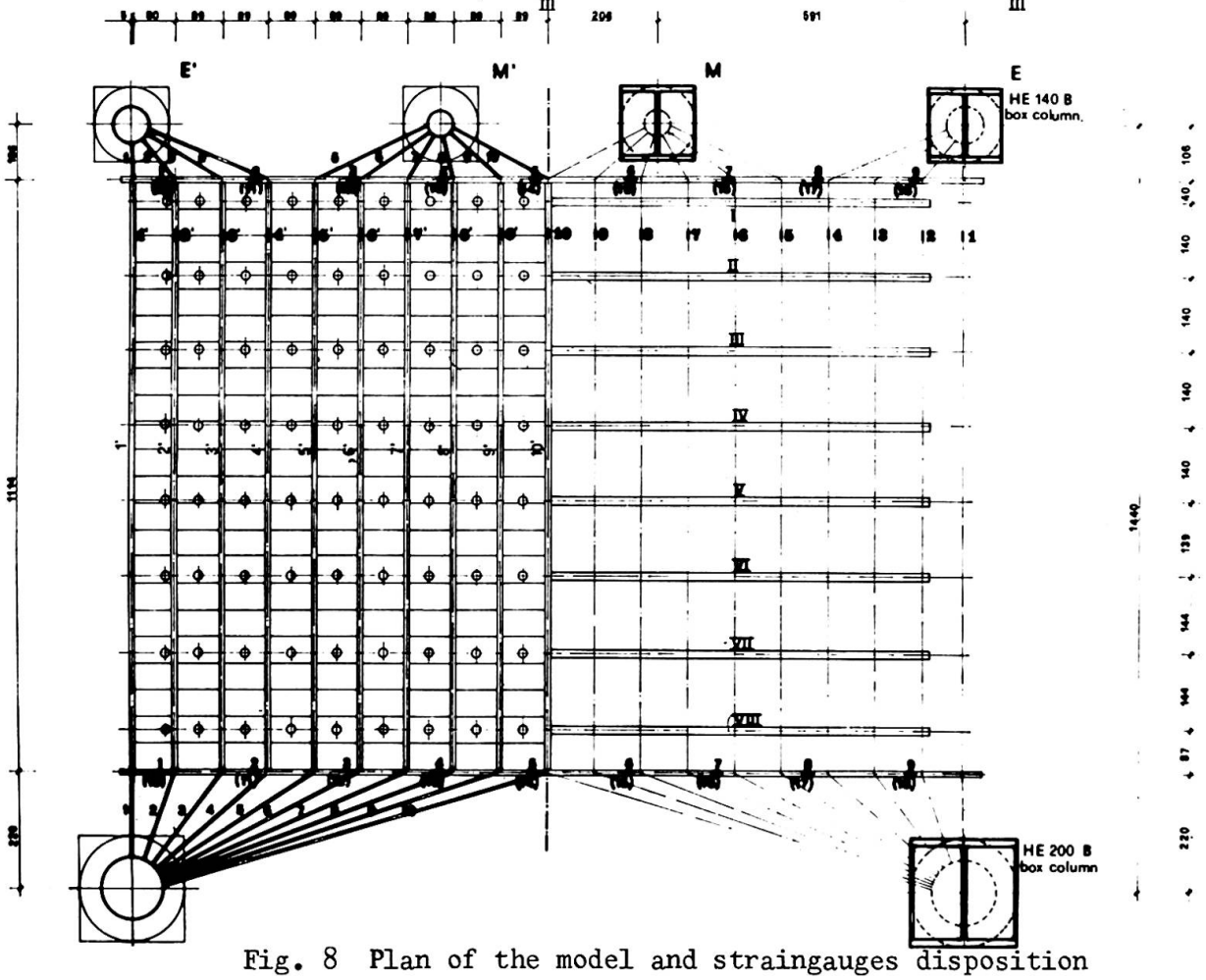

Fig. 8 Plan of the model and straingauges disposition

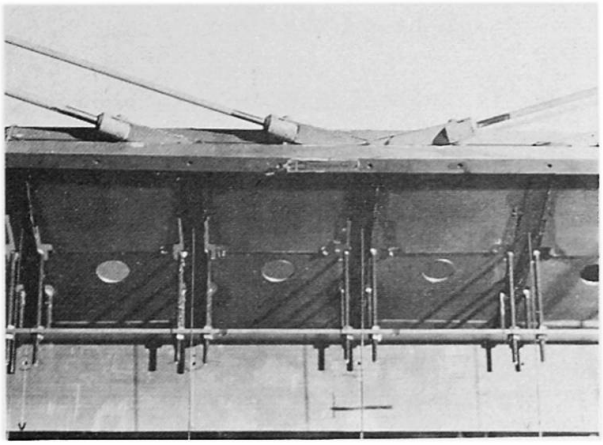

Fig. 9 Model detail

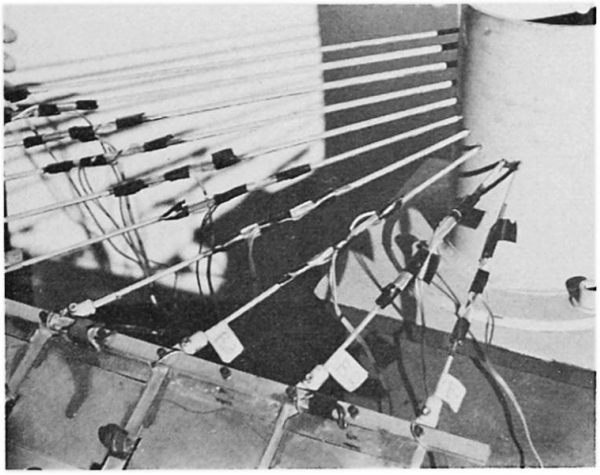

Fig. 10 Model:anchorage of the fan-like tendons

given the size of the actual structure, it has been considered convenient to assume the values: $\lambda=50$ and $\phi=2{,}200$ from which follows the ratio for the cross sections in tension (cables and tendons):

$$\frac{A^*}{A_m} = 13{,}200$$

The section has been chosen rectangular, 0.5mmx11.0mm, which is convenient for the application either of the straingauges and of the roof plates. From the previously determined parameters the tendons cross sections-made by steel rods having commercial sizes, which vary in steps of 0.5 mm - were derived. All arising approximations do not exceed a 4% error in diameter.

Both terminal cross beams were constructed by means of two bars spaced 2 mm from each other, assembled by bolts.This composite section, constant in height for the rear beam, and variable for the front beam, has been chosen in order to solve the problem of an efficient connection between the beam itself and the other two structural members converging in every joint. The resulting sections follow the similitude laws either as it refers to

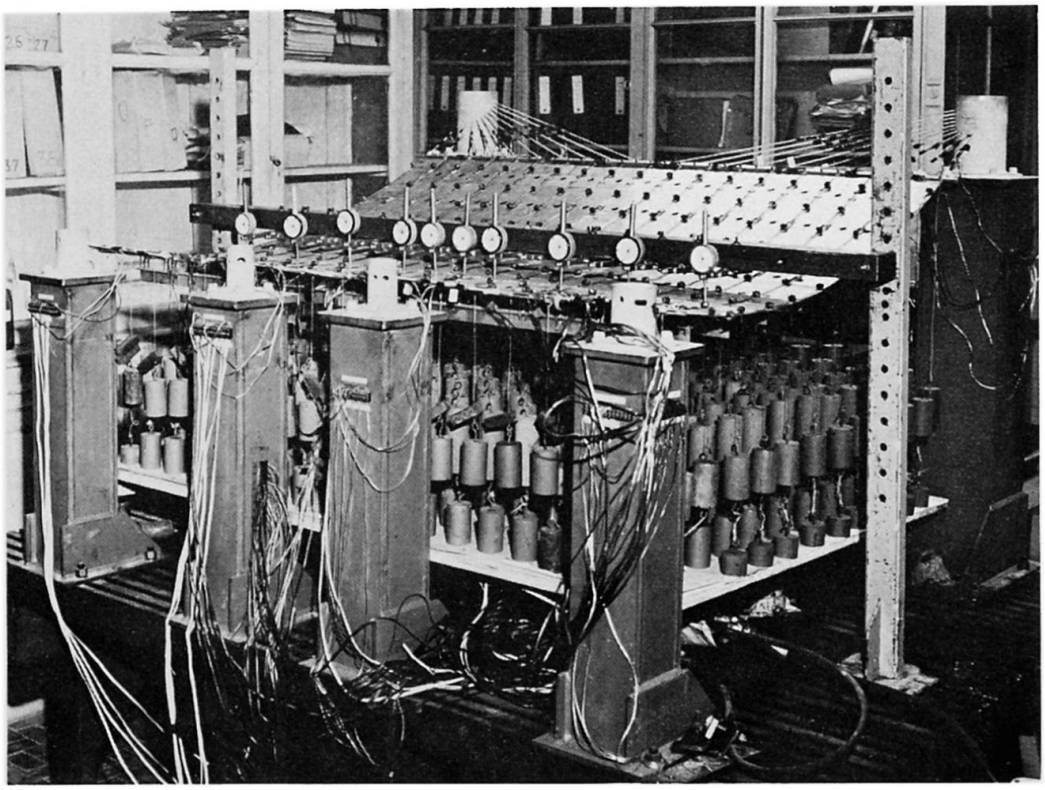

Fig. 11

Model:general view showing deflection gauges and loads.

the areas and the moments of inertia: as a matter of fact, the cross beams are submitted to high axial force.

In connecting the tendons to the outside walls and columns this latter part, (whose deformations are smaller than the roof ones) has not been realized but the tendons fixed to rigid steel tubes.

As it refers to intermediate cross beams, actually consisting of a double steel trusses, they are represented by anticorodal Tees, being impossible to re produce in detail the rather complicated truss structure.

Six linkage head ties (tubes) are fixed to six steel columns of a box profile composed by HEB I beams. Loads are realized by means of iron cylinders, 2.00 kg each for the dead load and 1.25 kg for the live load.

The loading equipment consists of a table raised and lowered by means of four hydraulic jacks, acted by a single hand pump. Through the table raising and lowering action are applied or taken away only the live load weights, while the dead load ones are always suspended to the roof.

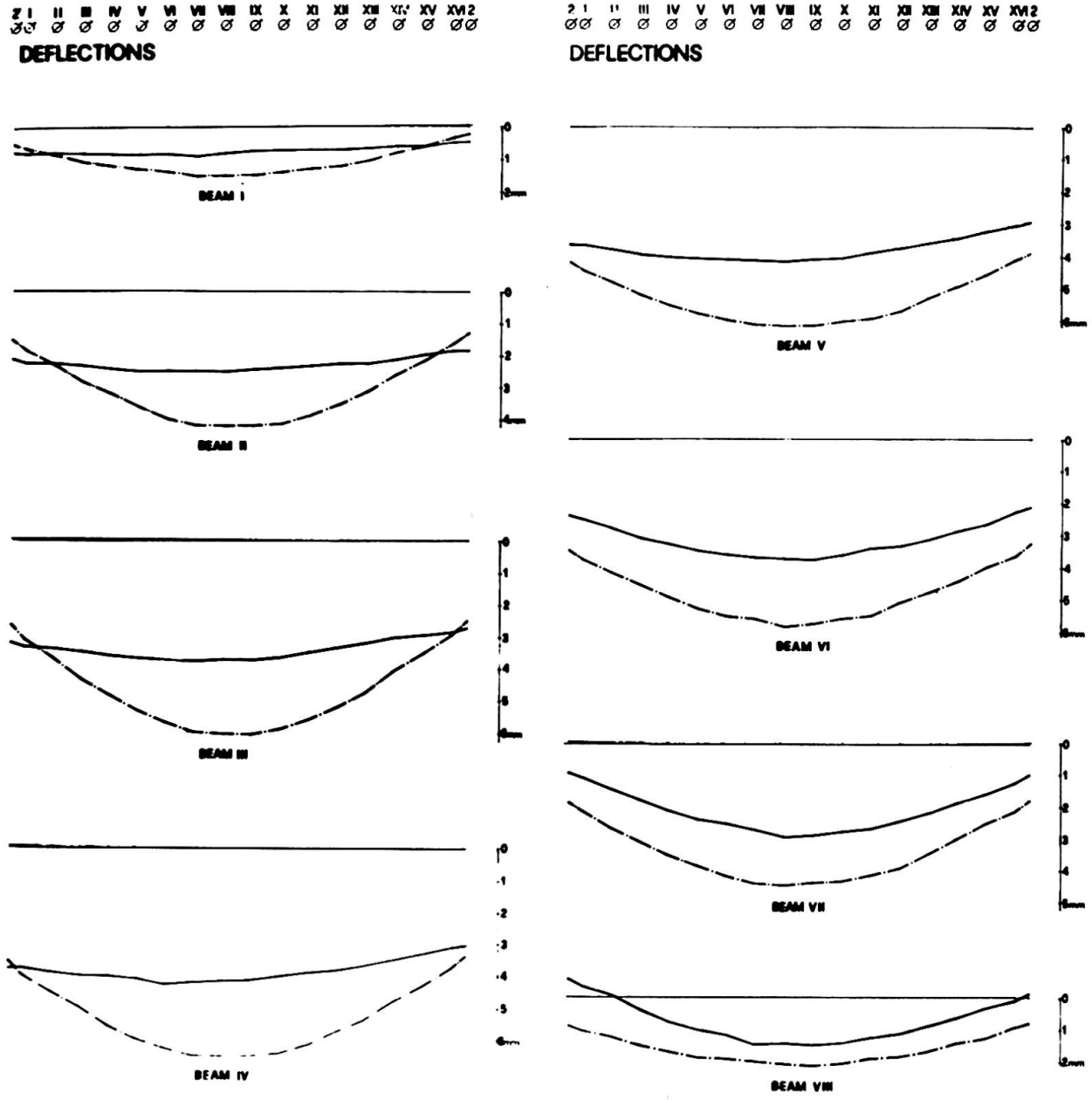

Fig. 12

2.2) Testing and results

The model tests resulted from the application of the live load to the structure already subjected to the dead load.

Two sets of measurements have been taken, one before the roof plates were mounted, the second with the plates in place.

Besides it has been tested the effect of the concentrated loads measuring the effects due to a 3 kg load applied in correspondence of five section every intermediate cross beam.

In the model, taking $\lambda = 50$, these displacements result in the order of 1 mm.

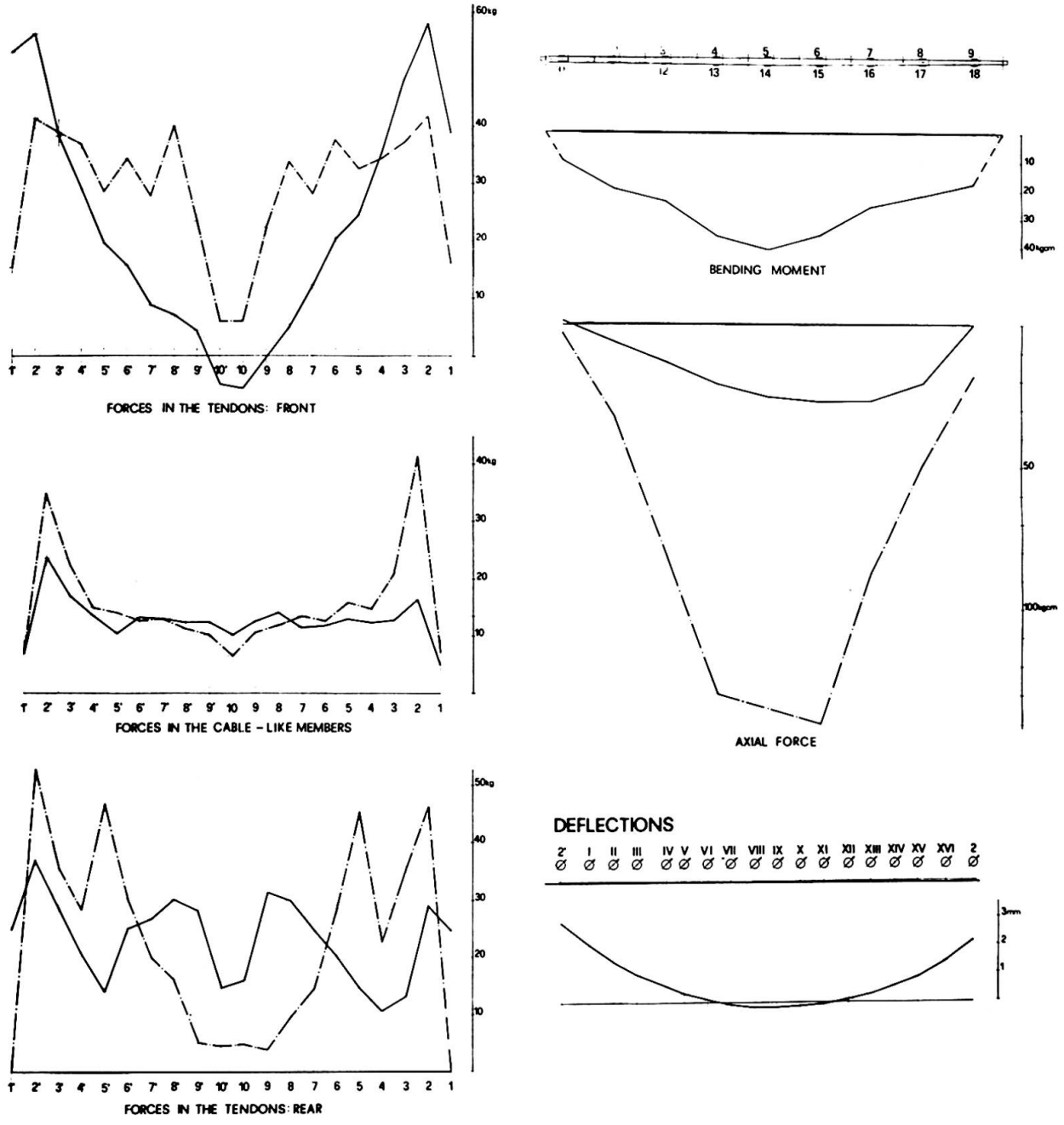

Fig. 13

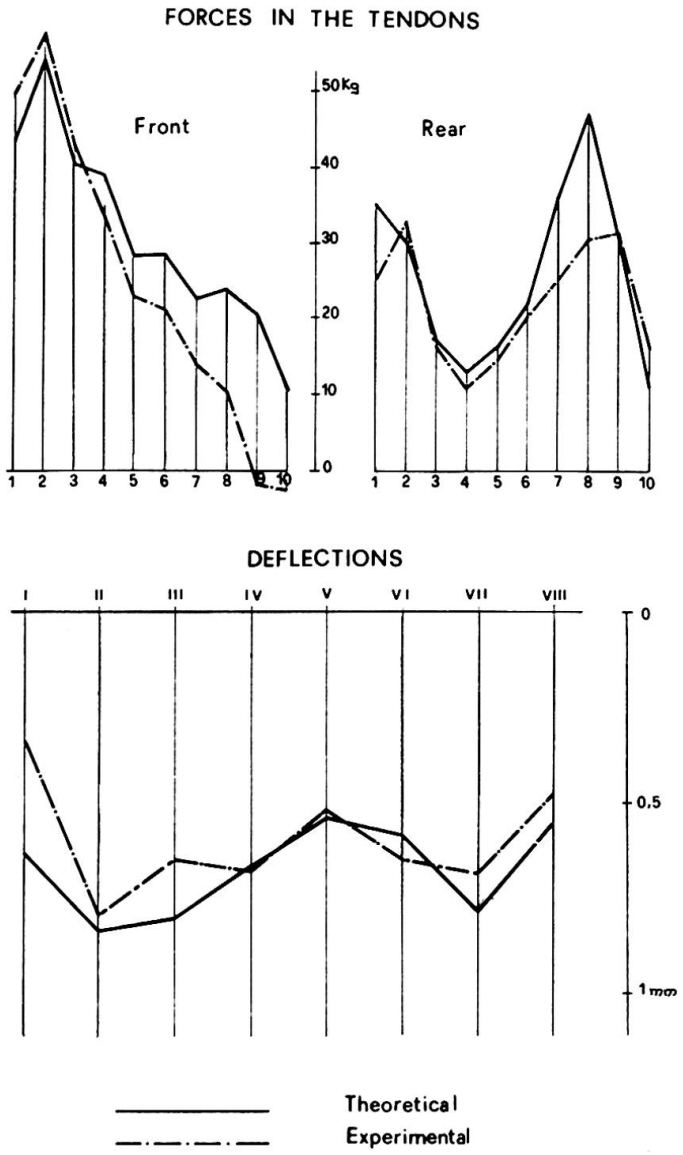

Fig. 14 Theoretical and experimental results

The main results of the model tests are given in Fig. 12 and 13, where the roof deformations (taken in correspondence of the cross beams) as well as the bending moments and the axial force distributions are represented.

In Fig. 14 the main experimental results are compared to the analytical ones, as far as the force distribution among the front tendons and the deflections of the transversal beams are concerned. It is evident the good correspondence existing between the two results.

Summary

The structures of the new hangar housing the jet Boeing 747 at the "Leonardo da Vinci" Fiumicino Airport (Rome) is described. Its main feature is the suspension roof, completely built in prestressed concrete. The structural elements are a series of parallel cable-like members, tied by transverse beams which are suspended to columns by means of fan-like tendons.
Stabilization against wind suction is provided by dead weight only.

Tests were made on a 1:50 scale metal model; details of the design as well as of the construction elements are given. Model tests results are in good agreement with the theoretical ones.

A Structural Model Study of a Hydraulic Intake Tower

Etude d'un modèle structurel d'une prise d'eau

Modelluntersuchung eines hydraulischen Einlaufs

Wm. G. GODDEN
Professor of Civil Engineering
University of California
Berkeley, USA

1. Introduction

In the design of any structure which will be subjected to water flow, the magnitude of the hydrodynamic forces may have to be determined, and the dynamic response of the structure predicted. In certain cases there is also a possibility of the hydrodynamic forces being increased by interaction with the vibration of the structure, causing a condition of hydroelastic instability.

A free-standing hydraulic intake tower is one such structure. This kind of tower, commonly used in reservoirs to draw off the water, is often tall and slender and hence liable to vibrate as a vertical cantilever. The section of the tower is commonly circular or square, and is fitted with intake valves at various levels to enable water to be drawn off at any required elevation. In operation the tower is subjected to the dynamic forces caused by water entering at the valves under considerable static head, dissipating much of its energy inside the tower, and flowing out at the base. The magnitude of these forces depends on the valves that are open and on the height of water in the reservoir. Further the tower is standing in water and its dynamic response will be influenced by the water both inside and outside the tower. There has been at least one case of serious vibration in a tower of this kind, a condition that might have led to structural damage if the flow of water had not been cut off.

The purpose of this model study was to establish the stability of a proposed intake tower design under all possible flow conditions, and to determine if any design modifications were required in the design to achieve this stability. As the hydraulic aspects of the tower had also to be studied, a combined hydraulic-structural model study was undertaken to reduce the total cost and time. The tower, to be constructed in Southern California, was also designed for seismic forces,hence it had considerable bending stiffness when considered as a long vertical cantilever. The stability of the design in this regard made it probable that it was also adequately stiff to resist the horizontal hydrodynamic forces, but this had to be established.

2. Description of the Structure

The prototype tower in this study is a 214 ft. high circular tower with an internal diameter of 32 ft., fitted with thirty six 6 ft. diameter butterfly valves arranged in groups of four at nine elevations. Each group of four valves is arranged as two opposing pairs, the groups are spaced at 17 ft. centers vertically and the lowest is 7 ft. above ground. When the reservoir is full the water level will be 158 ft. above ground.

When all valves are finally installed, all four valves at any given level

will either be open or closed, one or two levels will be open and these will be fully submerged. The maximum flow with all valves open will be 9600 cub. ft. per sec. During the initial phases of construction there will be only one pair of opposing valves at each level.

The appearance of the tower above ground will be similar to that of the model shown in Plate 1. Below ground the internal diameter tapers from 32 ft. to 19 ft. over a height of 75 ft., and below this there is an elbow section which joins the outlet tunnel which also has a diameter of 19 ft.

The foundation of the tower is interbedded sandstone and shale which will be pressure grouted after construction.

3. Considerations in the Design of the Model

Dynamic forces due to hydraulic flow are inertial forces and drag forces, and these two lead to conflicting similitude requirements. As gravity acts on both model and prototype, accelerations are the same in both, and this in turn gives rise to the velocity ratio $v_r = 1/L_r$ where subscript r denotes a dimensionless ratio between model and prototype, and L = length. Hence the ratio of inertial forces when water is used as the fluid in the model is $F_r = L_r^3$. To keep the drag forces to the same scale the Reynolds Number has to be the same in model and prototype, and this leads to a velocity requirement of $v_r = 1/L_r$. This conflict in velocities cannot be resolved in such a model study and hence a decision has to be made regarding the relative importance of inertial and drag forces. Clearly inertial effects are extremely important, and the only question is whether or not the drag forces are a significant factor. In this case it was decided to neglect the drag forces, but to keep the Reynolds Numbers as close as possible by making the linear scale of the model as large as possible. For the flow condition causing the maximum vibration of the tower the Reynold Numbers were 2.7×10^7 and 1.6×10^5 in prototype and model respectively. The final effect of this decision will not be known until tests are made on the prototype tower.

In using a physical model as part of a design process it is desirable to construct the model so that modifications to the design can be effected on the model with a minimum of difficulty to allow for possible design changes in the prototype. This demands that certain geometrical features be taken as fixed, and in this case it was the internal geometry of the section. The outside geometry was left open to modification, hence the mass and the overall bending and shear stiffnesses of the tower could be modified.

It was assumed that the important structural properties for this study were those associated with the vibration of the tower considered as a long vertical cantilever, hence the overall flexural and shear stiffnesses of the tower section and its mass distribution had to be correctly simulated. Those modes of vibration associated with the local deformation of the cross section corresponded with frequencies that were considered too high to be significant.

The tower was considered fixed at ground level, and the model supported in such a way that there was an effectively rigid connection at this elevation. The prototype design included an access bridge to the tower, but this was not to be considered unless the response of the model called for design modifications.

The interaction between the vibrating tower and the surrounding water was assumed to be correctly simulated by the model. The interaction effect is discussed below. There is some data available for this effect at model scale (1), but little at prototype scale and it is recognised that the effect may be

velocity dependent. As any scale effect would likely influence the magnitude of the coupled mass of water vibrating with the tower, once this scale effect is known it can be allowed for by the designed mass of the model. In this study as no information of this kind was available, it was assumed that there was no scale effect influencing the virtual coupled mass of water.

4. Design of the Model

The stiffness requirements and frequencies of the model were fixed from the values of F_r and v_r discussed above. To make the model true scale and in prototype material would have made it too stiff by a factor of L_r the geometric scale, and as a scale of $L_r = 1/30$ was used this would have meant a model 30 times too stiff. The stiffness could have been reduced in two ways: (a) by reducing the wall thickness as local deformation was not being studied, and (b) by using a more flexible material. The first of these would have resulted in a model with extremely thin walls and difficult to construct; the second would have required a lower value of E than can be found in suitable materials. Hence a combination of the two was used. Acrylic resin in the form of Plexiglas sheet was selected for the model material, and as this has an effective dynamic E approximately 1/5th that of concrete, the further 6 times reduction is stiffness had to be effected by reducing the wall thickness of the model to approximately 1/6th of its true-scale value.

There are two properties associated with model material that must be considered in an elastic dynamic study, stiffness and damping. The value of E is the dynamic modulus associated with the frequencies expected in the study. Tests on certain plastics show E to be frequency dependent, and if E varies significantly over the expected range of frequencies, such a material may be unsuitable.[5] Dynamic tests on Plexiglas showed that E is effectively constant at 6.5×10^5 psi above 6 Hz, and as the first natural frequency of the model in water was approximately 6.5 Hz this was considered suitable. Material damping presents problems when using certain plastics for dynamic modeling. The damping of Plexiglas is in the order of 4% critical, and this is somewhat higher than would be expected in an uncracked concrete tower. Provided that there is no interaction between the dynamic forces and the vibration of the structure, the effect of higher damping can be allowed for; if a feed-back phenomenon is present, this is not possible. It was decided to use Plexiglas and to recognise the problem of higher damping in the model.

Having decided on a distorted model, it was found convenient to make the basic model understiff and to bring it up to the design stiffness with detachable external ribs. Hence it was possible to increase the stiffness further if redesign was called for.

The natural weight of the model was approximately 100 lb., whereas the simulation of inertia forces called for a weight of 550 lb. This was achieved by adding external lead weight rings, bolted to the model in such a way that they held the section geometry on two normal diagonals (Plate 2). By this means the problem of the reduced local bending stiffness of the walls was overcome. The weights were designed not to interfere with the flow pattern external to the tube, and they could also be increased in value if design modifications required it.

The valves were modeled in Plexiglas (Plate 3), and were installed with the axis of the vane vertical. Open and closed valves were modeled and these were installed according to the required operational conditions. The situation arising during the opening or closing of the valves was not studied. The model above ground without valves or weight rings is shown in Plate 1.

Three large tanks were used, a constant head tank and a weir tank to control and measure the water flow, and an 8 ft. diameter tank (Fig. 1) in which the model was tested.

5. Instrumentation

Horizontal accelerations were monitored at six points in the tower, two accelerometers at each of three elevations (Fig. 1). The locations were selected to monitor the vibration of the tower simultaneously about two orthogonal axes and at elevations suited to measuring experimental mode shapes for the first three natural modes. Samll piezoelectric accelerometers were used with a frequency range down to 1 Hz and a sensitivity of 0.01g. Dynamic stresses were measured by resistance strain gages mounted in opposing pairs at the base of the tower.

Provision was made for processing the data in either digital or analog form. For digital processing the data could be stored on magnetic tape. For diaplay in analog form the data could be fed to a storage oscilloscope and photographed. It was found that the latter procedure was ideally suited to the entire program as it had two advantages: the instantaneous display of dynamic response is essential in any study where there is a possibility of resonance causing damage; also it was useful in the preliminary stages for studying the constructional problems associated with the dynamic characteristics of the supporting tank system. Two devices were used in connection with data display. The first was an operational amplifier which displayed the log of the acceleration vertically against time horizontally. This was used for damping studies (Plate 6). The second was a harmonic analyzer which displayed the intensity of any quantity against frequency, and was used to monitor the harmonic contents of the horizontal accelerations at the top of the tower (Plate 5).

A digital counter was used to measure natural periods, and this period could be measured at any preselected interval after initial excitation by the use of a specially designed zero-crossing counter.

6. Tower-Water Interaction

The principle effect of submergence on the dynamic response of the tower is the coupled virtual mass of water which lowers the natural frequencies of the tower as compared with the frequencies in air. This was studied extensively on a series of small models (2) as well as on the tower model, and the coupled mass of water determined from interaction graphs of the kind drawn in Fig. 2 for the tower model. In this graph m_o = mass/unit length of the tower in air, m = required coupled mass of water/unit length, f_o = first natural frequency of the tower in air, and f = frequency of the tower in water. The theoretical curves are based on a Rayleigh solution which assumes a constant mode shape and a coupled mass of water taken as a constant mass m per unit depth.

The mass coupling due to water outside the tower is expressed as a percentage of the mass per unit depth of the water displaced by the tower. From a series of tests conducted on tubes of different external diameters ranging from 1.0 in. to 13.44 in. (the latter being the tower model), the coupled mass factor was found to be sensibly constant at 75%. 100% of the mass of the water inside the tower was coupled with the vibrating tower.

Fig. 2 shows the results of tests conducted on the model tower with water rising simultaneously inside and outside. The form of the experimental curve, which closely follows the theoretical interaction curves, indicates that the simple interaction concept provides an accurate procedure for computing the first

natural frequency of a vertical tube standing in water whose surface is at any elevation below the top of the tube.

The damping, as measured from decay curves, was not measureably increased by submergence in still water, even when the water level was at its maximum and all valves were open.

7. Experimental Results

Data was taken for a wide variety of valve operational conditions; single valves open at various levels of submergence, two adjacent valves open, two opposing valves open, all four valves open, and these combinations for more than one level at a time up to and including all valves being open for the maximum flow condition.

The vibration of the tower appeared to be random in form and occurred simultaneously about both horizontal axes. The form of movement of the top of the tower as viewed in plan can be seen in Plate 4, which is the trace formed by the signals from the two accelerometers at the top of the tower being fed to the X and Y plates of the oscilloscope. The most useful display of the acceleration data was by taking the signal from one accelerometer, passing it through a spectral analyzer, and recording the resulting acceleration-frequency plot on a storage oscilloscope. Plate 5 shows the spectral analysis of the accelerations at the top of the tower about one axis. It was due to two adjacent valves being open at level 4 with all other valves closed, and the water level outside the tower being at its maximum elevation. This was the valve condition that produced the maximum vibration in the tower. It will be noted that the important dynamic response of the system was associated with the natural frequencies of the tower in water, the two major peaks in this particular diagram corresponding to the second and third natural frequencies. In all cases the maximum acceleration intensity was associated with the second mode, but the largest displacement amplitude was associated with the first mode. The acceleration response curves were all of the general form shown in Plate 5, and it appeared that within the range of frequencies under study the hydrodynamic forces produced something in the nature of a white noise excitation, the dynamic magnification at the natural frequencies causing the response peaks. It will be noted that the projected prototype displacements at the top of the tower are not large, the maximum amplitude in the first mode for any valve condition being 0.4 in., and this is considerably less than the design seismic displacements. Displacements in the higher modes were much smaller.

Considerable time was spent in searching for a more serious resonant condition, without result. There appeared to be no significant feed-back phenomenon between the excitation forces and the vibration of the tower. It was concluded from the model study that this particular design was dynamically stable for all possible conditions of hydraulic flow, within the limitations of the model study.

The effect of water depth on two different valve operational conditions can be seen in Figs. 3 and 4. Fig. 3 shows the effect of the water level outside the tower on the dynamic response when two adjacent valves were open at level 4 (see also Plate 5). The variation of vibration amplitudes in the first two modes was approximately linear with water level. This could be expected as the static pressure at the intake valves increases linearly. However, when valves were open at more than one level the effect was different. Fig. 4 shows the influence of water depth on dynamic response when all valves were open. In this case there was a critical depth of water associated with maximum vibration amplitudes, and this was not the maximum possible depth. As the water level outside the tower was raised above this critical elevation the water flowing into the tower through the

higher valves either interfered with the excitation caused at the lower valves, or the random nature of the excitations at the different levels tended to cancel each other, and there was a resulting reduction in dynamic response.

Similar data was taken for the bending stresses at the base of the tower, and it was found that the spectral analysis of bending stresses correlated closely with the values predicted from the modal displacements at the top of the tower derived from the accelerometer readings.

As a further check on the stability of the tower, effective damping tests were done both in still water and also during those flow conditions showing maximum vibration. These were done by externally exciting the tower during the flow condition and observing the decay curve while the flow was maintained. Plate 6 is an example using the signal from the top accelerometer. The system damping can be deduced from the envelope of the first part of the curve which represents the decay after the removal of the external excitation. The residual signal after the initial decay represents the dynamic response of the tower to the hydrodynamic forces. In all such tests the change in system damping caused by the hydraulic flow condition was minimal.

8. Conclusion

This particular model of a hydraulic intake tower was completely stable under all possible flow conditions. In using the experimental data to predict prototype response the limitations of the model are recognized, namely the effects of drag forces and system damping.

At the time of writing the prototype tower has not yet been constructed. It is hoped that the structure will be tested under conditions equivalent to those simulated by the model. Thus it should be possible to study the correlation between model and prototype dynamic behavior and to determine the extent to which dynamic model studies of this kind can be used in the design of hydraulic structures.

9. Acknowledgments

The author acknowedges the assistance received from Mr. E. W. Stroppini, Chief, Civil Design Section, Department of Water Resources, State of California, who sponsored the investigation, and from Professor J. Amorocho, University of California, Davis, who was in charge of the hydraulic studies.

10. References

1. Clough, R.W., "Effects of Earthquakes on Underwater Structures," International Earthquake Congress, Tokyo, 1960.

2. Godden, W.G., Tuncag, M., and Wasley, D.L., "Model Analysis of the Castaic Reservoir Intake Tower," Report No. 70-15, Structural Engineering Laboratory, University of California, Berkeley, U.S.A.

11. Summary

Experimental data is presented on the dynamic response of a structural model of a hydraulic intake tower. The effects of submergence on the natural frequencies are given together with the response of the system to the hydrodynamic forces associated with certain valve operational conditions. Using a combined structural-hydraulic model an attempt has been made to establish the structural adequacy of a proposed design.

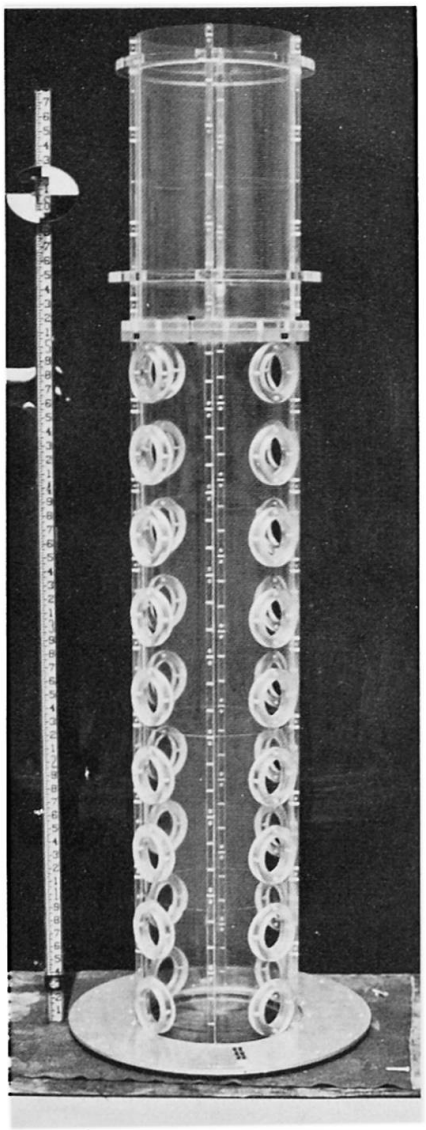

Plate 1. Model Tower
without Valves or Weights

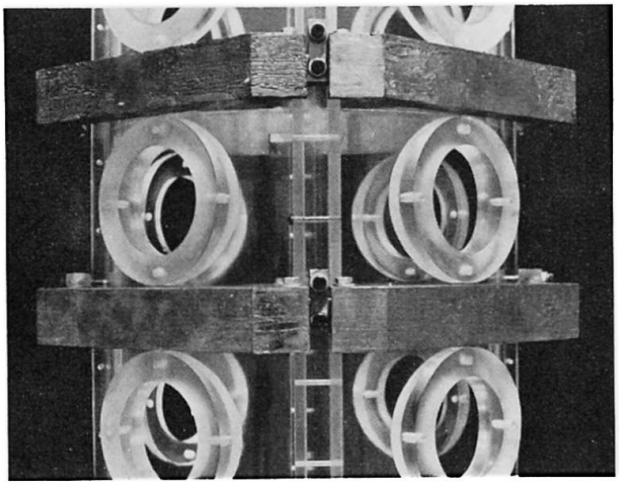

Plate 2. Fitted Weight Rings

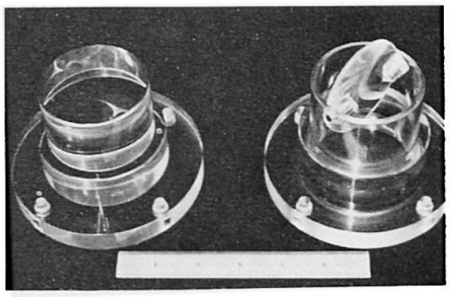

Plate 3. Valves Closed and Open

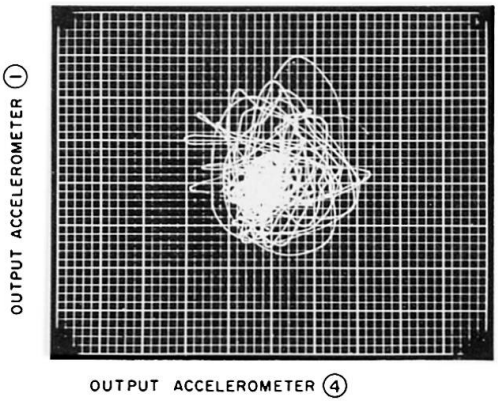

Plate 4. Response of Top of Tower

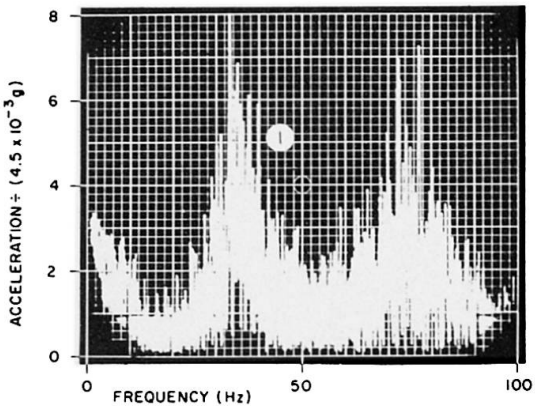

Plate 5. Spectral Analysis of Response

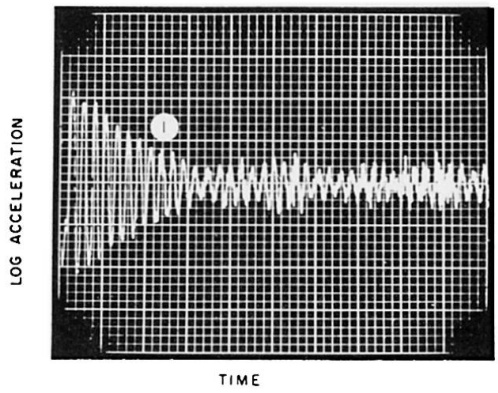

Plate 6. System Damping

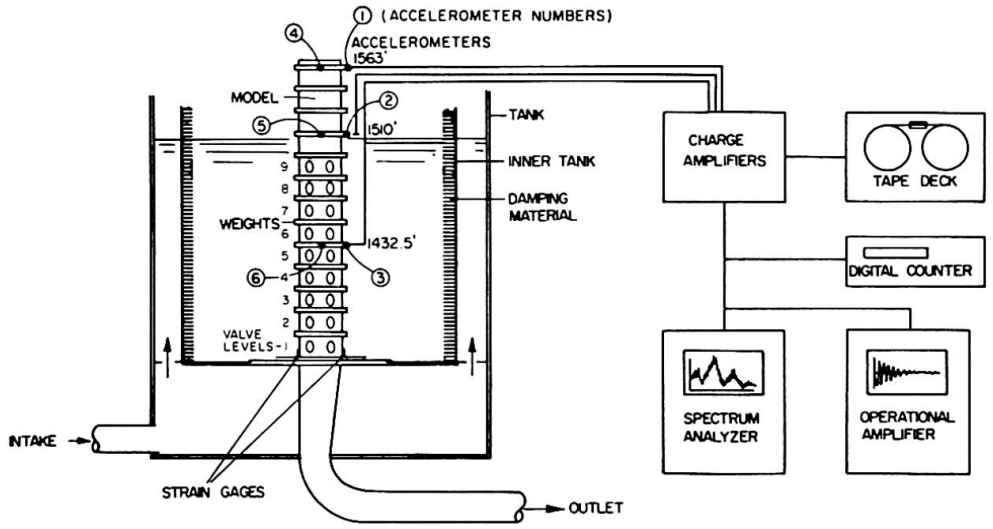

Fig. 1. Test Set-up and Instrumentation

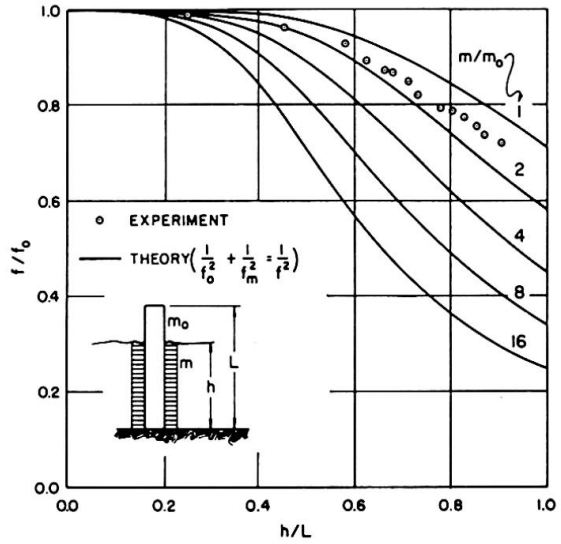

Fig. 2. Effect of Submergence on Natural Frequency

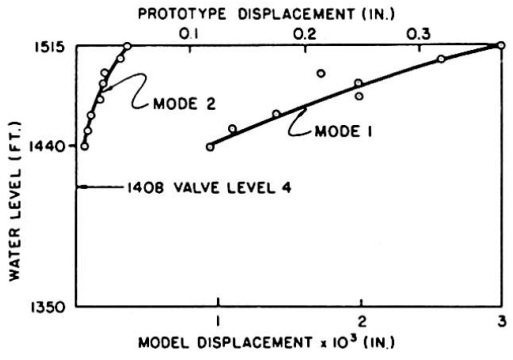

Fig. 3. Effect of Water Level Two Valves Open at Level 4

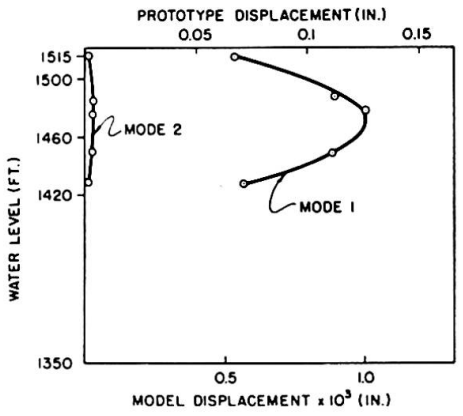

Fig. 4. Effect of Water Level All Valves Open

Tests of a 1/10-Scale Concrete Model to Aid Design of a Large Prestressed Bridge

Essais sur modèle en béton à l'échelle 1 : 10; complément pour l'étude du projet d'un grand pont précontraint

Versuche an einem Betonmodell im Massstab 1 : 10 als Hilfsmittel beim Entwurf einer grossen vorgespannten Brücke

W.G. CORLEY EIVIND HOGNESTAD
Manager, Structural Development Section, and Director
Engineering Development Department, respectively
Portland Cement Association
Skokie, Illinois, USA

1. HIGHLIGHTS

As noted by the Reporter, the use of structural models provides a powerful aid to analytical design. Models permit direct determination of elastic behavior of complex structures that must be simplified to permit structural analysis. Even more important, concrete models provide the only reliable means of determining the ultimate strength of complex concrete structures.

Planned for construction across the Potomac River near Washington, D.C., the proposed Three Sisters Bridge, shown in the artist's rendering in Fig. 1, is unique in several respects. In addition to its 750 ft. (228.6 m) main span, it has curved 440-ft. (134.1 m) side spans and the 110-ft. (33.5 m) roadway is widest of any post-tensioned, cantilevered bridge yet constructed. Consequently, it was decided that this design should be supplemented by the construction and testing to destruction of a 1/10-scale model of the prototype.

Fig. 1. Proposed I-266 Potomac River Bridge

---

* Manager, Structural Development Section, and Director, Engineering Development Department, respectively, Portland Cement Association, Old Orchard Road, Skokie, Illinois, 60076, U.S.A.

Under contract with the designers Howard, Needles, Tammen and Bergendoff, Consulting Engineers of New York City, a 1/10-scale concrete model of the Three Sisters Bridge was constructed and tested in the Structural Development Laboratory of the Portland Cement Association. Dimensions of the prototype bridge are shown in Fig. 2. Since the prototype is symmetrical about the center of the main span, only one-half of the bridge was modeled. At 1/10-scale, the model shown in Fig. 3 was 81-ft. 6-in. (24.8 m) long, 11-ft. (3.4 m) wide, about 6-ft. (1.8 m) deep at the pier and 1-ft. 3-in. (38 cm) deep at midspan and at the abutment. Constructed using materials having properties similar to those of the prototype, the model represented the "Direct" method of structural modeling as described in detail elsewhere. (1)

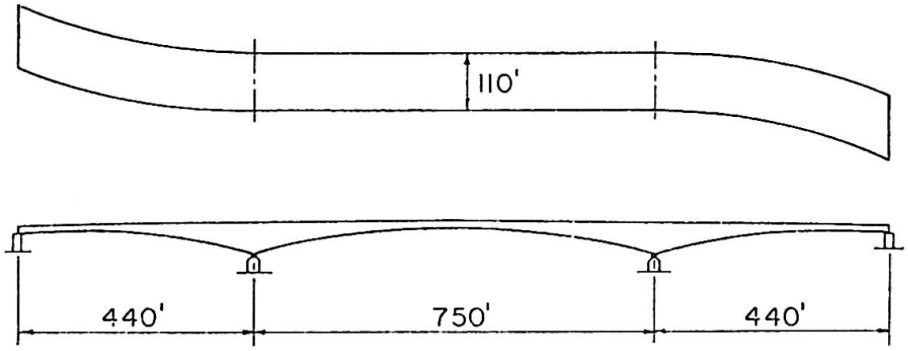

Fig. 2. Plan and elevation of prototype bridge

This report describes construction of the 1/10-scale prestressed concrete model, the testing procedure, instrumentation and data processing. Important results of service load tests, design ultimate load tests, and tests to destruction are reported. It is shown that the model supported the design service load without structural cracking and safely withstood the severe overload of 1.5 D + 2.5 (L + I)* required by "Section 1.6.6 - Load Factors," the AASHO Standard Specifications for Highway Bridges.(2) Furthermore, it withstood an overload of 1.5 + 6.0 (L + I) before the flexural capacity of the bridge was reached in the main span at the pier.

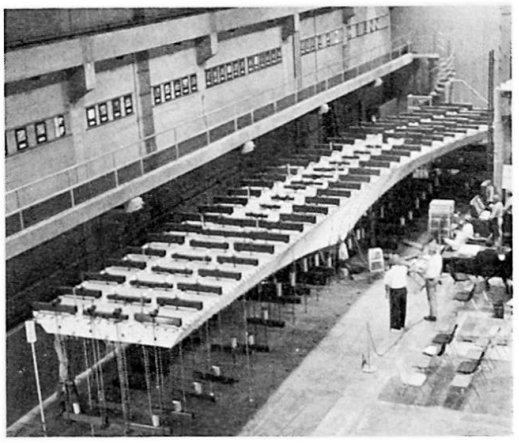

Fig. 3. Bridge Model

2. MODEL CONSTRUCTION

Assembly of Superstructure - Although the prototype is designed to be cast in place in segments, the model was constructed of precast 3-ft. (91.4 cm) segments that were sequentially grouted in position and post-tensioned together to form the complete bridge. This use of precast segments was strictly for convenience in the laboratory. To simulate field construction, continuity of non-prestressed reinforcement was maintained across all joints. Dimensions of a model segment near the pier are shown in Fig. 4. Details of construction and testing are given elsewhere. (3)

---

* D = effect of dead load
L = effect of design live load
I = impact of load

Using the cantilever method, the model bridge was constructed so that the superstructure was always heavier on the abutment side of the pier. Overturning of the partially completed bridge was prevented by a temporary support initially located 5.5 ft. (1.7 m) from the pier and later moved to a position 29.3 ft. (8.9 m) from the pier. This support was removed when the bridge was seated on the abutment. At all times after the first longitudinal tendons were stressed, a 3,000 lb. (1.36 t) weight representing the 300,000-lb. (136.4 t) weight of construction equipment on the prototype, was kept near each end of the model. It is intended that the same cantilever construction procedure will be used for the prototype.

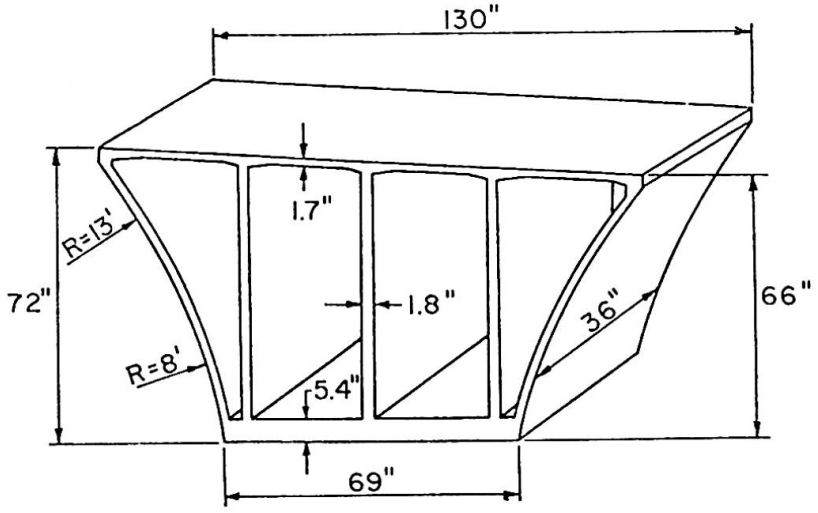

Fig. 4. Dimensions of model segment near pier

Construction of Segments - Each precast model bridge segment was constructed in three operations.(3) Roadway and soffit sections were precast separately and then joined together by casting webs and fascias. Figure 5 shows this procedure schematically.

Soffit sections were cast on a continuous platform built each side of the pier at the location where the model bridge was later to be assembled and tested. The platform served initially as a base for casting soffit sections and subsequently as a working platform during erection of the bridge.

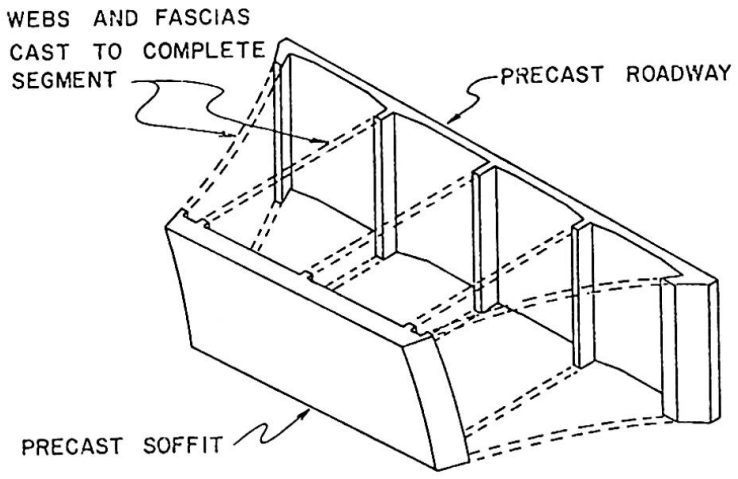

Fig. 5. Model bridge segment construction

Roadway sections were cast in pairs, deck surface down on special adjustable platforms. Continuity of the roadway section was ensured by aligning longitudinal ducts with metal templates and by casting each new section against a previously cast section.

The precast roadway and soffit sections were placed in an assembly frame that was adjusted to ensure longitudinal prestressing duct continuity and proper relative geometry. Web duct continuity between segments was established by use of adjustable templates. After forms were attached to the web and fascia stubs on the deck and soffit sections, the bridge segment was completed by casting the center portions of webs and fascias.

Erection of Segments - The erection of each piece of the bridge model began with lifting the segment onto an adjustable temporary scaffolding and clamping it to the completed portion of the bridge. The temporary scaffolding and

clamping were then adjusted until observation by surveying instruments (4) indicated that the segment was in its proper position relative to the completed portion of the bridge.

Once a segment was properly aligned, joint concrete was placed. To complete the erection cycle, tendons were stressed and the temporary supports were removed.

Method of Prestressing and Compensation for Losses - Prestressing tendons in the deck, soffit, webs, fascias and diaphragms were anchored at the dead end with a button head and at the stressing end with a friction anchor. (3) An adjustment device was placed between the friction anchor and the anchor plate to provide a means for precise tensioning of each tendon.

All tendons were stressed initially to 20 percent above the final desired value. This overstress was chosen to compensate for calculated losses from steel relaxation, concrete creep and shrinkage and tendon friction.

Similitude of Reinforcement - Grade 60 deformed bar reinforcement in the prototype was represented by galvanized welded wire fabric having a yield stress of about 60 ksi and meeting requirements of ASTM Designation: A185-68 and A82-66. Mesh sizes used were 2x2 in. (5x5 cm) - 12/12 and 2x2 in. (5x5 cm) - 14/14. The size and amount of mesh was varied to provide about the same percentage of reinforcement at each section in the model as in the prototype.

The 32 mm (1-1/4 in.) prestressing bars considered in the design of the prototype were represented by 5 mm (0.2 in.) or 1/4 in. (6.35 mm) prestressing wire in the model. The total prestressing force rather than the individual tendon force was modeled. Consequently, the 1/4-in. and 5 mm prestressing wires in the model represented approximately six and four tendons, respectively, in the prototype. Details of placement of the reinforcement are provided elsewhere. (3)

Properties of Concrete and Prestressing Reinforcement - A concrete mix with proportions of 1 part Type III cement to 5.25 parts Elgin fine aggregate was used to cast the segments. The 28-day strength and elastic modulus measured by compression tests of 6x12-in. (15x30 cm) cylinders are summarized in Table 1.

Joints between the segments were made from a low slump mortar of 1 part Type III cement and 3 parts masonry sand. The 28-day strengths measured by compression tests of 6x12-in. cylinders are listed in Table 1.

TABLE 1 - Properties of Model Concrete at 28 Days

Location of Concrete	Test of 6x12-in. (15x30 cm) Cylinders*	Average Values psi (kg/cm^2)
Segments	f'_c	5,870 (412)
Segments	E_c	3,350,000 (235,000)
Joints	f'_c	7,770 (546)

* f'_c = compressive strength; E_c = modulus of elasticity

Prestressing wire met the requirements of ASTM Designation: A421-65. Strengths obtained from tests of representative samples of wire used in the model are listed in Table 2.

TABLE 2 - Properties of Model Prestressing Reinforcement

Diameter	Yield Stress at 1% elongation f_y ksi (kg/cm²)	Strength f'_s ksi (kg/cm²)
5 mm	264 (18,500)	292 (20,500)
0.25 in. (6.35 mm)	218 (15,300)	254 (17,800)

3. TESTING PROCEDURE

Application of Loads During Construction - As construction of the model proceeded, forces were applied to simulate the dead load of the prototype. (1) At 1/10-scale, the model required application of nine times the self weight of each segment to reproduce prototype stresses. Load was applied by means of temporary hydraulic rams located below the test floor. (3, 4) Anchor nuts on the loading rods were then tightened against the lower side of the floor to hold the required force. Coil springs in the system permitted small movements of the bridge during construction while maintaining the total load within a minimum of 93 percent of that intended.

Application of Dead Load - Hydraulic loading equipment below the test floor was arranged to apply dead load and live load to the model using techniques described elsewhere. (3, 4) Two independent hydraulic systems were used to apply these loads.

The first step in the test sequence was to transfer the load from the springs to the hydraulic system and hold the prototype dead load (1.0 D), i.e., a load ten times the self weight of the model. A set of initial readings used as a "zero" reference for all tests was then taken.

Design Service Load Tests - After initial readings were taken under 1.0 D, lane loads and concentrated loads representing 1.0 (L + I) for HS20-44 loading (2) were added in 5 equal increments. All electronic instruments were read and the model was visually inspected at each increment. Under this design service load condition of 1.0 D + 1.0 (L + I), no cracking due to application of load was observed.

Dead Load Tests - After completion of the design service load test, the dead load was increased from 1.0 D to 1.3 D in six equal increments. All electronic gages were read and the model was visually inspected at each increment. No cracking due to application of this load was observed.

Design Ultimate Load Test - The dead load was first increased from 1.0 D to 1.3 D in three equal increments. Then four smaller, equal increments of load were added to bring the total up to 1.5 D. Finally, live load was applied in four increments until a total of 1.5 D and 2.5 (L + I) was carried by the model. All electronic gages were read and the model was visually inspected after each increment.

Under application of the Design Ultimate Load, cracks were observed both over the pier and near the abutment. Although some inelastic deformation was evident, the model safely supported this extreme overload.

Test to Destruction - The dead load was first increased from 1.0 D to 1.3 D in one increment and to 1.5 D in a second increment. Live load was then

applied to bring the total to 1.5 D +4.0 (L + I) with five stops to take readings. The live load was then reduced to zero and the model was held at 1.5 D overnight.

The next day live load was again increased and another set of readings was taken at 1.5 D +4.0 (L + I). Two more increments of 1.0 (L + I) were then applied and all instruments were read. While maintaining a load of 1.5 D + 6.0 (L + I), the flexural capacity of the main span at the pier was reached and the load dropped off suddenly. When this occurred, crushing of the concrete over the entire cross section released all longitudinal prestress and deflections of the model released all applied load. This completed structural testing of the 1/10-scale model.

4. INSTRUMENTATION AND DATA PROCESSING

Loads, reactions, reinforcement strains, concrete strains, web and fascia horizontal deflections, superstructure deflections and rotations were measured during the test using procedures described elsewhere. (3, 4)

Eighteen load cells were used to measure forces. Ten cells under the pier and two at the side span abutment measured reactions. Applied loads were monitored both with pressure cells in each hydraulic system and with six load cells distributed through the dead load and live load systems.

Bonded electrical strain gages and Whittemore mechanical gages were placed on eleven main deck tendons above the pier and on four soffit tendons at the calculated location of maximum positive moment. Tendon forces were also sensed with a load cell at each end of one long longitudinal deck tendon and with one load cell each on a soffit tendon, a web diagonal tendon and fascia tendon.

Strain gages were placed on the concrete surface at 360 locations. This included gages on nine heavily instrumented cross sections, two diaphragms, and on the soffit near the pier. At each heavily instrumented cross section, longitudinal gages were provided over each web on both deck and soffit, over the fascias on the deck and at mid-depth of two webs and one fascia. At sections near the pier, additional longitudinal gages were placed on all webs and fascias near the bottom of the deck.

Lateral deflection at mid-depth of each web and fascia was measured at a location midway between the pier diaphragm and the first intermediate diaphragm in both the main span and the side span. To accomplish this, a vertical framework was attached near the top and bottom of each web and fascia to support a linear variable differential transformer (4) displacement sensor at mid-height.

Deflections of the superstructure were measured at 26 locations including the quarter points and mid-lengths of each span and the free end of the main span cantilever. A linear potentiometer connected to the test floor directly below each measuring point was used to sense the vertical movements.

Rotation was measured over a 24-in. gage length including the first longitudinal deck tendon cutoff each side of the pier. Both rotation and web lateral deflection were continuously traced on oscillographic recorders. Selected load versus rotation, load versus vertical deflection, and load versus web lateral deflection outputs were displayed continuously on X-Y recorders with the Y-axis representing applied load.

At each load increment, all data were recorded. Loads, reactions, strains and deflections were recorded on printed and punched tape using a high speed VIDAR digital data acquisition system shown in Fig. 6. The punched tape can be

used to feed the data directly into an IBM 1130 Computer. Recording of 400 channels of information with this equipment required about 40 seconds.

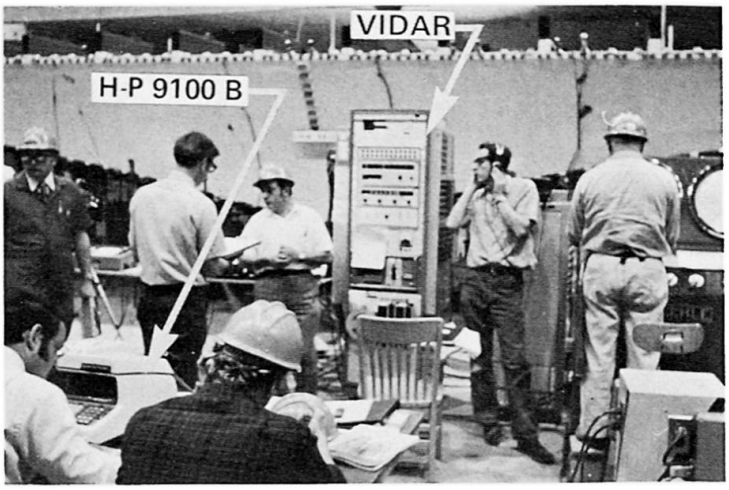

FIG. 6. Test control center

As soon as a complete set of data was recorded on the VIDAR, selected readings were fed into a Hewlett-Packard 9100B (H-P 9100B) desk computer located in the test control center as shown in Fig. 6. This computer was programmed to give measured values of reactions, key stresses and deflections. As the test progressed, the measured values were compared with previously calculated values. This immediate access to important reduced data permitted the test to proceed rapidly while still maintaining complete control.

After each test was completed, the data were reduced and analyzed with the help of an IBM 1130 Computer. All readings were converted to strain, load or deflection and tabulated. The data were then analyzed to determine force distributions in the model, principal stresses at selected locations, load versus deformation relationships and other selected information.

In a separate operation, the H-P 9100B desk computer was used in combination with an on-line calculator plotter to plot load versus deformation data. This permitted a large amount of data to be plotted and studied in a very short time.

5. TEST RESULTS

Performance During Construction - Observed reactions, strains and deflections during construction of the bridge model were all within anticipated limits. The bridge model was observed to respond "elastically" as each new segment was erected and dead load was applied. In addition, no cracks attributed to applied load were found.

Performance Under Design Service Load - Under the Design Service Load of $1.0\,D + 1.0\,(L + I)$, the concrete model was observed to perform as anticipated. No cracks caused by applied load were found. Strains and deflections measured at critical locations were observed to be proportional to the applied load, indicating that the structure remained essentially "elastic." A comparison of measured and calculated load deflection curves for mid span (end of cantilever) deflections is shown in Fig. 7. Calculated deflections were based on an uncracked section and measured material properties.

Behavior at service load was within limits generally assumed in design. These experimental results indicate that the serviceability requirements implied by the AASHO Specifications (2) are met by the design.

Performance Under Design Ultimate Load - After the service load tests, the design ultimate load of $1.5\,D + 2.5\,(L + I)$ was applied to the concrete model. Under this extreme overload some inelastic strains and deflections were observed, and cracks occurred both in the negative moment region over the pier and in the positive moment region near the abutment. All of the inelastic behavior observed under application of design ultimate load was within ranges anticipated.

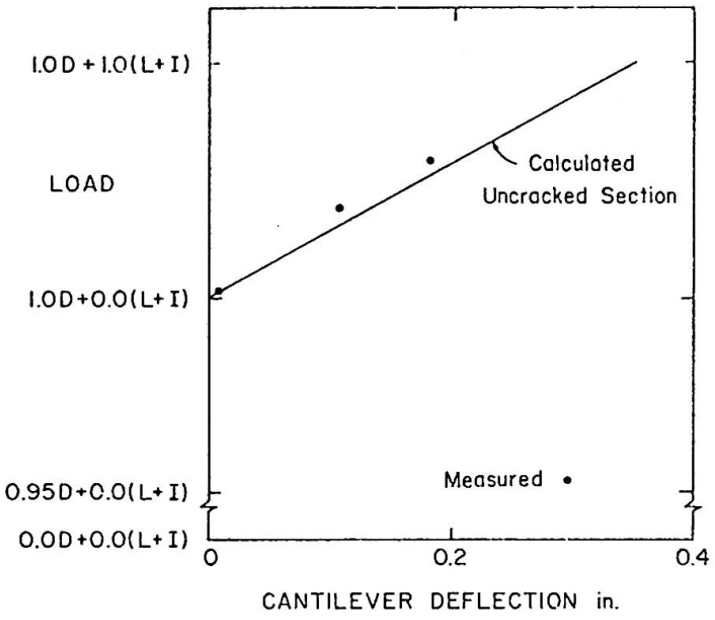

FIG. 7. Cantilever deflection - service load test

Figure 8 shows calculated and measured load versus deflection relationships for mid span (end of cantilever). Calculated deflections were based on an uncracked section and measured material properties. As can be seen, the observed deflections were in satisfactory agreement with those calculated.

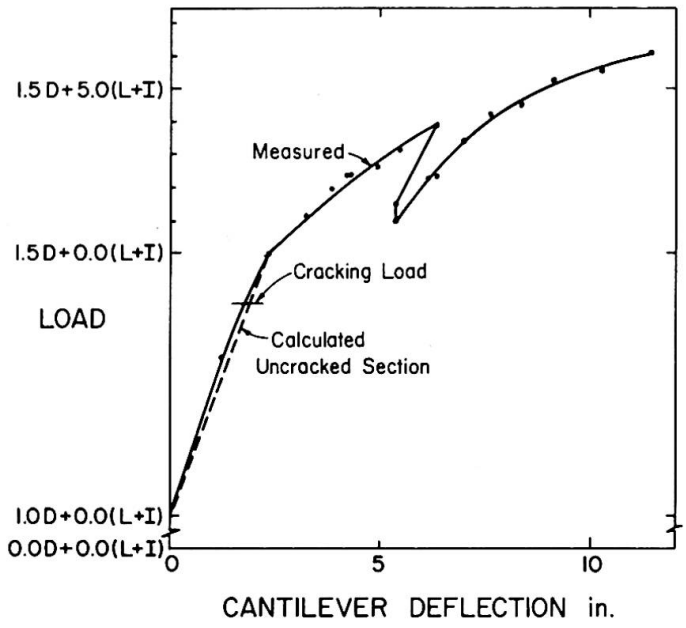

FIG. 8. Cantilever load vs. deflection - test to destruction

After the overload was removed and the condition of 1.0 D had been restored, all cracks were observed to have closed until they were barely visible to the naked eye. This behavior indicated and measured strains confirmed that the longitudinal prestressing tendons remained "elastic" under application of the design ultimate load.

Performance Under Test to Destruction - As overload was added during the test to destruction, additional flexural and torsional cracking developed. However, no large cracks were observed either in the webs or the fascias of the model.

After a total load of 1.5 D + 4.0 (L + I) had been applied, it was observed that an increase in load caused significant spalling of the concrete at the first joint in the main span. Measured strains indicated that general crushing of the concrete occurred as the load went from 1.5 D + 5.0 (L + I) to 1.5 D + 6.0 (L + I). At this load, the flexural capacity of the main span was reached and the test ended. Fig. 9 shows the pier region after the test.

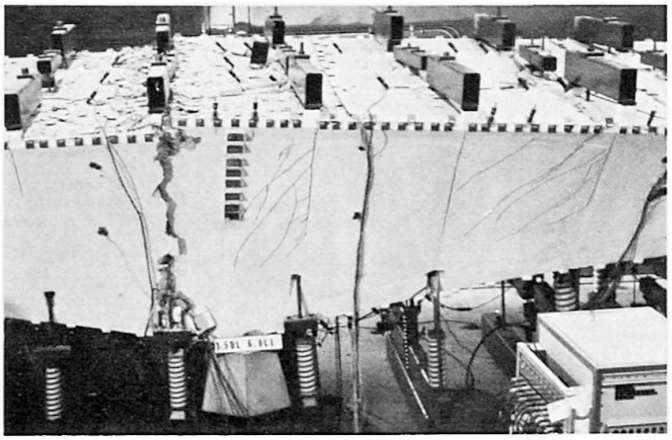

FIG. 9. Pier region after test

A comparison of measured moment capacity with that calculated on the basis of Article 1.6.10 of the AASHO Specifications (2) and using measured material properties gives a ratio of $M_{u\,(test)}/M_{u\,(calc)} = 1.15$. A similar comparison using moments calculated on the basis of compatibility of deformations and equilibrium of forces gives a ratio of $M_{u\,(test)}/M_{u\,(calc)} = 0.99$. These comparisons indicate that measured and calculated values of flexural strength are in satisfactory agreement.

6. ACKNOWLEDGEMENTS

This work was done under contract with the designers, Howard, Needles, Tammen and Bergendoff, Consulting Engineers of New York City. Mr. Gerard F. Fox is the partner-in-charge of design and Mr. Fred H. Sterbenz is the Project Engineer. Mr. A. Gordon Lorimer is the Consulting Architect on the project.

Mr. G. I. Sawyer, Assistant Director, Department of Traffic and Highways, District of Columbia, is the Owner's Representative. This work was carried out under Federal Aid Project No. DC-VA-I-266-2(102)1. The work was aided by staff of the Federal Highway Administration, U.S. Department of Transportation.

The model was constructed and tested in the Structural Development Laboratory of the Portland Cement Association. Professional staff members responsible for construction and testing of the model were Dr. J. E. Carpenter, Dr. H. G. Russell, N. W. Hanson, Dr. A. E. Cardenas, T. Helgason, Dr. J. M. Hanson and Felix Barda. Mr. A. P. Christensen and other personnel from the Transportation Development Section provided valuable assistance in the design and construction of the model.

Dr. Roy E. Rowe, Director of Research and Development, Cement and Concrete Association, Great Britain, served as Models Consultant.

7. REFERENCES

1. Mattock, A. H., "Structural Model Testing - Theory and Application," Journal of the Portland Cement Association, Research and Development Laboratories, Vol. 4, No. 3, September 1963, pp. 12-23; PCA Development Bulletin D56.

2. "Standard Specifications for Highway Bridges," Tenth Edition, 1969, The American Association of State Highway Officials, Washington, D. C.

3. Corley, W. G., Carpenter, J. E., Russell, H. G., Hanson, N. W., Cardenas, A. E., Helgason, T., Hanson, J. M., and Hognestad, E., "Construction and Testing of 1/10-Scale Micro-Concrete Model of New Potomac River Crossing, I-266," Journal of the Prestressed Concrete Institute, V. 16, No. 6, Nov.-Dec. 1971, pp. 70-84.

4. Hognestad, E., Hanson, N. W., Kriz, L. B., and Kurvits, O. A., "Facilities and Test Methods of PCA Structural Laboratory," Journal of the Portland Cement Association, Research and Development Laboratories, Vol. 1, No. 1, 1959, pp. 12-20 and 40-44; Vol. 1, No. 2, 1959, pp. 30-37; Vol. 1, No. 3, 1959, pp. 35-41; PCA Development Bulletin D33.

8. SUMMARY

Previous model tests such as those of the Medway Bridge constructed in Southern England have shown the usefulness of a concrete model to aid in design. Tests of the Three Sisters Bridge model have carried the design process another step forward by providing a direct link between the model and the computer.

Results of this test indicate that all of the unusual features of the bridge are adequately accounted for in the design. Service load performance met or surpassed the design requirements and the required safety against overload was exceeded.